HELLENIC REPUBLIC

National and Kapodistrian University of Athens

EST. 1837

Orbital instabilities induced by tidal interactions in a gravitationally driven neutron-star binary.

Eftychios Kontadakis[1]

[1]Postgraduate Student, National and Kapodistrian University of Athens, felkon0@gmail.com

August 21, 2024

Master's Thesis
Examination comittee:
T. A. Apostolatos (Main supervisor)
N. Vlahakis
K. Gazeas
Section of Astrophysics, Astronomy and Mechanics

Acknowledgements

I want to express my utmost gratitude to my supervisor and teacher, T. A. Apostolatos for introducing me in this field, for patiently guiding me through it and for supporting me in my current and future endeavors. I'm also thankful for all the Astrophysics,Astronomy and Mechanics sector's professor's, lecturer's, secretary's and student's efforts to make this journey both meaningful and enjoyable.
I also want to thank my parents for supporting me all these years and listening to me explaining the weekly challenges I faced working on this (even though they did not understand me most of the time). Last but not least, I want to thank my cat for always sleeping on my notes.

Abstract

After the first detection of gravitational waves (GW) originating from coalescing black holes from LIGO in 2015, every doubt regarding their existence disappeared. In 2024, we count more than 90 unique detections of gravitational waves, most of them from coalescing black hole binaries (BBH). Only 2 of those detections originated from coalescing neutron star binaries (BNS), named GW190425 and GW180718, the latter event was also captured by Fermi LAT (GRB170817). The GW signal combined with the electromagnetic observations will play a vital role in the difficult task of unlocking the secrets hidden inside these compact objects. Further understanding of neutron star coalescences is required. The first goal of this work is to infer how the tidally induced quadrupole moment will affect the gravitational wave phase. Existing work on this assumes circular orbits, thus the second and primary goal of this paper is to investigate if elliptical orbits can appear during the inspiral, or if some exchange between the energy of the tidally induced quadrupolar oscillations and the energy of the two companion's motion around their center of mass can lead to some kind of "oscillation" between circular and elliptical orbits.

Keywords: Binary, Neutron Star, Orbits, Instabilities, Tidal Effects

Περίληψη

Μετά την πρώτη καταγραφή βαρυτικών κυμάτων από διπλό σύστημα μελανών οπών, από τον ανιχνευτή LIGO το 2015 , κάθε αμφιβολία για την ύπαρξη τους ανήκει πλέον στο παρελθόν, πόσο μάλλον όταν σήματα από τέτοια συστήματα συνεχίζουν να καταγράφονται από τους ανιχνευτές μας (Virgo & LIGO). Πλέον μετράμε πάνω από 90 ξεχωριστές καταγραφές βαρυτικών κυμάτων οι περισσότερες εκ των οποίων είναι από συγκλίνοντα διπλά συστήματα μελανών οπών. Μόλις δύο από αυτές τις παρατηρήσεις είναι από διπλό σύστημα αστέρων νετρονίων που συγκλίνει, οι γνωστές με τα ονόματα GW190425 και GW180718, η τελευταία κατά μια εκπληκτική σύμπτωση έγινε αισθητή τόσο από τους βαρυτικούς ανιχνευτές όσο και από το Fermi LAT (GRB170817) . Για χρόνια οι επιστήμονες προσπαθούν να ξεκλειδώσουν τα μυστικά που κρύβουν στο εσωτερικό τους οι αστέρες νετρονίων. Τα βαρυτικά κύματα σε συνδυασμό με ηλεκτρομαγνητικές παρατηρήσεις χρησιμοποιούνται για την επίτευξη του στόχου αυτού. Συνεπώς, είναι σημαντική η κατανόηση του ίδιου του φαινομένου της σύγκλισης δύο αστέρων νετρονίων και τις επιδράσεις των διαφόρων χαρακτηριστικών τους στο σήμα των βαρυτικών κυμάτων . Η παρούσα εργασία έχει ως πρώτο στόχο την κατανόηση της διαφοροποίησης που θα προκαλέσει στη φάση του βαρυτικού κύματος η ύπαρξη τετραπολικής ροπής των αστέρων η οποία θα διεγερθεί από την επίδραση του παλιρροϊκού πεδίου του συνοδού τους. Η υπάρχουσα θεώρηση είναι ότι οι αστέρες νετρονίων εκτελούν κυκλικές κινήσεις κατά την σύγκλιση τους, για αυτό ο δεύτερος και κυριότερος στόχος είναι η διερεύνηση του αν είναι εφικτή η εμφάνιση ελλειπτικών τροχιών κατά την σύγκλιση, ή ακόμα αν υπάρχει κάποιου είδους «ταλάντωση» της ίδιας της κίνησης από κυκλική σε ελλειπτική με ανταλλαγή ενέργειας μεταξύ ιδιοταλάντωσης των αστέρων και της κίνησης τους γύρω από το κέντρο μάζας τους.

Λέξεις Κλειδιά: Διπλό Σύστημα, Αστέρες Νετρονίων, Τροχιές, Αστάθειες, Παλιρροϊκά Φαινόμενα

Contents

1 Introduction

A binary system, is a dynamical system consisting of two bodies orbiting each other. When these bodies are compact celestial objects like Black Holes (BH), Neutron Stars (NS) or White Dwarfs (WD). they are simply called compact binaries. In these binaries, the main acting force is gravity pulling the objects towards each other and locking them in an orbital motion. One of the main features of these binaries, that separate them from other celestial binaries like star binaries is the emission of strong gravitational waves, namely perturbations of spacetime propagating outwards in every direction . Gravitational waves carry a portion of the binary's energy causing a gradual decrease of it's total energy and as a result, a decrease in the distance between the objects that comprise it. This decrease in the distance between them is linked with the increase of the frequency at which the binary rotates, and thus the frequency of the signal emitted. As the two companion bodies rotate faster , more energy is emitted as gravitational waves causing them to close in on each other even more rapidly. The system keeps going faster and faster until the two objects finally merge.

This is the general evolution of a compact binary. However, the exact evolution and the final merger product differs for binaries of different composition. For example, a Binary Black Hole (BBH), which consists of two Black Holes, and a Binary Neutron Star (BNS), which consists of two neutron stars, show significant differences in both evolution and signal. The same goes for a binary consisting of two White Dwarfs and all the other possible combinations (BH-NS,BH-WD,NS-WD). This work is focused on Binary Neutron Stars (BNSs) and in the tidal effects that mark their evolution and are embedded in the emitted gravitational wave signal. Work on this already exists and a first correction to the phase of the gravitational wave due to these tidal effects has been calculated analytically[13]. This calculation however is based on the hypothesis that BNSs rotate in quasi-circular orbits (i.e. circular orbits that decrease in radius much slower than the two companion stars rotate around their common center), a hypothesis that is backed up by several papers[5][16][24]. We plan to put this hypothesis to yet another test, to see if the tidally excited oscillations of the two companion stars can give rise to instabilities and perhaps disrupt that quasi-circular motion.

2 Requirements

In this segment we will introduce all the different tools, relations and information necessary for the upcoming calculations.

2.1 Gravitational Quadrupole Moment

In order to understand how and under which circumstances does a body or a system emit gravitational waves, we first need to understand Gravitational Quadrupole Moment (Q_{ij}). This physical quantity is usually a 3x3 tensor that describes the deformation of a distribution of mass. This tensor is all zeros when an object is spherically symmetric[23], such an object is what we call an undeformed object. If such an object becomes stretched along an axis by an outside force, then it is no longer spherically symmetric and it's quadrupole moment is no longer zero, thus, it is now deformed. Rigid bodies are not the only mass distributions that have a quadrupole moment , a system consisting of two point masses orbiting a common center (i.e. a binary) can also be considered as such. A binary system is far from spherically symmetric and as a result it's quadrupole moment is not zero as well. To calculate the quadrupole moment of a distribution of n masses we use the expression

$$Q_{ij} = \sum_n m_n \left(x_{n,i} x_{n,j} - |r_n|^2 \delta_{ij}/3 \right) \tag{1}$$

where m_n is the point mass, $x_{n,i}$ are the components of the position vector of that point mass, r_n is the distance of the mass from the center of the system and δ_{ij} is the Kronecker delta. If that distribution of masses is a continuous system with density ρ, we swap the sum with a volume integral[13]:

$$Q_{ij} = \int \rho \left(x_i x_j - |r|^2 \delta_{ij}/3 \right) d^3x \tag{2}$$

Lastly, for a two-body system consisting of two masses m_1, m_2 rotating around their center of mass, with the origin system in that center of mass, the quadrupole moment can be simplified greatly.

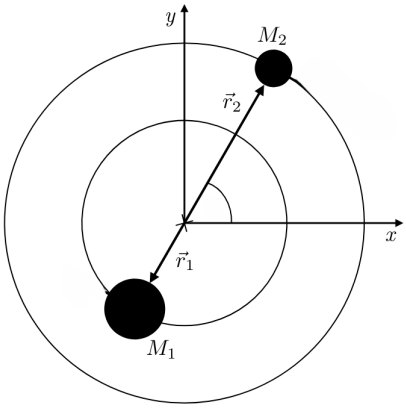

Figure 1: A binary's rotation around the center of mass.

For an origin system at the center of mass $m_1\mathbf{r_1} + m_2\mathbf{r_2} = 0$ and $\mathbf{r} = \mathbf{r_1} - \mathbf{r_2}$. Because $\mathbf{r_1}, \mathbf{r_2}$ are collinear we can write $r = r_1 + r_2$ and $m_1 r_1 = m_2 r_2$. Using that last relation:

$$\begin{aligned} m_2 r_1 + m_1 r_1 &= m_2 r_1 + m_2 r_2 \Rightarrow \\ M r_1 &= m_2 r \Rightarrow \\ r_1 &= \frac{m_2 r}{M} \text{ and similarly,} \\ r_2 &= \frac{m_1 r}{M} \end{aligned}$$

The quadrupole of two point masses m_1, m_2 with position vectors $\mathbf{r_1}, \mathbf{r_2}$ is given by:

$$Q_{ij} = m_1 \left(x_{1,i} x_{1,j} - |r_1|^2 \delta_{ij}/3 \right) + m_2 \left(x_{2,i} x_{2,j} - |r_2|^2 \delta_{ij}/3 \right)$$

Using the above relations:

$$Q_{ij} = \frac{m_1 m_2}{M} \frac{m_2}{M} \left(x_i x_j - r^2 \delta_{ij}/3 \right) + \frac{m_1 m_2}{M} \frac{m_1}{M} \left(x_i x_j - r^2 \delta_{ij}/3 \right)$$

And finally,

$$Q_{ij} = \mu \left(x_i x_j - r^2 \delta_{ij}/3 \right) \tag{3}$$

where $\mu = \frac{m_1 m_2}{m_1 + m_2}$, x_i is the relative position vector of the two bodies and r is the distance between them.

We will calculate the exact quadrupole for a simplified binary system consisting of two point masses orbiting a common center in circular orbits with a Keplerian angular velocity $\omega_k = \sqrt{\frac{M}{r^3}}$. For such a system, the point vectors components are simply $x_1 = rcos(\omega_k t)$, $x_2 = rsin(\omega_k t)$ and assuming the binary rotates in a plane $x_3 = z = 0$. The components of the quadrupole are:

$$\begin{aligned} Q_{11} = \mu xx - \mu r^2 \delta_{xx}/3 \Rightarrow Q_{11} &= \mu r^2 cos^2(\omega_k t) - \mu r^2/3 \\ Q_{12} &= \mu r^2 \cos(\omega_k t) \sin(\omega_k t) \\ Q_{21} &= \mu r^2 \cos(\omega_k t) \sin(\omega_k t) \\ Q_{22} &= \mu r^2 \sin^2(\omega_k t) - \mu r^2/3 \\ Q_{33} &= -\mu r^2/3 \\ Q_{13} = Q_{23} = Q_{31} = Q_{32} &= 0 \end{aligned}$$

Written as a matrix:

$$Q_{ij} = \mu r^2 \begin{pmatrix} \cos^2(\omega_k t) - 1/3 & \cos(\omega_k t) \sin(\omega_k t) & 0 \\ \cos(\omega_k t) \sin(\omega_k t) & \sin^2(\omega_k t) - 1/3 & 0 \\ 0 & 0 & -1/3 \end{pmatrix}$$

Which can also be written as:

$$Q_{ij} = \mu r^2 \begin{pmatrix} \cos(2\omega_k t)/2 + 1/6 & sin(2\omega_k t)/2 & 0 \\ \sin(2\omega_k t)/2 & -\cos(2\omega_k t)/2 + 1/6 & 0 \\ 0 & 0 & -2/6 \end{pmatrix} \tag{4}$$

2.2 Gravitational Waves

In order for gravitational waves to be emitted, a system must have a time-varying quadrupole. In other words, having a non zero quadrupole moment is not sufficient for waves to emerge, non zero time derivatives of that quadrupole moment are also required. Specifically, the power radiated as gravitational waves depends on the 3rd time derivative of the system's quadrupole and is given by the formula[13]:

$$\dot{E} = -\frac{1}{5} \langle \dddot{Q}_{ij} \dddot{Q}_{ij} \rangle \tag{5}$$

This relation is known as the Quadrupole Formula and was first obtained by Einstein in 1918[12]. This version is written in geometrized units (see 2.4). Because gravitational waves are a direct product of quadrupoles, for a simple time varying binary quadrupole like the one in 4, we have shown in a simple way, that the gravitational wave has double the frequency of the rotational motion ($f_{GW} = 2f$). We can also see that the faster the objects rotate around their common center, the stronger the gravitational radiation emitted. Of course, more massive objects also emit more powerful waves. As a result, the strongest gravitational waves are emitted by binaries comprised of massive objects that can at the same time get close enough to each other, so that their orbital frequency can be relatively large. Compact binaries meet these criteria. Despite them being one of the strongest gravitational wave emitters, gravity itself is a relatively weak force, at the same time, similarly to electromagnetic radiation, the signal's amplitude drops as an inverse-square law, making it difficult to detect and almost indistinguishable from the noise.

2.3 Detecting Gravitational Waves

Due to a relatively small Signal to Noise ratio (S/N) detecting gravitational waves had been an ongoing challenge for more than 50 years. The first gravitational wave detectors (Weber bars) were developed and built back in the 1960s by Joseph Weber[26], but no gravitational signal was ever detected. Modern gravitational wave detectors, were first built and began operation early in the

2000s. The LIGO laser interferometers (Livingston & Hanford) were the first to be constructed in 2002, and Virgo, a laser interferometer located in Santo Stefano a Macerata, near the city of Pisa joined the effort one year later in 2003. Many years went by with no detection, and the interferometers were shut down for major upgrades. The advanced LIGO interferometers began operation in 2015 and the first ever gravitational wave signal from a BBH was recorded in September of the same year by both LIGO detectors [9].

The advanced Virgo was also completed and began observations in 2017[9] and 3 years later in 2020, the Japanese interferometer KAGRA joined the observation runs[9]. Most of the detected signals originated from BBHs, only two of the total signals detected to date are thought to have been emitted by a BNS. These two are GW170817 and GW190425 with the first of the two being accompanied by an electromagnetic signal detected by Fermi-GBM around the same sky region (GRB170817)[2]. Despite their size, advanced optics, strong lasers and noise reduction techniques a gravitational wave signal is still very difficult to differentiate from the noise. To give you a perspective on the noise that can affect the inteferometers, the teams running the interferometers have to account for seismic noise from passing vehicles and noise from the microscopic movement of atoms in the mirrors (thermal noise) among many other noise sources (Seismic, Quantum, Laser etc.)[1]. Due to all these noise sources, and due to the relatively small amplitude of the gravitational wave signal itself, the latter is buried in the background noise. A signal example can be seen in Figure 2.

A waveform like the one in that figure is not visible when looking at the signal, thus to find the hidden gravitational wave, we use a technique called Match Filtering, i.e. we apply model waveforms to the signal until they match with the actual gravitational waveform[4]. These model waveform templates are made using existing knowledge of compact binary mergers and rely on our theoretical understanding and on analytical and numerical calculations around the phenomenon. As a result, better understanding of the "mechanics" of compact binaries and the parameters affecting the generated gravitational wave is very important to this whole process.

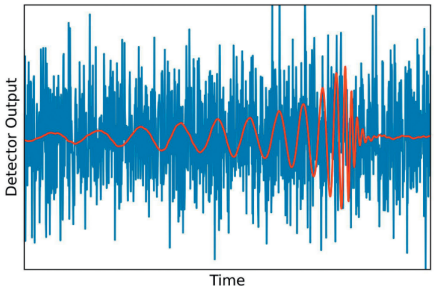

Figure 2: An example of the gravitational wave signal (Red), buried in the background noise (Blue) of the detector.This simulated signal corresponds to the merger of a binary system of two black holes of 40 solar masses[29]

2.4 Geometrized Unit System

All the calculations in this work are done in geometrized units. The geometrized unit system is the system emerging from setting $G = c = 1$ where G is the gravitational constant and c is the speed of light[20]. By setting these equal to unity, the length, mass and time units become equivalent with each other. In other words, we can express every length in time units, or every time in length units and every other combination. The conversions are derived from the relations $G = 1$ and $c = 1$ and they are summed up in the following table:

2.5 Tidal deformability

When a rigid body is placed on another object's gravitational field, different parts of it will experience different forces depending on their relative distance from the other object. This is what we call a tidal interaction, a difference in other words in force from one part of the rigid body to the other. That difference in force, can cause a rigid body to start stretching and twisting, changing

Units	Time	Length	Mass
s	1	$1/3 \cdot 10^{-5}$	$1/2 \cdot 10^{-5}$
km	$3 \cdot 10^5$	1	1.5
$M_\odot$	$2 \cdot 10^5$	2/3	1

Table 1: All the different unit conversions between length, mass and time units in the geometrized unit system.

it's original shape. In other words, it can deform it. The inner composition of the body determines how easily it gets deformed when placed in a given gravitational field. The physical quantity that describes how easy or hard it is to deform an object, is called tidal deformability (λ) and it is defined as[10]:

$$\lambda \equiv -\frac{Q_{ij}}{\mathcal{E}_{ij}} \tag{6}$$

Where Q_{ij} is the body's quadrupole and $\mathcal{E}_{ij}$ is the gravitational tidal field. For a spherical rigid body, we can use dimensional analysis to derive a more commonly used expression for the tidal deformability[10]:

$$\lambda = \frac{2}{3} k_2 R^5 \tag{7}$$

where R is the body's radius and k_2 is the tidal love number, which also depends on the body's internal structure. This tidal love number can be calculated independently from λ. For this calculation, we will use the fitting formula derived by Hinderer[15]:

$$k_2 \approx \frac{3}{2}\left(-0.41 + \frac{0.56}{n^{0.33}}\right)\left(\frac{M}{R}\right)^{-0.003} \tag{8}$$

This formula has an accuracy of 6% for polytropic indices $0.5 \leq n \leq 1.0$ and Mass to Radius ratios $0.1 \leq M/R \leq 0.24$. Because some of the neutron star models (see 2.6) we are going to use have $n = 1.5$, this relation can not be expected to have the same accuracy predicted by Hinderer, for these models we will take into account errors much larger than 6% and set it to about 15% to see how our results vary with such differences in love number values. Due to an erratum in [15] we are not certain whether the fitting formula is still valid, so we will also try smaller love numbers from the corrected table values (See Appendix A)

Having the tidal love number k_2 we can go back to 7 and extract the tidal deformability λ. Of course this tidal deformability is different for different radii,masses and polytropic indices, on other words, for different neutron star equations of state models.

2.6 Neutron Star Equation Of State Models

The ultimate goal of understanding binary neutron star mergers is to gain valuable insights on their internal composition and how matter behaves in the extreme conditions of their interiors. In other words, we wish to find the equation of state that describes matter in these conditions. Plethora of models have been created, predicting different masses,radii and other parameters[10]. Because these parameters affect the tidal deformability, they also affect the quadrupole moment induced by the tidal field 6, which in turn affects the gravitational wave signal as discussed in 2.2. As a result, we can take the reverse route, by using gravitational wave signals to put constraints on these parameters, and limit the realistic equation of state models.
In this work we are going to use polytropic equations of state:

$$P = K\rho^{1+1/n}$$

where P is the pressure, ρ is the density , K is a constant and n is the polytropic index. Specifically we are going to use the following 5 models[25]:

All of these models have mass to radius ratios (M/R) within the acceptable limits set in equation 8's accuracy. However, the polytropic indices of $n = 1.5$ are outside the 6% accuracy limit, so we are going to assume that the accuracy is much lower, namely 15% which is more than the expected continuation of the accuracy percentage from $n = 0.5$ ($\approx 1-4\%$ accuracy) and $n = 0.7$ ($\approx 1-2\%$ accuracy) to $n = 1.0$ ($\approx 1-8\%$ accuracy) and $n = 1.2$ ($\approx 2-9\%$ accuracy). These accuracy percentages are derived by comparing the exact k_2 extracted analytically with the ones calculated using the fitting formula[15] (See Appendix A for details).

Model number	n	ρ_c (g/cm^3)	α_0	M ($M_\odot$)	R (km)	M/R
A	1.5	1.00×10^{15}	13.552	0.945	14.07	0.099
B	1	6.584×10^{14}	9.669	1.4	15.00	0.138
C	1.5	1.260×10^{15}	8.205	1.4	15.00	0.138
D	1	2.455×10^{15}	4.490	1.4	9.80	0.211
E	1.5	8.156×10^{15}	2.146	1.4	9.00	0.230

Figure 3: Parameter's of Neutron Star (polytropic index n,central density ρ_c, central energy density to central pressure ratio α_0, mass M , Radius R and their ratio) for different Equations of State[25].

2.7 Additional tools and theoretical background

We will now introduce some very important tools and specific theoretical background for our calculations.

2.7.1 Virial Theorem

One of these tools is the well known Virial theorem. This relation is useful for a wide variety of systems, with the important prerequisite that the point masses/objects that comprise these systems have finite point vectors and velocities[14].
For a system consisting of i point masses with point vectors $\mathbf{r_i}$ and moments $\mathbf{p_i}$, deriving the theorem starts with the scalar:

$$G = \sum_i \mathbf{p_i}\ \mathbf{r_i}$$

By taking this scalar's time derivative:

$$\frac{dG}{dt} = \sum_i \mathbf{p_i}\ \dot{\mathbf{r}}_\mathbf{i} + \sum_i \dot{\mathbf{p}}_\mathbf{i}\ \mathbf{r_i}$$

The first and second term of the right hand side of this relation can be written as:

$$\sum_i \mathbf{p_i}\ \dot{\mathbf{r}}_\mathbf{i} = \sum_i m_i \mathbf{u_i}^2 = 2T$$

$$\sum_i \dot{\mathbf{p}}_\mathbf{i}\ \mathbf{r_i} = \sum_i \mathbf{F_i}\ \mathbf{r_i}$$

where T is the kinetic energy of the system and $\mathbf{F_i}$ is the force felt by the particle i. The time derivative now becomes:

$$\frac{dG}{dt} = 2T + \sum_i \mathbf{F_i}\ \mathbf{r_i}$$

We will now take the time average of this relation over a time interval τ [14]:

$$\frac{1}{\tau}\int_0^\tau \frac{dG}{dt}d\tau \equiv \overline{\frac{dG}{dt}} = 2\overline{T} + \overline{\sum_i \mathbf{F_i}\ \mathbf{r_i}}$$

Here is where the assumption of finite point vectors and velocities comes in. Assuming this is the case, the scalar G is bound by an upper limit G_{max} and a lower limit G_{min}. By taking a large enough time interval τ we can assume $\overline{\frac{dG}{dt}}$ is as close to zero as we need it to be. Thus, we get:

$$2\overline{T} + \overline{\sum_i \mathbf{F_i}\ \mathbf{r_i}} = 0$$

If we assume a single point mass in a central force's field and swap the force with it's potential, we get:

$$2\overline{T} - \overline{\frac{\partial V}{\partial r}r} = 0$$

Finally, for a potential of the form $V = \alpha r^n$, we get the final expression of the Virial theorem:

$$\overline{T} = \frac{n}{2}\overline{V} \tag{9}$$

2.7.2 Harmonic Oscillators

Another important part of the needed theoretical background to understand the phenomenon is harmonic oscillators. A harmonic oscillator is a system consisting of a body moving around an equilibrium position under the influence of an external restoring force with a potential of the form $V = \frac{1}{2}kx^2$[18], where k is a constant and x is the displacement of the body relative to the equilibrium position.

If the only acting force is this restoring force, the harmonic oscillator is called simple and it's equation of motion is given by:

$$m\ddot{x} + kx = 0$$

Where m is the body's mass. Because this is a linear differential equation we expect solutions in the form of exponentials[18] $x = e^{pt}$. By putting this back to the differential equation we can calculate p:

$$p = \pm i\sqrt{\frac{k}{m}} \equiv \pm i\omega_0$$

Thus, the solution takes the form:

$$x = Ae^{i\omega_0 t} + Be^{-i\omega_0 t}$$

where A and B are complex numbers, that must be complex conjugates so that x is real[18]. By also using Euler's formula: $e^{i\omega_0 t} = \cos(\omega_0 t) + i\sin(\omega_0 t)$ we get the final solution:

$$x = C\cos(\omega_0 t) + D\sin(\omega_0 t)$$

where C and D are constants, dependent on the initial conditions.

We are particularly interested in the driven simple harmonic oscillator, where apart from the restoring force there is also an exterior force acting on the body. Assuming this exterior force is of a cosinusoidal form, for example $F = F_1\cos(\omega_1 t)$, where F_1, ω_1 constants, we get a new differential equation:

$$m\ddot{x} + kx = F_1\cos(\omega_1 t)$$

Similarly to the simple harmonic oscillator, we will solve this by moving to complex space and assume exponential solutions $z = Ae^{pt}$[18]:

$$m\ddot{z} + kz = F_1 e^{(i\omega_1 t)}$$

Where the real part of z will be the the solution of the initial differential equation. The solution, will be the sum of the complementary solution (i.e. the solution of the same equation with the right hand side set to 0, in this case the simple harmonic oscillation solution) and the particular solution which satisfies the above equation.

We have already derived the complementary solution thus we move to the particular by substituting $z = Ae^{pt}$:

$$mp^2Ae^{pt} + kAe^{pt} = F_1 e^{i\omega_1 t}$$

It is clear that $p = i\omega_1$,thus we get:

$$\begin{aligned} -m\omega_1^2 A + kA = F_1 \Rightarrow \\ A(k/m - \omega_1^2) = F_1/m \Rightarrow \\ A = \frac{F_1}{m(\omega_0^2 - \omega_1^2)} \end{aligned}$$

As a result,

$$z = \frac{F_1}{m(\omega_0^2 - \omega_1^2)} e^{i\omega_1 t}$$

The particular solution of the initial differential equation is the real part of z:

$$x = \frac{F_1}{m(\omega_0^2 - \omega_1^2)} \cos\omega_1 t$$

Finally by summing this with the complementary solution we get the full solution:

$$x = \frac{F_1}{m(\omega_0^2 - \omega_1^2)} \cos\omega_1 t + C\cos(\omega_0 t) + D\sin(\omega_0 t) \tag{10}$$

where once again C and D are dependent on the initial conditions.

2.7.3 Solving systems of linear homogeneous differential equations with constant coefficients

A system of first order, linear and homogeneous differential equations is of the general form:

$$\begin{array}{ccccccccccccccc}
a'_{11}\dot{x}_1 & + & a'_{12}\dot{x}_2 & +\cdots+ & a'_{1n}\dot{x}_n & + & a_{11}x_1 & + & a_{12}x_2 & +\cdots+ & a_{1n}x_n & = & 0 \\
a'_{21}\dot{x}_1 & + & a'_{22}\dot{x}_2 & +\cdots+ & a'_{2n}\dot{x}_n & + & a_{21}x_1 & + & a_{22}x_2 & +\cdots+ & a_{2n}x_n & = & 0 \\
 & & & & & & & & & & & \vdots & \\
a'_{m1}\dot{x}_1 & + & a'_{m2}\dot{x}_2 & +\cdots+ & a'_{mn}\dot{x}_n & + & a_{m1}x_1 & + & a_{m2}x_2 & +\cdots+ & a_{mn}x_n & = & 0.
\end{array}$$

A homogeneous system is equivalent to a matrix equation of the form:

$$\mathbf{A'x'} + \mathbf{Ax} = \mathbf{0}$$

where $\mathbf{A'}$ and $\mathbf{A}$ are two $m \times n$ matrices, $\mathbf{x}$ is a column vector with n entries, $\mathbf{x'}$ is it's first time derivative, and $\mathbf{0}$ is the zero vector with m entries.

We can extend to second order linear equations by simply adding another matrix $\mathbf{A''}$ and the second derivative of $\mathbf{x}$, $\mathbf{x''}$:

$$\mathbf{A''x''} + \mathbf{A'x'} + \mathbf{Ax} = \mathbf{0}$$

We can repeat for 3rd or greater order.Because of it's linearity, we can expect solutions of the form[8]:

$$\mathbf{x} = \mathbf{C}e^{i\lambda t}$$

where λ is a constant and $\mathbf{C}$ is a column vector with no time dependence and n entries just like $\mathbf{x}$. By substituting this back to the differential equation:

$$\begin{aligned}
-\mathbf{A''C}\lambda^2 + \mathbf{A'C}i\lambda + \mathbf{AC} = \mathbf{0} \Rightarrow \\
(-\mathbf{A''}\lambda^2 + \mathbf{A'}i\lambda + \mathbf{A})\mathbf{C} = \mathbf{0} \Rightarrow \\
\mathbf{\Pi C} = \mathbf{0}
\end{aligned}$$

where $\mathbf{\Pi} = (-\mathbf{A''}\lambda^2 + \mathbf{A'}i\lambda + \mathbf{A})$ is a $m \times n$ matrix just like $\mathbf{A}, \mathbf{A'}, \mathbf{A''}$. However, if we assume we have as many equations as the variables in them, then $m = n$ and all these matrices are square matrices. . In order for the system to have solutions other than the column vector of n zeros ($\mathbf{C} = \mathbf{0}$), the determinant $Det(\Pi)$ must be equal to zero[8]. If we rearrange the matrix so that λ^2 terms exist in the diagonal of $\mathbf{\Pi}$, we can then see that this λ^2 is an eigenvalue of $\mathbf{\Pi}$ and $\mathbf{C} = c\mathbf{u}$, where $\mathbf{u}$ is the eigenvector for said eigenvalue and c is a constant obtainable with initial conditions.

Consequently, for a system of linear homogeneous differential equations with constant coefficients, the solution is of the form[8]:

$$\mathbf{x} = c\mathbf{u}e^{i\lambda t} \tag{11}$$

where λ and $\mathbf{u}$ are the eigenvalues and eigenvectors of the matrix $\mathbf{\Pi} = (-\mathbf{A''}\lambda^2 + \mathbf{A'}i\lambda + \mathbf{A})$. An important detail here is that if this λ^2 becomes negative, λ becomes imaginary and that's what we call an instability.

2.7.4 Adding perturbations/corrections and linearization of equations

Usually, when we want to check for instabilities in a system, we add small perturbations in it's variables, we linearize the equations and solve them[28]. The same principle is applied when we want to add corrections in a solution due to a relatively small term in the equations.

To demonstrate this process, we will consider a simple harmonic oscillator, the solution of which we already derived back in 2.7.2:

$$\ddot{x} + \frac{k}{m}x = 0$$

With a solution:

$$x = A\cos(\omega_0 t) + B\sin(\omega_0 t)$$

We will add a non-linear term ax^2 with a relatively small coefficient a:

$$\ddot{x} + \frac{k}{m}x = -ax^2$$

To solve this equation we will consider the series $x = x_1 + x_2$ where $x_2 \ll x_1$ and $\omega = \omega_0 + \omega_1$ where we can even set $\omega_1 = 0$ with a change in the origin system of time[19].

Solving for the first order, $x = x_1$

$$x_1 = Acos(\omega_0 t)$$

By substituting $x = x_1 + x_2$ and keeping up to second order terms:

$$\begin{aligned}
\ddot{x_2} + \frac{k}{m}x_2 &= -ax_1^2 \\
\ddot{x_2} + \frac{k}{m}x_2 &= -aA^2\cos^2(\omega_0 t) \\
\ddot{x_2} + \frac{k}{m}x_2 &= -\frac{1}{2}aA^2 - \frac{1}{2}aA^2\cos(2\omega_0 t)
\end{aligned}$$

This is now a linear inhomogeneous equation which can be solved for x_2 [19]:

$$x_2 = -\frac{aA^2}{2\omega_0^2} + \frac{aA^2}{6\omega_0^2}\cos 2\omega_0 t$$

With both x_1, x_2 we have the full solution of the original equation $x = x_1 + x_2$.

2.7.5 Hamilton's Principle

Another very important tool we are going to use is the derivation of the equations of motion using Hamilton's principle. Let's consider a particle driven by a force F described by a potential V, so that:

$$\vec{F} = -\vec{\nabla}V$$

We want to derive the particle's equations of motion. The first way to do that, is to go straight to Newton's Laws. However, there is another way through Hamilton's principle. According to Hamilton's principle, a particle that begins it's motion from a point A at t_A and reaches another point B at t_B follows the route for which the action, i.e. the quantity

$$\mathcal{S} = \int_{t_A}^{t_B} \mathcal{L}dt$$

becomes stationary [17].
The quantity $\mathcal{L}$ is called Lagrangian and it is defined as the difference between the kinetic energy (T) and the potential energy (V) of the particle $\mathcal{L} = T - V$. To extract the equations of motion we use the Euler-Lagrange equations:

$$\frac{\partial \mathcal{L}}{\partial x_i} - \frac{d}{dt}\left(\frac{\partial \mathcal{L}}{\partial \dot{x}_i}\right) = 0 \tag{12}$$

We are going to use these equations for the Lagrangian of a simple harmonic oscillator:

$$\mathcal{L} = \frac{1}{2}m\dot{x}^2 - \frac{1}{2}kx^2$$

With the Lagrangian, we calculate the terms of 12:

$$\begin{aligned}
\frac{\partial \mathcal{L}}{\partial x_i} &= \frac{\partial \mathcal{L}}{\partial x} = -kx \\
\frac{d}{dt}\left(\frac{\partial \mathcal{L}}{\partial \dot{x}_i}\right) &= \frac{d}{dt}\left(\frac{\partial \mathcal{L}}{\partial \dot{x}}\right) = \frac{d}{dt}(m\dot{x}) = m\ddot{x}
\end{aligned}$$

and derive the same equation of motion we solved in 2.7.2:

$$m\ddot{x} + kx = 0$$

There is also another way to reach the same equation and that's by differentiating the action directly:

$$\mathcal{S} = \int_{t_A}^{t_B} \mathcal{L} dt = \int_{t_A}^{t_B} \left(\frac{1}{2} m\dot{x}^2 - \frac{1}{2} kx^2 \right) dt \Rightarrow$$
$$\delta\mathcal{S} = \int_{t_A}^{t_B} \left(\frac{1}{2} 2m\dot{x}\delta\dot{x} - \frac{1}{2} 2kx\delta x \right) dt \Rightarrow$$
$$\delta\mathcal{S} = \int_{t_A}^{t_B} \left[m(\dot{x}\delta x)' - m\ddot{x}\delta x - kx\delta x \right] dt \Rightarrow$$
$$\delta\mathcal{S} = \int_{t_A}^{t_B} \left[m(\dot{x}\delta x)' \right] dt - \int_{t_A}^{t_B} \left(m\ddot{x}\delta x + kx\delta x \right) dt \Rightarrow$$

The first integral equals to zero as an exact differential. The second integral remains:

$$\frac{\delta\mathcal{S}}{\delta x} = -\int_{t_A}^{t_B} \left(m\ddot{x}\frac{\delta x}{\delta x} + kx\frac{\delta x}{\delta x} \right) dt$$

For $\frac{\delta\mathcal{S}}{\delta x} = 0$ the action becomes stationary, which leads to:

$$m\ddot{x}\frac{\delta x}{\delta x} + kx\frac{\delta x}{\delta x} = 0 \Rightarrow$$

and finally, we reach the same conclusion:

$$m\ddot{x} + kx = 0$$

2.8 Neutron Star Binaries

Having all the tools we will need, we now focus on the main subject of this work, which is Binary Neutron Stars (BNSs). A BNS's evolution is split in three main periods[27], with the first one being the inspiral phase, during which the motion is dominated by Newtonian gravity while the tidal interactions are considered as corrections, during this phase the binary evolution is adiabatic (the orbital timescale is much smaller than the damping scale). The two gravitational wave signals detected from BNSs (GW170817 & GW190425), originated from a system in the inspiral phase, i.e. with frequencies up to $f = 500Hz$[2]. In the second intermediate phase, the system still evolves in an adiabatic manner, but as the companion stars get closer to each other, the tidal interactions become important and can no longer be considered as corrections. The final coalescing phase, is the merger phase of the binary, with a rapid evolution which along with the intermediate phase can not be solved analytically and must be treated numerically[27].

In greater separations, a BNS can be considered a binary of two point masses for which's motion the resulting quadrupole was already computed in 2.1 and is given by 4. The same can be said for a BBH, however even though the event horizon of a black hole can be deformed slightly [22] [21], black holes are thought to have love numbers equal to zero[7][11], while Neutron Stars have Love numbers typically in the range of $k_2 = 0.2 - 0.3$ [10]. This means, that even though BBHs and BNSs can both be treated as point mass binaries for big enough separations, that begins to change as tidal effects come into play. During the evolution of a BNS, the tidal interactions give rise to oscillations of the stars themselves, for which we consider n different oscillating shells for fundamental f-modes with $l = 2$ .These oscillations change the shape of the rigid body and thus create an additional quadrupole that adds upon the signal. This means, that the total quadrupole of the system is the combination of both rotational quadrupole Q_{ij}^{rot} which is the one we calculated in 4 and the sum of the n oscillating shells quadrupoles $Q_{ij} = \sum_n Q_{ij}^n$, or[13]:

$$Q_{ij}^T = Q_{ij} + Q_{ij}^{rot}$$

We will focus on the inspiral phase which has been already described analytically. The action for the inspiral phase of a neutron star binary that describes the motion of the two bodies (m_1,m_2), plus the induced oscillation of one of them (assumed m_1) by the gravitational field of the other (m_2) is given by[13]:

$$S = \int dt \left[\frac{1}{2}\mu \dot{r}^2 + \frac{1}{2}\mu r^2 \dot{\Phi}^2 + \frac{M\mu}{r} \right] - \frac{1}{2} \int dt Q_{ij} \mathcal{E}_{ij} + \sum_n \int dt \frac{1}{4\lambda_{1,n}\omega_n^2} \left[\dot{Q}_{ij}^n \dot{Q}_{ij}^n - \omega_n^2 Q_{ij}^n Q_{ij}^n \right] \quad (13)$$

where $\mu = \frac{m_1 m_2}{m_1 + m_2}$ is the reduced mass, r is the separation, Φ is the phase of the motion, Q_{ij} is the quadrupole of the neutron star, $\lambda_{1,n}$ is the tidal deformability of the nth neutron star's oscillating shell, ω_n is the frequency at which that shell oscillates and Q_{ij}^n is it's quadrupole. Using this action, just like we did in 2.7.5 we can extract the equations of motion for both the separation r and for the quadrupoles Q_{ij}^n.

3 Extracting the effective tidal deformability

In this section we will present the calculations that lead to the effective tidal deformability and the change in the phase of the gravitational wave signal derived by Flanagan & Hinderer[13][1].

3.1 From the Equation of Motion to the NS Quadrupoles

The equations of motion derived from the action 13, with the addition of the leading order gravitational wave dissipation terms [13] (last term for each equation), are:

$$\ddot{x}^i + \frac{M}{r^2}n^i = \frac{m_2}{2\mu}Q_{jk}\partial_i\partial_j\partial_k\frac{1}{r} - \frac{2}{5}x_j\frac{d^5Q_{ij}^T}{dt^5} \tag{14}$$

$$\ddot{Q_{ij}^n} + \omega_n^2 Q_{ij}^n = m_2\lambda_{1,n}\omega_n^2\partial_i\partial_j\frac{1}{r} - \frac{2}{5}\lambda_{1,n}\omega_n^2\frac{d^5Q_{ij}^T}{d^5t} \tag{15}$$

Where $Q_{ij}^T = Q_{ij} + \mu x_i x_j - \mu r^2\delta_{ij}/3$ with $Q_{ij} = \sum Q_{ij}^n$ and $n^i = x^i/r$. We are going to solve equation 15 ignoring the GW dissipation terms, to derive the quadrupole of the NS.

The quadrupole of the rotation of the binary system, ignoring the wobble of the NS, is calculated by $Q_{ij}^{rot} = \mu x_i x_j - \mu r^2\delta_{ij}/3$. Assuming circular orbits, $x_1 = x = r\cos\Phi, x_2 = y = r\sin\Phi$, where $\Phi = \omega t + \Phi_0$, and $z = 0$, the resulting quadrupole is given by 4:

$$Q_{ij}^{rot} = \mu r^2\begin{pmatrix}\cos(2\Phi)/2 + 1/6 & sin(2\Phi)/2 & 0\\ \sin(2\Phi)/2 & -\cos(2\Phi)/2 + 1/6 & 0\\ 0 & 0 & -2/6\end{pmatrix}$$

This matrix can be split into two matrices as follows:

$$Q_{ij}^{rot} = \mu r^2\left[\frac{1}{2}\begin{pmatrix}\cos(2\Phi) & sin(2\Phi) & 0\\ \sin(2\Phi) & -\cos(2\Phi) & 0\\ 0 & 0 & 0\end{pmatrix} + \frac{1}{6}\begin{pmatrix}1 & 0 & 0\\ 0 & 1 & 0\\ 0 & 0 & -2\end{pmatrix}\right] = \mu r^2\left[\frac{1}{2}\mathbf{B} + \frac{1}{6}\mathbf{A}\right]$$

If we calculate the term $D_{ij} = \partial_i\partial_j\frac{1}{r}$ we find that it can also be expressed as a linear combination of the same matrices $\mathbf{A}, \mathbf{B}$:

$$\begin{aligned}
D_{xx} &= \partial_x^2\frac{1}{r} = \frac{3}{r^3}\left(\cos^2\Phi - 1/3\right)\\
D_{yy} &= \partial_y^2\frac{1}{r} = \frac{3}{r^3}\left(\sin^2\Phi - 1/3\right)\\
D_{xy} = D_{yx} &= \partial_x\partial_y\frac{1}{r} = \frac{3}{r^3}\cos(\Phi)\sin(\Phi)\\
D_{zx} = D_{xz} &= D_{yz} = D_{zy} = 0\\
D_{zz} &= \frac{3}{r^3}(-1/3)
\end{aligned}$$

And finally:

$$D_{ij} = \frac{3}{r^3}\left[\frac{1}{2}\mathbf{B} + \frac{1}{6}\mathbf{A}\right] \tag{16}$$

Due to all terms except Q_{ij}^n being a linear combination of $\mathbf{A}, \mathbf{B}$ the expected solution of 15 must also be a linear combination of the same matrices (similarly to the forced oscillator in 2.2):

$$Q_{ij}^n = Q'^n\mathbf{A} + Q^n\mathbf{B}$$

As a result the total quadrupole and the quadrupole of the wobble can be written as:

[1] These calculations are our own attempt of extracting those relations as Flanagan & Hinderer's calculations are not presented analytically in their aforementioned paper.

$$Q_{ij}^T = Q'\mathbf{A} + Q\mathbf{B}$$
$$Q_{ij} = (Q' - \frac{1}{6}\mu r^2)\mathbf{A} + (Q - \frac{1}{2}\mu r^2)\mathbf{B}$$

We will now put this back in 15 to calculate Q, Q':

$$(Q - \frac{1}{2}\mu r^2)\frac{\partial^2 \mathbf{B}}{\partial t^2} + \omega_n^2 \left[(Q' - \frac{1}{6}\mu r^2)\mathbf{A} + (Q - \frac{1}{2}\mu r^2)\mathbf{B}\right] = m_2\lambda_{1,n}\omega_n^2 \frac{3}{r^3}\left[\frac{1}{2}\mathbf{B} + \frac{1}{6}\mathbf{A}\right]$$

The parameters of the two matrices must match in each side of the equation, thus the latter splits in two equations, one to calculate Q' and one to calculate Q. For the parameters of matrix **A**:

$$\omega_n^2(Q' - \frac{1}{6}\mu r^2) = m_2\lambda_{1,n}\omega_n^2 \frac{3}{r^3}\frac{1}{6}$$
$$Q' = \frac{1}{6}\mu r^2 + \frac{m_2\lambda_{1,n}}{2r^3}$$

In these calculations we assumed only one oscillating shell, we can simply include all of them by summing them:

$$Q' = \frac{1}{6}\mu r^2 + \sum_n \frac{m_2\lambda_{1,n}}{2r^3} \tag{17}$$

We repeat the process for matrix **B**:

$$(Q - \frac{1}{2}\mu r^2)\frac{\partial^2 \mathbf{B}}{\partial t^2} + \omega_n^2(Q - \frac{1}{2}\mu r^2)\mathbf{B} = m_2\lambda_{1,n}\omega_n^2 \frac{3}{r^3}\frac{1}{2}\mathbf{B}$$
$$(Q - \frac{1}{2}\mu r^2)(-4\omega^2\mathbf{B}) + \omega_n^2(Q - \frac{1}{2}\mu r^2)\mathbf{B} = m_2\lambda_{1,n}\omega_n^2 \frac{3}{r^3}\frac{1}{2}\mathbf{B}$$
$$(1 - 4x_n^2)(Q - \frac{1}{2}\mu r^2) = m_2\lambda_{1,n}\frac{3}{r^3}\frac{1}{2}$$
$$Q = \frac{1}{2}\mu r^2 + m_2\lambda_{1,n}\frac{3}{r^3}\frac{1}{2(1 - 4x_n^2)}$$

Where $x_n = \omega/\omega_n$. Adding the sum we get:

$$Q = \frac{1}{2}\mu r^2 + \sum_n \frac{3m_2\lambda_{1,n}}{2(1 - 4x_n^2)r^3} \tag{18}$$

Thus, the tidally induced quadrupole can be written as:

$$Q_{ij} = \sum_n \left(\frac{m_2\lambda_{1,n}}{2r^3}\mathbf{A} + \frac{3m_2\lambda_{1,n}}{2(1 - 4x_n^2)r^3}\mathbf{B}\right) \tag{19}$$

and the total quadrupole:

$$Q_{ij}^T = \left(\frac{1}{6}\mu r^2 + \sum_n \frac{m_2\lambda_{1,n}}{2r^3}\right)\mathbf{A} + \left(\frac{1}{2}\mu r^2 + \sum_n \frac{3m_2\lambda_{1,n}}{2(1 - 4x_n^2)r^3}\right)\mathbf{B} \tag{20}$$

Having calculated the total quadrupole we are now ready to go back to the action of the system.

3.2 Deriving the equations for radius, energy and its time derivative in relation to the angular velocity

We rewrite the action of the system written in equation 13:

$$S = \int dt \left[\frac{1}{2}\mu\dot{r}^2 + \frac{1}{2}\mu r^2\dot{\Phi}^2 + \frac{M\mu}{r}\right] - \frac{1}{2}\int dt Q_{ij}\mathcal{E}_{ij} + \sum_n \int dt \frac{1}{4\lambda_{1,n}\omega_n^2}\left[\dot{Q}_{ij}^n\dot{Q}_{ij}^n - \omega_n^2 Q_{ij}^n Q_{ij}^n\right]$$

The action is split strategically in three parts, the first integral contains the kinetic energy and gravitational potential of the rotating binary, the last integral contains the kinetic energy (first term) and potential (second term) of the tidally induced oscillation. The integral in the middle contains the tidal term of the gravitational potential which acts as the exchange of energy between the two sub-systems. This will prove really important when we calculate the total energy of the

system. In order to calculate the action, we will need to calculate the following matrix scalar products:

$$\mathbf{A}^2 = \begin{pmatrix} 1 & 0 & 0 \\ 0 & 1 & 0 \\ 0 & 0 & -2 \end{pmatrix} \cdot \begin{pmatrix} 1 & 0 & 0 \\ 0 & 1 & 0 \\ 0 & 0 & -2 \end{pmatrix} = 1 + 1 + 4 = 6$$

$$\mathbf{A} \cdot \mathbf{B} = \begin{pmatrix} 1 & 0 & 0 \\ 0 & 1 & 0 \\ 0 & 0 & -2 \end{pmatrix} \cdot \begin{pmatrix} \cos(2\Phi) & sin(2\Phi) & 0 \\ \sin(2\Phi) & \cos(2\Phi) & 0 \\ 0 & 0 & 0 \end{pmatrix} = 0$$

$$\mathbf{B} \cdot \mathbf{A} = 0$$

$$\mathbf{B}^2 = \begin{pmatrix} \cos(2\Phi) & sin(2\Phi) & 0 \\ \sin(2\Phi) & \cos(2\Phi) & 0 \\ 0 & 0 & 0 \end{pmatrix} \cdot \begin{pmatrix} \cos(2\Phi) & sin(2\Phi) & 0 \\ \sin(2\Phi) & \cos(2\Phi) & 0 \\ 0 & 0 & 0 \end{pmatrix} = 2\cos(2\Phi)^2 + 2\sin(2\Phi)^2 = 2$$

Using these we can easily compute the matrix scalar products:

$$Q_{ij}\mathcal{E}_{ij} = -m_2 \frac{3}{r^3}\left[\sum_n \frac{m_2\lambda_{1,n}}{2r^3} + \sum_n \frac{3m_2\lambda_{1,n}}{2(1-4x_n^2)r^3}\right]$$

$$Q_{ij}^n Q_{ij}^n = 6\left(\frac{m_2\lambda_{1,n}}{2r^3}\right)^2 + 2\left(\frac{3m_2\lambda_{1,n}}{2(1-4x_n^2)r^3}\right)^2$$

$$\dot{Q}_{ij}^n \dot{Q}_{ij}^n = 8\omega^2\left(\frac{3m_2\lambda_{1,n}}{2(1-4x_n^2)r^3}\right)^2$$

As a result the action can be written:

$$S = \int dt\left[\frac{1}{2}\mu\dot{r}^2 + \frac{1}{2}\mu r^2\dot{\Phi}^2 + \frac{M\mu}{r}\right] + \frac{1}{2}\int dt m_2 \frac{3}{r^3}\left[\sum_n \frac{m_2\lambda_{1,n}}{2r^3} + \sum_n \frac{3m_2\lambda_{1,n}}{2(1-4x_n^2)r^3}\right]$$
$$+\sum_n \int dt \frac{1}{4\lambda_{1,n}\omega_n^2}\left\{8\omega^2\left(\frac{3m_2\lambda_{1,n}}{2(1-4x_n^2)r^3}\right)^2 - \omega_n^2\left[6\left(\frac{m_2\lambda_{1,n}}{2r^3}\right)^2 + 2\left(\frac{3m_2\lambda_{1,n}}{2(1-4x_n^2)r^3}\right)^2\right]\right\}$$

3.2.1 Calculating the radius

We will now differentiate the action in terms of r. δS in terms of δr:

$$\delta S = \int dt\left[\mu r\delta\dot{r} + \mu\delta r\dot{r}\omega^2 - \frac{M\mu}{r^2}\delta r\right] - \frac{1}{2}\int dt m_2\left[\sum_n \frac{3m_2\lambda_{1,n}6}{2r^7}\delta r + \sum_n \frac{9m_2\lambda_{1,n}6}{2(1-4x_n^2)r^7}\delta r\right]$$
$$-\sum_n \int dt\frac{1}{2}\left\{4x_n^2\frac{9m_2^2\lambda_{1,n}6}{4(1-4x_n^2)^2r^7}\delta r - 3\frac{m_2^2\lambda_{1,n}6}{4r^7}\delta r - \frac{9m_2^2\lambda_{1,n}6}{4(1-4x_n^2)^2r^7}\delta r\right\}$$

Assuming circular orbits, $\dot{r} = 0$. For a stationary action in terms of r:

$$\frac{\delta S}{\delta r} = 0 \Longrightarrow$$
$$\mu r\omega^2 - \frac{M\mu}{r^2} - \sum_n \frac{3m_2^2\lambda_{1,n}3}{2r^7} - \sum_n \frac{9m_2^2\lambda_{1,n}3}{2(1-4x_n^2)r^7} - \sum_n x_n^2\frac{9m_2^2\lambda_{1,n}3}{(1-4x_n^2)^2r^7} + 3\sum_n \frac{m_2^2\lambda_{1,n}3}{4r^7} + \sum_n \frac{9m_2^2\lambda_{1,n}3}{4(1-4x_n^2)^2r^7} = 0$$

Because we can combine the terms,

$$\sum_n x_n^2\frac{9m_2^2\lambda_{1,n}3}{(1-4x_n^2)^2r^7} - \sum_n \frac{9m_2^2\lambda_{1,n}3}{4(1-4x_n^2)^2r^7} = \sum_n \frac{9m_2^2\lambda_{1,n}3}{4(1-4x_n^2)r^7}$$

we get:

$$\mu r\omega^2 - \frac{M\mu}{r^2} - \sum_n \frac{3m_2^2\lambda_{1,n}3}{2r^7} - \sum_n \frac{9m_2^2\lambda_{1,n}3}{2(1-4x_n^2)r^7} + \sum_n \frac{9m_2^2\lambda_{1,n}3}{4(1-4x_n^2)r^7} + 3\sum_n \frac{m_2^2\lambda_{1,n}3}{4r^7} = 0$$

and finally,

$$\mu r^3\omega^2 - M\mu - \sum_n \frac{9m_2^2\lambda_{1,n}}{4r^5} - \sum_n \frac{27m_2^2\lambda_{1,n}}{4(1-4x_n^2)r^5} = 0 \tag{21}$$

The first two terms are the dominant ones in the inspiral phase, the last two terms become important when the two bodies are close to merging. As a result we can assume that the radius can be written as $r = r_k + \delta r$, a dominant r_k and a fluctuation of that r_k (as we did in 2.7.4). In a first order of magnitude, we ignore the two last terms as small and we get the expression of the Kepler radius $r_k = M^{1/3}\omega^{-2/3}$ which is to be expected. In a second order of magnitude:

$$\begin{aligned}
3\mu r_k^2\omega^2\delta r &= \sum_n \frac{9m_2^2\lambda_{1,n}}{4r_k^5} + \sum_n \frac{27m_2^2\lambda_{1,n}}{4(1-4x_n^2)r_k^5} \\
\mu r_k^2\omega^2\delta r &= \sum_n \frac{3m_2^2\lambda_{1,n}}{4r_k^5} + \sum_n \frac{9m_2^2\lambda_{1,n}}{4(1-4x_n^2)r_k^5} \\
\delta r &= \frac{3}{4}\frac{m_2m_1\omega^{-2}}{\mu r_k^2}\sum_n \frac{m_2m_1^{-1}\lambda_{1,n}}{r_k^5}\left(1 + \frac{3}{(1-4x_n^2)}\right)
\end{aligned}$$

Because $\frac{m_2m_1\omega^2}{\mu} = (M^{1/3}\omega^{-2/3})^3 = r_k^3$, we can write:

$$\delta r = r_k\frac{3}{4}\sum_n \chi_n g_1(x_n) \tag{22}$$

where $g_1(x) = 1 + \frac{3}{(1-4x^2)}$ and $\chi_n = \frac{m_2m_1^{-1}\lambda_{1,n}}{r_k^5}$ Finally, we have the full expression of $r(\omega)$, which matches with the one derived in [13]:

$$r(\omega) = r_k\left[1 + \frac{3}{4}\sum_n \chi_n g_1(x_n)\right] \tag{23}$$

3.2.2 Calculating the Energy

To calculate the energy of the system we will need to think of the system as the combination of two systems, as we did in the action 13, the first system will only have the Newtonian gravitational potential, expressing the rotating motion of the binary, and the second system will contain the kinetic energy and potential of the tidally induced oscillations. The tidal potential will not be included in the calculation because it serves as the exchange in energy between the two systems. Working in the two systems separately we have:

$$V_g = -\frac{\mu M}{r}$$

Because the bodies have finite point vectors and velocities, we can use the Virial theorem for $n = -1$ (see 2.7.1). The total energy of the rotation is given by:

$$E_{rot} = -\frac{\mu M}{2r}$$

For the oscillation's potential we have:

$$\begin{aligned}
V_{osc} &= \sum_n \frac{1}{4\lambda 1,n\omega_n^2}(-\omega_n^2 Q_{ij}^n Q_{ij}^n) \\
V_{osc} &= -\frac{3}{8}\frac{1}{r^6}\sum_n m_2^2\lambda 1,n - \frac{9}{8}\frac{1}{r^6}\sum_n \frac{m_2^2\lambda 1,n}{(1-4x_n^2)^2}
\end{aligned}$$

Again, using Virial theorem for $n = -6$, we get the total energy of the oscillation:

$$E_{osc} = +\frac{6}{8}\frac{1}{r^6}\sum_n m_2^2\lambda 1,n + \frac{9}{4}\frac{1}{r^6}\sum_n \frac{m_2^2\lambda 1,n}{(1-4x_n^2)^2}$$

Adding these up we get the total energy:

$$E = -\frac{\mu M}{2r} + \frac{6}{8}\frac{1}{r^6}\sum_n m_2^2\lambda 1, n + \frac{9}{4}\frac{1}{r^6}\sum_n \frac{m_2^2\lambda 1, n}{(1-4x_n^2)^2}$$
$$rE = -\frac{\mu M}{2} + \frac{6}{8}\frac{1}{r^5}\sum_n m_2^2\lambda 1, n + \frac{9}{4}\frac{1}{r^5}\sum_n \frac{m_2^2\lambda 1, n}{(1-4x_n^2)^2}$$

On the first order of magnitude:

$$r_k E_k = -\frac{\mu M}{2}$$

Where E_k is the Kepler energy.

$$E_k = -\frac{\mu M}{2r_k} = -\frac{\mu}{2}(M\omega)^{2/3} \tag{24}$$

On the second order of magnitude:

$$\delta r E_k + r_k \delta E = \frac{6}{8}\frac{1}{r_k^5}\sum_n m_2^2\lambda 1, n + \frac{9}{4}\frac{1}{r_k^5}\sum_n \frac{m_2^2\lambda 1, n}{(1-4x_n^2)^2}$$
$$-r_k\frac{\mu M}{2r_k}\frac{3}{4}\sum_n \chi_n\left(1+\frac{3}{(1-4x_n^2)}\right) + r_k\delta E = \frac{6}{8}\frac{1}{r_k^5}\sum_n m_2^2\lambda 1, n + \frac{9}{4}\frac{1}{r_k^5}\sum_n \frac{m_2^2\lambda 1, n}{(1-4x_n^2)^2}$$
$$-\frac{\mu M}{2r_k}\frac{3}{4}\sum_n \chi_n\left(1+\frac{3}{(1-4x_n^2)}\right) + \delta E = \frac{6}{8}\frac{\mu M}{r_k}\sum_n \chi_n + \frac{9}{4}\frac{\mu M}{r_k}\sum_n \chi_n\frac{1}{(1-4x_n^2)^2}$$
$$\delta E = +\frac{\mu M}{2r_k}\frac{9}{4}\sum_n \chi_n\left(1+\frac{1}{(1-4x_n^2)}+\frac{2}{(1-4x_n^2)^2}\right)$$

The three terms in the parenthesis:

$$1+\frac{1}{(1-4x_n^2)}+\frac{2}{(1-4x_n^2)^2} = 1+\frac{3-4x_n^2}{(1-4x_n^2)^2} = g_2(x_n)$$

So the final expression for the change in energy δE is:

$$\delta E = +\frac{\mu M}{2r_k}\frac{9}{4}\sum_n \chi_n g_2(x_n) \tag{25}$$

and the total energy $E(\omega)$ of the system also matches the one in [13]:

$$E(\omega) = -\frac{\mu}{2}(M\omega)^{2/3}\left[1-\frac{9}{4}\sum_n \chi_n g_2(x_n)\right] \tag{26}$$

3.2.3 Calculating the energy loss due to gravitational wave emission

To calculate the energy loss due to gravitational wave emission, we will have to use the quadrupole formula (5):

$$\dot{E} = -\frac{1}{5}\langle \dddot{Q}_{ij}^T \dddot{Q}_{ij}^T\rangle \tag{27}$$

We have already calculated Q_{ij}^T back in 20 and we will now calculate it's 3rd time derivative:

$$\dddot{Q}_{ij}^{\ T} = Q\ddddot{\mathbf{B}} = Q\omega^3 8\begin{pmatrix}\sin(2\Phi) & -\cos(2\Phi) & 0\\ -\cos(2\Phi) & -\sin(2\Phi) & 0\\ 0 & 0 & 0\end{pmatrix}$$

With this we calculate the energy loss:

$$\dot{E} = -\frac{128}{5}Q^2\omega^6$$
$$\dot{E} = -\frac{128}{5}\omega^6\left(\frac{1}{4}\mu^2 r^4 + \frac{3}{4}\mu\sum_n \frac{m_2\lambda_{1,n}}{(1-4x_n^2)r}\right)$$
$$\frac{\dot{E}}{r^4} = -\frac{128}{5}\omega^6\left(\frac{1}{4}\mu^2 + \frac{3}{4}\mu\sum_n \frac{m_2\lambda_{1,n}}{(1-4x_n^2)r^5}\right)$$

In a first order of magnitude we ignore the sum term and we get:

$$\dot{E}_k = -\frac{32}{5} M^{4/3} \mu^2 \omega^{10/3} \tag{28}$$

In the second order of magnitude:

$$\frac{\delta \dot{E}}{r_k^4} - \frac{4\dot{E}_k \delta r}{r_k^5} = -\frac{128}{5}\omega^6 \frac{3}{4}\mu \sum_n \frac{m_2 \lambda_{1,n}}{(1-4x_n^2) r^5}$$

$$\frac{\delta \dot{E}}{\dot{E}_k} = 3\sum_n \chi_n \left(1 + \frac{3}{(1-4x_n^2)}\right) + 6\sum_n \frac{\chi_n M}{m_2(1-4x_n^2)}$$

$$\delta \dot{E} = \dot{E}_k 6 \sum_n \chi_n \left(\frac{1}{2} + \frac{3}{2(1-4x_n^2)} + \frac{M}{m_2(1-4x_n^2)}\right)$$

$$\delta \dot{E} = \dot{E}_k 6 \sum_n \chi_n \left((\frac{M}{m_2} + 2 - 2x_n^2)/(1-4x_n^2)\right)$$

The change in energy loss due to the oscillation is given by:

$$\delta \dot{E} = \dot{E}_k 6 \sum_n \chi_n g_3(x_n) \tag{29}$$

where $g_3(x) = (\frac{M}{m_2} + 2 - 2x^2)/(1-4x^2)$. The total energy loss of the system is given by:

$$\dot{E}(\omega) = -\frac{32}{5} M^{4/3} \mu^2 \omega^{10/3} \left[1 + 6\sum_n \chi_n g_3(x_n)\right] \tag{30}$$

, which also matches with Flanagan-Hinderer's formula [13].

3.3 Finding the change in the gravitational wave phase

We want to calculate the change in the phase of the gravitational wave signal from the additional tidally induced Quadrupole. We already know the phase $\Phi(t) = \omega t + \Phi_0$ of the rotating binary but in general that angular frequency is time dependent, it slowly increases the closer the two companion stars are. A more accurate description of the gravitational wave's waveform would be written as follows[3]:

$$h(t) = A(t) e^{-i\phi(t)} \text{ where } \phi(t) = \int_{t_0}^{t} \omega_{gw}(t')dt'$$

It is clear that:

$$\omega_{gw} = \frac{d\phi}{dt} \text{ and } \frac{d\omega_{gw}}{dt} = \frac{d^2\phi}{dt^2}$$

But we also know that $\omega_{gw} = 2\omega$. As a result:

$$2\frac{d\omega}{dt} = \frac{d^2\phi}{dt^2}$$

We want to calculate the phase of the gravitational wave signal, using all the knowledge we acquired in the previous section. To do that, we use the chain rule.

$$\frac{dE}{dt} = \frac{dE}{d\omega}\frac{d\omega}{dt} = \frac{1}{2}\frac{dE}{d\omega}\frac{d^2\phi}{dt^2}$$

Thus, we can calculate the phase of the gravitational wave signal, or at least it's second time derivative using the formula:

$$\frac{d^2\phi}{dt^2} = 2\frac{dE/dt}{dE/d\omega} \tag{31}$$

To calculate that we simply have to replace the energy loss and energy derivative over ω. But we do not have the expressions for the energy and energy loss in the time domain, we have calculated them in the frequency domain. So we will need to use the frequency domain counterpart of 31 [3]:

$$\frac{d^2\Psi}{d\omega^2} = 2\frac{dE/d\omega}{dE/dt} \tag{32}$$

Where $\Psi = \Psi(f)$ is the phase of the waveform in the frequency domain. We will have to use Fourier transform to find the waveform in the frequency domain and the relation between the two phases.

$$\tilde{h(f)} = \int_{t_0}^{t} h(t) e^{i2\pi ft} dt = \int_{t_0}^{t} A(t) e^{i(2\pi ft - \phi(t))} dt$$

In this integral $\phi(t)$ and $2\pi ft$ change rapidly in relation to $A(t)$ thus, we can use the stationary phase approximation:

$$\frac{d(2\pi ft - \phi(t))}{dt}|_{t=t^*} = 0 \Longrightarrow 2\pi f = \dot{\phi}(t^*)$$

We expand the phase around t^*:

$$\phi(t) = \phi(t^*) + \dot{\phi}(t^*)(t - t^*) + \ddot{\phi}\frac{(t-t^*)^2}{2}$$

We put this back into the waveform

$$\tilde{h(f)} \approx A(t^*) \int_{t_0}^{t} e^{i(2\pi ft - \phi(t^*) - 2\pi ft + 2\pi ft^* - \ddot{\phi}\frac{(t-t^*)^2}{2})} dt$$

$$\tilde{h(f)} \approx A(t^*) e^{i(2\pi ft^* - \phi(t^*))} \int_{t_0}^{t} e^{i(-\ddot{\phi}\frac{(t-t^*)^2}{2})} dt$$

The integral:

$$\int_{t_0}^{t} e^{i(-\ddot{\phi}(t^*)\frac{(t-t^*)^2}{2})} dt = \sqrt{\frac{2\pi}{\ddot{\phi}(t^*)}} e^{-i\pi/4}$$

Which leads to the final expression of the waveform[3]:

$$\tilde{h(f)} \approx A(t^*) \sqrt{\frac{2\pi}{\ddot{\phi}(t^*)}} e^{i(2\pi ft^* - \phi(t^*) - \pi/4)} \tag{33}$$

Where the terms in the exponential are the phase in the frequency domain:

$$\Psi(f) = 2\pi ft^* - \phi(t^*) - \pi/4 \tag{34}$$

We now use 31:

$$\frac{d^2\phi}{dt^2} = 2\frac{dE/dt}{dE/d\omega} \Longrightarrow \frac{d\omega}{dt} = \frac{dE/dt}{dE/d\omega} \text{ because } \frac{d\phi}{dt} = 2\omega$$

Using these two we can calculate:

$$\frac{d\phi}{d\omega} = \frac{d\phi}{dt}\frac{dt}{d\omega} = 2\omega\frac{dE/d\omega}{dE/dt} \Longrightarrow$$

$$\phi(\omega) = \phi_c - \int_{\omega}^{\omega_c} 2\omega' \frac{dE/d\omega'}{dE/dt} d\omega' \tag{35}$$

Where ϕ_c and ω_c represent the phase and the angular frequency at an early stage of the system. This relation is key to calculate $\Psi(f)$, but we will also need to repeat the same process for time(t):

$$\frac{dt}{d\omega} = \frac{dE/d\omega}{dE/dt} \Longrightarrow$$

$$t = t_c - \int_{\omega}^{\omega_c} \frac{dE/d\omega'}{dE/dt} d\omega' \tag{36}$$

Using 35 and 36 in 33 we get the final expression:

$$\Psi(f) = 2\pi ft_c - \phi_c - \pi/4 - \int_{\omega}^{\omega_c} 2(\omega - \omega')\frac{dE/d\omega'}{dE/dt} d\omega' \tag{37}$$

The term in the integral contains the second order of magnitude terms we need to calculate $\delta\psi$. We write $\dot{E} = \dot{E}_k + \delta\dot{E}$ and $E = E_k + \delta E$.

$$\frac{dE/d\omega'}{dE/dt} = \frac{dE_k/d\omega' + d\delta E/d\omega'}{\dot{E}_k + \delta\dot{E}} = \left(\frac{dE_k}{d\omega'} + \frac{d\delta E}{d\omega'}\right)\left(\frac{\dot{E}_k - \delta\dot{E}}{{\dot{E}_k}^2}\right)$$

Which can be written as follows:

$$\frac{dE/d\omega'}{dE/dt} = \frac{dE_k}{d\omega'}/\dot{E}_k + \frac{d\delta E/d\omega'}{\dot{E}_k} - \frac{\delta\dot{E}(dE_k/d\omega')}{{\dot{E}_k}^2}$$

The first terms in this expression along with the first three terms of 37 are related to the first order of $\Psi(f)$ the last two terms are related to the second order correction to the phase. After careful and meticulous calculations:

$$\frac{d\delta E/d\omega'}{\dot{E}_k} - \frac{\delta\dot{E}(dE_k/d\omega')}{{\dot{E}_k}^2} = -\frac{15}{16}\frac{m_2^2}{\mu^2 M^5}\upsilon' M \sum_n \lambda_{1,n}\left(\frac{2M}{m_2(1-4x_n^2)} + \frac{22-117x_n^2+348x_n^4-352x_n^6}{(1-4x_n^2)^3}\right)$$

Here we changed from ω to υ where $\upsilon = (\pi M f)^{1/3}$ to better match the post Newtonian analysis. Finally, by putting this back in 37:

$$\delta\Psi = -\frac{15}{16}\frac{m_2^2}{\mu^2 M^5}\sum_n \lambda_{1,n}\int_{\upsilon_i}^{\upsilon} d\upsilon'\upsilon'(\upsilon^3 - \upsilon'^3)g_4(x_n) \tag{38}$$

where $g_4(x) = \frac{2M}{m_2(1-4x^2)} + \frac{22-117x^2+348x^4-352x^6}{(1-4x^2)^3}$. This expression is simplified when we assume $\omega \ll \omega_n$ which translates into $x_n \ll 1$. This assumption instantly turns the integral into a simple calculation because $g_4(x_n) = 2M/m_2 + 22$ which can also be written as:

$$g_4(x_n) = 2\frac{\mu M}{m_2^2}\left(\frac{M}{m_1} + 11\frac{m_2}{m_1}\right)$$

Putting this back into 38, and disregarding υ_i as small $\upsilon_i \ll \upsilon$,due to it referring to an early stage of the binary where angular velocities are still small, we get:

$$\delta\Psi = -\frac{30}{16}\frac{1}{\mu M^4}\left(\frac{M}{m_1} + 11\frac{m_2}{m_1}\right)\left(\frac{3\upsilon^5}{10}\right)\sum_n \lambda_{1,n}$$

We remember that $\lambda_1 = \sum_n \lambda_{1,n}$[13]:

$$\delta\Psi = -\frac{9}{16}\frac{\upsilon^5}{\mu M^4}\left(\frac{M}{m_1} + 11\frac{m_2}{m_1}\right)\lambda_1$$

But this is only for one oscillating body in the field of the second body, if we assume both companions are oscillating and include the change in the phase from the second body oscillating in the field of the first, we get the final expression for the total change in the phase[13]:

$$\delta\Psi = -\frac{9}{16}\frac{\upsilon^5}{\mu M^4}\left[\left(\frac{M}{m_1} + 11\frac{m_2}{m_1}\right)\lambda_1 + \left(\frac{M}{m_2} + 11\frac{m_1}{m_2}\right)\lambda_2\right] \tag{39}$$

The term in the brackets is often referred to as the "Effective Tidal Deformability" $(\tilde{\Lambda})$:

$$\tilde{\Lambda} = \left[\left(\frac{M}{m_1} + 11\frac{m_2}{m_1}\right)\lambda_1 + \left(\frac{M}{m_2} + 11\frac{m_1}{m_2}\right)\lambda_2\right] \tag{40}$$

39 is a 5PN order term, and it is the first term containing information about the tidal deformabilities of the two companion stars $(\lambda_{1,2})$. Terms containing these tidal deformabilities in a separate , discrete manner are of higher PN order[10] and thus are still way out of reach of our current detector's capabilities. This effective tidal deformability is still difficult to detect and measure, but it's a first look to the inner composition of Neutron Stars through gravitational wave signals.

4 Assumptions and their accuracy

During this process, there is a number of assumptions being made. To have a better visualization of these assumptions, they are listed below:

1. The first and most important assumption is that the binary rotates in a circular orbit($r = const$).
2. The second and well hidden assumption is that the bulge of the neutron stars always faces the companion or has a small angle delay($\Phi_0 = const$).
3. The third assumption is that that the self-oscillation of the neutron stars is much faster than the rotating motion of the binary,$\omega \ll \omega_n$ (this is the last assumption leading to the final result 40).
4. We have ignored other corrections such as higher f-modes ($l \geq 3$),nonlinear hydrodynamic,spin, Post 1-Newtonian and linearization corrections.

The last corrections are checked in (Flanagan & Hinderer) and found to result in errors smaller than 10% for two identical stars with $n = 1, m = 1.4M_\odot$ and $R = 15km$ rotating with $f = 400Hz$, errors smaller than the current uncertainty in λ itself.

The third assumption's accuracy is vital because it directly simplifies the result of the analysis and can be easily calculated, for a binary system with the same characteristics, as follows:

We simplify the calculation by assuming all modes oscillate with the same $\omega_n = \omega_0$. Let $\omega = \omega_0/k$ where k is a constant. We can then write $\omega/\omega_0 = 1/k = x$ using this we can simplify $g_4(x) = \frac{2M}{m_2} + 22 + (\frac{8M}{m_2} + 147)x^2$. As expected if we put this back in 38 the first order term is none other than 39. The second order term is:

$$\delta\Psi_2 = -\frac{15}{16}\frac{m_2^2}{\mu^2 M^5}\sum_n \lambda_{1,n}\int_{v_i}^{v} dv' v'(v^3 - v'^3)(\frac{8M}{m_2} + 147)x^2$$

We remember that $x = \omega/\omega_n = v'^3/(M\omega_0)$ and $M = 2m_2$ which is then combined with the above integral:

$$\delta\Psi_2 = -\frac{15}{16}\frac{m_2^2}{\mu^2 M^5}\sum_n \lambda_{1,n}\int_{v_i}^{v} dv' v'(v^3 - v'^3)(163)v'^6/(M\omega_0)^2$$

This integral can be easily computed ignoring u_i as much smaller than u as we did in the original calculation of 39. The resulting second order correction to $\delta\Psi$:

$$\delta\Psi_2 = -\frac{15}{16}\frac{m_2^2}{\mu^2 M^5}\sum_n \lambda_{1,n}(\frac{v^8}{8}v^3 - \frac{v^{11}}{11})(163)\frac{1}{(M\omega_0)^2}$$

$$\delta\Psi_2 = -\frac{15}{16}\frac{m_2^2}{\mu^2 M^5}u^5\sum_n \lambda_{1,n}(\frac{3}{88})(163)\frac{u^6}{(M\omega_0)^2}$$

$$\delta\Psi_2 = -\frac{15}{16}\frac{m_2^2}{\mu^2 M^5}u^5\lambda_1(\frac{3}{88})(163)x^2$$

We will now compare this with the first order:

$$\frac{\delta\Psi_2}{\delta\Psi} = \frac{-\frac{15}{16}\frac{m_2^2}{\mu^2 M^5}u^5\lambda_1(\frac{3}{88})(163)x^2}{-\frac{9}{16}\frac{v^5}{\mu M^4}(13)\lambda_1} = \frac{15}{9}\frac{m_2^2}{\mu M}\frac{\frac{3}{88}}{13}163x^2$$

Finally,

$$\frac{\delta\Psi_2}{\delta\Psi} = 0.732x^2 \tag{41}$$

which for $f \leq 400Hz$ and $f_0 \geq 1000Hz$,typical values of observed frequencies, is:

$$\frac{\delta\Psi_2}{\delta\Psi} = 0.732x^2 = 0.183(f/f_0)^2 \leq 0.029$$

The first two assumptions are the primary goal of this work. In the same context of a neutron star binary and the same focus on the phase shift due to tidal effects, is it possible to lift the first two assumptions? Can the energy transfer between the two systems give rise to a non negligible change in the radius? Is it possible to also "unlock" the bulge from facing the companion and perhaps let it oscillate with a small amplitude around that direction?

5 Lifting the lock in the radius and the angle of the bulge

We will repeat the process as a whole but we will change the first two assumptions. Instead of a constant radius (r) we will allow a small time dependent change to that radius ($r + \epsilon(t)$), and instead of a constant angle (Φ_0) we will replace it with a time dependent ($\Phi_0(t)$) which does not deviate much from the constant value ($\Phi_0(t) - \Phi_0 \approx 0$). We put these small changes back into the equations of motion:

$$\ddot{x}^i + \frac{M}{r^2}n^i = \frac{m_2}{2\mu}Q_{jk}\partial_i\partial_j\partial_k\frac{1}{r} - \frac{2}{5}x_j\frac{d^5Q^T_{ij}}{dt^5}$$

$$\ddot{Q^n_{ij}} + \omega_n^2 Q^n_{ij} = m_2\lambda_{1,n}\omega_n^2\partial_i\partial_j\frac{1}{r} - \frac{2}{5}\lambda_{1,n}\omega_n^2\frac{d^5Q^T_{ij}}{d^5t}$$

Just as we did in the previous analysis the last two terms will be ignored:

$$\ddot{x}^i + \frac{M}{r^2}n^i = \frac{m_2}{2\mu}Q_{jk}\partial_i\partial_j\partial_k\frac{1}{r} \tag{42}$$

$$\ddot{Q^n_{ij}} + \omega_n^2 Q^n_{ij} = m_2\lambda_{1,n}\omega_n^2\partial_i\partial_j\frac{1}{r} \tag{43}$$

These two equations contain the information needed to find those small time dependent changes$(\epsilon(t), \Phi_0(t))$ but it also contains the information to calculate the change in the quadrupole (Q^n_{ij}) which arises from the time dependencies added in the radius and angle.

5.1 Adding the perturbations and important "prep" work

Let's tackle the first equation 42. In the previous analysis the radius was extracted directly from the action 13 and this equation was not used at all. We will now do it with this equation to make sure the result is the same. We will first need to calculate the term on the right hand of the equation:

$$\partial_i\partial_j\partial_k\frac{1}{r} = \partial_i(\partial_j\partial_k\frac{1}{r})$$

we have already calculated the parenthesis earlier $\partial_j\partial_k\frac{1}{r} = \frac{3}{r^3}\left[\frac{1}{2}\mathbf{B} + \frac{1}{6}\mathbf{A}\right]$ so we only need to do one extra step.

$$\partial_i\partial_j\partial_k\frac{1}{r} = \partial_i(\frac{3}{r^3}\left[\frac{1}{2}\mathbf{B} + \frac{1}{6}\mathbf{A}\right])$$

which for $i = 1, 2, 3$ gives

$$\partial_x\partial_j\partial_k\frac{1}{r} = -\frac{9cos\Phi}{r^4}\left[\frac{1}{2}\mathbf{B} + \frac{1}{6}\mathbf{A}\right])$$

$$\partial_y\partial_j\partial_k\frac{1}{r} = -\frac{9sin\Phi}{r^4}\left[\frac{1}{2}\mathbf{B} + \frac{1}{6}\mathbf{A}\right])$$

$$\partial_z\partial_j\partial_k\frac{1}{r} = 0$$

Now we are ready to put $r' = r + \epsilon(t)$ and $\Phi'(t) = \omega t + \Phi_0(t)$ into 42. This equation is written in Cartesian coordinates so we will need to translate those small changes into the new x', y'

$$x' = r\cos(\Phi') + \epsilon\cos(\Phi') \text{ and } y' = r\sin(\Phi') + e\sin(\Phi')$$

$$\dot{x'} = -r\frac{\partial\Phi'}{\partial t}\sin(\Phi') + \frac{\partial\epsilon}{\partial t}\cos(\Phi') - \epsilon\frac{\partial\Phi'}{\partial t}\sin(\Phi')$$

$$\dot{y'} = r\frac{\partial\Phi'}{\partial t}\cos(\Phi') + \frac{\partial\epsilon}{\partial t}\sin(\Phi') + \epsilon\frac{\partial\Phi'}{\partial t}\cos(\Phi')$$

$$\ddot{x'} = -r\frac{\partial^2\Phi'}{\partial t^2}\sin(\Phi') - r\left(\frac{\partial\Phi'}{\partial t}\right)^2\cos(\Phi') + \frac{\partial^2\epsilon}{\partial t^2}\cos(\Phi') - 2\frac{\partial\epsilon}{\partial t}\frac{\partial\Phi'}{\partial t}\sin(\Phi') - \epsilon\frac{\partial^2\Phi'}{\partial t^2}\sin(\Phi') - \epsilon\left(\frac{\partial\Phi'}{\partial t}\right)^2\cos(\Phi')$$

$$\ddot{y'} = r\frac{\partial^2\Phi'}{\partial t^2}\cos(\Phi') - r\left(\frac{\partial\Phi'}{\partial t}\right)^2\sin(\Phi') + \frac{\partial^2\epsilon}{\partial t^2}\sin(\Phi') + 2\frac{\partial\epsilon}{\partial t}\frac{\partial\Phi'}{\partial t}\cos(\Phi') + \epsilon\frac{\partial^2\Phi'}{\partial t^2}\cos(\Phi') - \epsilon\left(\frac{\partial\Phi'}{\partial t}\right)^2\sin(\Phi')$$

After calculating the time derivatives of Φ' and keeping only up to second order terms:

$$\frac{\partial \Phi'}{\partial t} = \omega + \dot{\Phi}_0$$
$$\left(\frac{\partial \Phi'}{\partial t}\right)^2 = \omega^2 + 2\omega\dot{\Phi}_0$$
$$\frac{\partial^2 \Phi'}{\partial t^2} = \ddot{\Phi}_0$$

We get the full expressions for all the derivatives of x and y:

$$\ddot{x'} = -r\ddot{\Phi}_0 \sin(\Phi') - r\omega^2 \cos(\Phi') - 2r\omega\dot{\Phi}_0 \cos(\Phi') - 2\dot{\epsilon}\omega \sin(\Phi') + \ddot{\epsilon}\cos(\Phi') - \epsilon\omega^2 \cos(\Phi')$$
$$\ddot{y'} = r\ddot{\Phi}_0 \cos(\Phi') - r\omega^2 \sin(\Phi') - 2r\omega\dot{\Phi}_0 \sin(\Phi') + 2\dot{\epsilon}\omega \cos(\Phi') + \ddot{\epsilon}\sin(\Phi') + \epsilon\omega^2 \sin(\Phi')$$

5.2 The perturbed equations of motion

We begin for i=1 in equation 42.

$$\ddot{x'} + \frac{M}{r'^2}\frac{x'}{r'} = \frac{m_2}{2\mu} Q_{jk} \partial_x \partial_j \partial_k \frac{1}{r'}$$
$$\ddot{x'} - \frac{2M}{r^3}\epsilon\cos(\Phi') + \frac{M}{r^2}\cos\Phi = \frac{m_2}{2\mu} Q_{jk} \frac{9cos\Phi}{r^4}\left[\frac{1}{2}\mathbf{B} + \frac{1}{6}\mathbf{A}\right])$$

Here Q_{jk} is expected to be a combination of $\mathbf{A}$ and $\mathbf{B}$ just like before although that's not certain since we will now change the equations and a new matrix may appear. The new matrix should only contain second order terms so that when keeping the first order terms the results should match the previous analysis. Still the combination will not be the same as before instead of the already calculated Q'^n, Q^n we assume that a correction will appear, due to the time dependent phase and radius, and we write:

$$Q^n_{jk} = (Q'^n + \delta Q'^n)\,\mathbf{A} + (Q^n + \delta Q^n)\,\mathbf{B} \tag{44}$$

Keeping only first order terms:

$$-r\omega^2\cos(\Phi') + \frac{M}{r^2}\cos(\Phi') = \frac{m_2}{2\mu}\left[Q'^n + Q^n\right]\left(\frac{-9\cos(\Phi')}{r^4}\right)$$
$$-\omega r^3 + M = \frac{m_2}{2\mu}\left[Q'^n + Q^n\right]\left(-\frac{9}{r^2}\right)$$

Which gives the exact $r(\omega)$ we found in the previous analysis straight from the action.
Keeping second order terms:

$$-r\ddot{\Phi}_0 \sin(\Phi') - 2r\omega\dot{\Phi}_0\cos(\Phi') - 2\dot{\epsilon}\omega\sin(\Phi') + \ddot{\epsilon}\cos(\Phi') - \epsilon\omega^2\cos(\Phi') - \frac{2M}{r^3}\epsilon\cos\Phi'$$
$$= \frac{m_2}{2\mu}\left[Q'^n + Q^n\right]\frac{36\cos(\Phi')\epsilon}{r^5} - \frac{m_2}{2\mu}\left[\delta Q'^n + \delta Q^n\right]\frac{9\cos(\Phi')}{r^4} \Longrightarrow$$
$$(-r\ddot{\Phi}_0 - 2\dot{\epsilon}\omega)\sin(\Phi') +$$
$$(-2r\omega\dot{\Phi}_0 + \ddot{\epsilon} - \epsilon\omega^2 - \frac{2M}{r^3}\epsilon - \frac{m_2}{2\mu}\left[Q'^n + Q^n\right]\frac{36\epsilon}{r^5} + \frac{m_2}{2\mu}\left[\delta Q'^n + \delta Q^n\right]\frac{9}{r^4})\cos(\Phi') = 0$$

The only way for this equation to be true for all Φ' is for the parameters of $\cos(\Phi'), \sin(\Phi')$ to be 0 independently, thus we get 2 differential equations:

$$-r\ddot{\Phi}_0 - 2\dot{\epsilon}\omega = 0 \tag{45}$$
$$-2r\omega\dot{\Phi}_0 + \ddot{\epsilon} - \epsilon\omega^2 - \frac{2M}{r^3}\epsilon - \frac{m_2}{2\mu}\left[Q'^n + Q^n\right]\frac{36\epsilon}{r^5} + \frac{m_2}{2\mu}\left[\delta Q'^n + \delta Q^n\right]\frac{9}{r^4} = 0 \tag{46}$$

If we repeat the process for i=2 the results stay the same, thus we move on to 43. When we add the time dependent components in 43 a new matrix appears from differentiating $\mathbf{B}$ over time. We name that matrix Γ:

$$\mathbf{\Gamma} = \begin{pmatrix} -\sin(2\Phi) & \cos(2\Phi) & 0 \\ \cos(2\Phi) & \sin(2\Phi) & 0 \\ 0 & 0 & 0 \end{pmatrix} \tag{47}$$

This matrix must be added to Q_{ij}

$$Q^n_{ij} = (Q'^n + \delta Q'^n)\,\mathbf{A} + (Q^n + \delta Q^n)\,\mathbf{B} + (Q''^n + \delta Q''^n)\,\mathbf{\Gamma} \tag{48}$$

Here $\mathbf{\Gamma}$ is expected to only have a second order term because as discussed earlier the first order term should be equal to 0, so that we can get the same first order result with the previous analysis where $\mathbf{\Gamma}$ didn't appear. For now, we will keep the first order term of $\mathbf{\Gamma}$ in order to see if it vanishes on it's own. However, does including this new matrix to the calculations in 42 change the result?

Due to the matrix scalar products $\mathbf{\Gamma A} = \mathbf{\Gamma B} = 0$, including the new matrix to the calculations does not change the result (Γ only appears in the term $Q_{jk}\frac{9\cos(\Phi)}{r^4}\left[\frac{1}{2}\mathbf{B} + \frac{1}{6}\mathbf{A}\right]$). Thus, we are ready for 43:

$$\begin{aligned}
&\ddot{Q}^n_{ij} + \omega_n^2 Q^n_{ij} = m_2\lambda_{1,n}\omega_n^2\partial_i\partial_j\frac{1}{r} \Longrightarrow \\
&\frac{\partial^2 Q'^n}{\partial t^2}\mathbf{A} + \frac{\partial^2 Q^n}{\partial t^2}\mathbf{B} + 2\frac{\partial Q^n}{\partial t}\frac{\partial \mathbf{B}}{\partial t} + Q^n\frac{\partial^2\mathbf{B}}{\partial t^2} + \frac{\partial^2 Q''^n}{\partial t^2}\mathbf{\Gamma} + 2\frac{\partial Q''^n}{\partial t}\frac{\partial \mathbf{\Gamma}}{\partial t} + Q''^n\frac{\partial^2\mathbf{\Gamma}}{\partial t^2} \\
&+ \omega_n^2\left[(Q'^n + \delta Q'^n)\,\mathbf{A} + (Q^n + \delta Q^n)\,\mathbf{B} + \delta Q''^n\mathbf{\Gamma}\right] \\
&= m_2\lambda_{1,n}\omega_n^2\frac{3}{r^3}\left[\frac{1}{2}\mathbf{B} + \frac{1}{6}\mathbf{A}\right] - m_2\lambda_{1,n}\omega_n^2\frac{9}{r^4}\epsilon\left[\frac{1}{2}\mathbf{B} + \frac{1}{6}\mathbf{A}\right]
\end{aligned}$$

We calculate the following:

$$\begin{aligned}
\frac{\partial \mathbf{B}}{\partial t} &= 2\frac{\partial \Phi'}{\partial t}\mathbf{\Gamma} \\
\frac{\partial^2 \mathbf{B}}{\partial t^2} &= 2\frac{\partial^2 \Phi'}{\partial t^2}\mathbf{\Gamma} - 4\left(\frac{\partial \Phi'}{\partial t}\right)^2\mathbf{B} \\
\frac{\partial \mathbf{\Gamma}}{\partial t} &= -2\frac{\partial \Phi'}{\partial t}\mathbf{B} \\
\frac{\partial^2 \mathbf{\Gamma}}{\partial t^2} &= -2\frac{\partial^2 \Phi'}{\partial t^2}\mathbf{B} - 4\left(\frac{\partial \Phi'}{\partial t}\right)^2\mathbf{\Gamma}
\end{aligned}$$

Again, this equation is satisfied when each of the parameters of the matrices $\mathbf{A}, \mathbf{B}$ and $\mathbf{\Gamma}$ are independently 0. Thus, we get 3 differential equations, one for each matrix.
For matrix $\mathbf{A}$:

$$\delta\ddot{Q}'^n + \omega_n^2\left(Q'^n + \delta Q'^n\right) = \frac{1}{2}m_2\lambda_{1,n}\omega_n^2\frac{1}{r^3} - \frac{3}{2}m_2\lambda_{1,n}\omega_n^2\frac{\epsilon}{r^4} \tag{49}$$

For matrix $\mathbf{B}$:

$$\begin{aligned}
&\delta\ddot{Q}^n + \omega_n^2\left(Q^n + \delta Q^n\right) - 4(\omega^2 + 2\omega\dot{\Phi}_0)\left(Q^n + \delta Q^n\right) - 4(\omega + \dot{\Phi}_0)\delta\dot{Q}''^n - 2\ddot{\Phi}_0\left(Q''^n + \delta Q''^n\right) \\
&= \frac{3}{2}m_2\lambda_{1,n}\omega_n^2\frac{1}{r^3} - \frac{9}{2}m_2\lambda_{1,n}\omega_n^2\frac{\epsilon}{r^4}
\end{aligned} \tag{50}$$

For matrix $\mathbf{\Gamma}$:

$$\delta\ddot{Q}''^n + \omega_n^2\left(Q''^n + \delta Q''^n\right) - 4(\omega^2 + 2\omega\dot{\Phi}_0)\left(Q''^n + \delta Q''^n\right) + 4(\omega + \dot{\Phi}_0)\delta\dot{Q}^n + 2\ddot{\Phi}_0\left(Q^n + \delta Q^n\right) = 0 \tag{51}$$

We will now take this three equations and split them in first and second order terms just as we did for 45 and 46.
We start with 49, keeping only 1st order terms:

$$\omega_n^2 Q'^n = \frac{1}{2}m_2\lambda_{1,n}\omega_n^2\frac{1}{r^3}$$

Which gives the same result as before:

$$Q'^n = \frac{1}{2}\frac{m_2\lambda_{1,n}}{r^3}$$

The second order terms give:

$$\delta\ddot{Q}'^n + \omega_n^2\delta Q'^n = -\frac{3}{2}m_2\lambda_{1,n}\omega_n^2\frac{\epsilon}{r^4} \tag{52}$$

We move on to 50. The first order terms:

$$\omega_n^2 Q^n - 4\omega^2 Q^n = \frac{3}{2} m_2 \lambda_{1,n} \omega_n^2 \frac{1}{r^3}$$

Which again gives the same result as before:

$$Q^n = \frac{3}{2} \frac{m_2 \lambda_{1,n}}{(1-4x_n^2) r^3}$$

The second order:

$$\delta\ddot{Q}^n + \omega_n^2 \delta Q^n - 4\omega^2 \delta Q^n - 8\omega\dot{\Phi}_0 Q^n - 4\omega\delta\dot{Q}'^n - 2\ddot{\Phi}_0 Q'^n = -\frac{9}{2} m_2 \lambda_{1,n} \omega_n^2 \frac{\epsilon}{r^4} \tag{53}$$

Finally for 51, the first order terms give:

$$\omega_n^2 Q'^n - 4\omega^2 Q'^n = 0$$

Which can only be true if $Q'^n = 0$. As expected the first order component of $\mathbf{\Gamma}$ vanishes.
The second order terms:

$$\delta\ddot{Q}'^n + \omega_n^2 \delta Q'^n - 4\omega^2 \delta Q'^n + 4\omega\delta\dot{Q}^n + 2\ddot{\Phi}_0 Q^n = 0 \tag{54}$$

The final result is a system of 5 differential (45,46,52,53,54) equations
and 5 variables $(\epsilon(t), \Phi_0(t), \delta Q^n, \delta Q'^n, \delta Q'^n)$.The system can be simplified a bit as 45 is already simple:

$$\ddot{\Phi}_0 = -\frac{2\dot{\epsilon}\omega}{r} \Longrightarrow \dot{\Phi}_0 = -\frac{2\omega\epsilon}{r} + c$$

Including this and $Q'^n = 0$ we write the remaining 4 equations again:

$$\begin{aligned}
&\ddot{\epsilon} + 3\omega^2\epsilon - \frac{2M}{r^3}\epsilon - \frac{m_2}{2\mu}\left[Q'^n + Q^n\right]\frac{36\epsilon}{r^5} + \frac{m_2}{2\mu}\left[\delta Q'^n + \delta Q^n\right]\frac{9}{r^4} = 0 \\
&\frac{3}{2} m_2 \lambda_{1,n} \omega_n^2 \frac{\epsilon}{r^4} + \delta\ddot{Q}'^n + \omega_n^2 \delta Q'^n = 0 \\
&\frac{9}{2} m_2 \lambda_{1,n} \omega_n^2 \frac{\epsilon}{r^4} + 16\omega^2 \frac{\epsilon}{r} Q^n + \delta\ddot{Q}^n + \omega_n^2 \delta Q^n - 4\omega^2 \delta Q^n - 4\omega\delta\dot{Q}'^n = 0 \\
&-4\omega\frac{\dot{\epsilon}}{r} Q^n + 4\omega\delta\dot{Q}^n + \delta\ddot{Q}'^n + \omega_n^2 \delta Q'^n - 4\omega^2 \delta Q'^n = 0
\end{aligned}$$

5.3 Solving the system of differential equations

This is a system of linear homogeneous differential equations with constant coefficients (adiabatically), thus we will consider solutions of the form (see 2.7.4):

$$\begin{aligned}
\epsilon(t) &= E e^{i\Omega t} \\
\Phi_0(t) &= \phi_0 e^{i\Omega t} \\
\delta Q'^n(t) &= q'^n e^{i\Omega t} \\
\delta Q^n(t) &= q^n e^{i\Omega t} \\
\delta Q'^n(t) &= q'^n e^{i\Omega t}
\end{aligned}$$

We substitute these back into the equations:

$$\begin{aligned}
&\left(-\Omega^2 + 3\omega^2 - \frac{2M}{r^3} - \frac{m_2}{2\mu}\left[Q'^n + Q^n\right]\frac{36}{r^5}\right) E + \frac{9m_2}{2\mu r^4} q'^n + \frac{9m_2}{2\mu r^4} q^n = 0 \\
&\left(\frac{3}{2}\frac{m_2 \lambda_{1,n} \omega_n^2}{r^4}\right) E + (-\Omega^2 + \omega_n^2) q'^n = 0 \\
&\left(\frac{3}{2}\frac{m_2 \lambda_{1,n}}{r^4}\frac{(3\omega_n^2 + 4\omega^2)}{(1-4x_n^2)}\right) E + (-\Omega^2 + \omega_n^2 - 4\omega^2) q^n - 4\omega i\Omega q'^n = 0 \\
&\frac{-4i\omega\Omega Q^n}{r} E + 4i\omega\Omega q^n + (-\Omega^2 + \omega_n^2 - 4\omega^2) q'^n = 0
\end{aligned}$$

This is now a linear system of 4 equations and 4 variables. We will attempt to solve this system with the matrix:

$$\begin{pmatrix} -\Omega^2+3\omega^2-\frac{2M}{r^3}-\frac{m_2}{2\mu}\left[Q'^n+Q^n\right]\frac{36}{r^5} & \frac{9m_2}{2\mu r^4} & \frac{9m_2}{2\mu r^4} & 0 \\ \frac{3}{2}\frac{m_2\lambda_{1,n}\omega_n^2}{r^4} & (-\Omega^2+\omega_n^2) & 0 & 0 \\ \frac{3}{2}\frac{m_2\lambda_{1,n}}{r^4}\frac{(3\omega_n^2+4\omega^2)}{(1-4x_n^2)} & 0 & (-\Omega^2+\omega_n^2-4\omega^2) & -4\omega i\Omega \\ \frac{-4i\omega\Omega Q^n}{r} & 0 & 4\omega i\Omega & (-\Omega^2+\omega_n^2-4\omega^2) \end{pmatrix} \tag{55}$$

If a non trivial solution for this system exists, then the determinant of this matrix must be equal to zero. The given equation can be solved to give us the eigenvalue Ω^2, the assumed common frequency of all the perturbations. But first, the determinant of this matrix is:

$$\begin{aligned} Det = 4i\omega\Omega\Bigg(&-\frac{63im^2\lambda\omega_n^2\omega\Omega}{r^8\mu}-\frac{81im^2\lambda\omega_n^2\omega\Omega}{r^8\left(1-4x^2\right)\mu}-\frac{8iM\omega_n^2\omega\Omega}{r^3}+12i\omega_n^2\omega^3\Omega+\frac{36im^2\lambda\omega\Omega^3}{r^8\mu}+\frac{81im^2\lambda\omega\Omega^3}{r^8\left(1-4x^2\right)\mu} \\ &+\frac{8iM\omega\Omega^3}{r^3}-4i\omega_n^2\omega\Omega^3-12i\omega^3\Omega^3+4i\omega\Omega^5\Bigg)+\left(\omega_n^2-4\omega^2-\Omega^2\right)\Bigg(\frac{3\left(3\omega_n^2+4\omega^2\right)\left(-\frac{9m\omega_n^2}{2r^4\mu}+\frac{9m\Omega^2}{2r^4\mu}\right)}{2r^4\left(1-4x^2\right)} \\ &-\frac{27m^2\lambda\omega_n^2}{4r^8\mu}+\left(\omega_n^2-\Omega^2\right)\left(-\frac{18m\left(\frac{m\lambda}{2r^3}+\frac{3m\lambda}{2r^3(1-4x^2)}\right)}{r^5\mu}-\frac{2M}{r^3}+3\omega^2-\Omega^2\right)\Bigg) \end{aligned}$$

Expanding this and rearranging the terms gives us a 8th degree polynomial of Ω. This polynomial is of the form:

$$Det = W_4\Omega^8+W_3\Omega^6+W_2\Omega^4+W_1\Omega^2+W_0 \tag{56}$$

where:

$$\begin{aligned} W_4 &= 1 \\ W_3 &= \frac{9m_2^2\lambda}{r^8\mu}+\frac{27m_2^2\lambda}{r^8\left(1-4x_n^2\right)\mu}+\frac{2M}{r^3}-3\omega_n^2+5\omega^2+16i^2\omega^2 \\ W_2 &= \frac{81m_2\omega_n^2}{4r^8\left(1-4x_n^2\right)\mu}-\frac{135m_2^2\lambda\omega_n^2}{4r^8\mu}-\frac{81m_2^2\lambda\omega_n^2}{r^8\left(1-4x_n^2\right)\mu}-\frac{6M\omega_n^2}{r^3}+3\omega_n^4-\frac{27m_2\omega^2}{r^8\left(1-4x_n^2\right)\mu}+\frac{72m_2^2\lambda\omega^2}{r^8\mu} \\ &\quad+\frac{144i^2m_2^2\lambda\omega^2}{r^8\mu}+\frac{216m_2^2\lambda\omega^2}{r^8\left(1-4x_n^2\right)\mu}+\frac{324i^2m_2^2\lambda\omega^2}{r^8\left(1-4x_n^2\right)\mu}+\frac{16M\omega^2}{r^3}+\frac{32i^2M\omega^2}{r^3}-7\omega_n^2\omega^2-16i^2\omega_n^2\omega^2-8\omega^4-48i^2\omega^4 \\ W_1 &= \frac{81m_2\omega_n^4}{2r^8\left(1-4x_n^2\right)\mu}+\frac{81m_2^2\lambda\omega_n^4}{2r^8\mu}+\frac{81m_2^2\lambda\omega_n^4}{r^8\left(1-4x_n^2\right)\mu}+\frac{6M\omega_n^4}{r^3}-\omega_n^6-\frac{27m_2\omega_n^2\omega^2}{r^8\left(1-4x_n^2\right)\mu}-\frac{198m_2^2\lambda\omega_n^2\omega^2}{r^8\mu} \\ &\quad-\frac{252i^2m_2^2\lambda\omega_n^2\omega^2\Omega^2}{r^8\mu}-\frac{432m_2^2\lambda\omega_n^2\omega^2}{r^8\left(1-4x_n^2\right)\mu}-\frac{324i^2m_2^2\lambda\omega_n^2\omega^2}{r^8\left(1-4x_n^2\right)\mu}-\frac{32M\omega_n^2\omega^2}{r^3}-\frac{32i^2M\omega_n^2\omega^2}{r^3}-\omega_n^4\omega^2 \\ &\quad-\frac{108m_2\omega^4}{r^8\left(1-4x_n^2\right)\mu}+\frac{144m_2^2\lambda\omega^4}{r^8\mu}+\frac{432m_2^2\lambda\omega^4}{r^8\left(1-4x_n^2\right)\mu}+\frac{32M\omega^4}{r^3}+32\omega_n^2\omega^4+48i^2\omega_n^2\omega^4-48\omega^6 \\ W_0 &= -\frac{81m_2\omega_n^6}{4r^8\left(1-4x_n^2\right)\mu}-\frac{63m_2^2\lambda\omega_n^6}{4r^8\mu}-\frac{27m_2^2\lambda\omega_n^6}{r^8\left(1-4x_n^2\right)\mu}-\frac{2M\omega_n^6}{r^3}+\frac{54m_2\omega_n^4\omega^2}{r^8\left(1-4x_n^2\right)\mu}+\frac{126m_2^2\lambda\omega_n^4\omega^2}{r^8\mu}+\frac{216m_2^2\lambda\omega_n^4\omega^2}{r^8\left(1-4x_n^2\right)\mu} \\ &\quad+\frac{16M\omega_n^4\omega^2}{r^3}+3\omega_n^6\omega^2+\frac{108m_2\omega_n^2\omega^4}{r^8\left(1-4x_n^2\right)\mu}-\frac{252m_2^2\lambda\omega_n^2\omega^4}{r^8\mu}-\frac{432m_2^2\lambda\omega_n^2\omega^4}{r^8\left(1-4x_n^2\right)\mu}-\frac{32M\omega_n^2\omega^4}{r^3}-24\omega_n^4\omega^4+48\omega_n^2\omega^6 \end{aligned}$$

We want to find the roots of this polynomial. The exact solutions are not easily extracted, thus we will plot it. But before that, we must consider realistic values for all the different parameters$(m_1, m_2, R, n, \omega_n, \omega, r)$.

1. For the neutron star properties, we consider the same combination Flanagan and Hinderer used in their paper[13], two identical neutron stars with $m1 = m2 = m = 1.4M_\odot = 2.1km$, a radius $R = 15km$ and a polytropic index $n = 1.0$.

2. With this parameters locked it is possible to calculate the approximate love number using the formula[15] $k_2 \approx \frac{3}{2}\left(-0.41 + \frac{0.56}{n^{0.33}}\right)\left(\frac{M}{R}\right)^{-0.003}$ and the tidal deformability $\lambda = \frac{2}{3}R^5 k_2$. The resulting $\lambda_1 = 114.000km^5$, when transformed, this matches with the one in [13] ($\lambda = 1.7 \cdot 10^{35} gcm^2 s^2$ for $n = 1.0$).

3. We know that the separation r and angular velocity ω are dependent on each other, thus we will use three different relations between them. The first one is the $r(\omega)$ in equation 23, which is the same one Flanagan and Hinderer derived in their paper[13]. I am naming this relation ω_{fh} for simplicity. The second relation is derived from solving equation 21 for ω without considering the tidal terms necessarily small. However, we still assume that all the shells oscillate with the same frequency,$\omega_n = \omega_0 = 0.021km^{-1}$ the equivalent of $f_n = 1000Hz$. This equation is a simple quadratic polynomial with two solutions:

$$-16\mu r^8\omega^4 + \left(4\mu r^8\omega_n^2 + 16M\mu r^5 + 36m_2^2\lambda_1\right)\omega^2 - \left(9m_2^2\lambda_1\omega_n^2 + 4M\mu r^3\omega_n^2 + 27m_2^2\lambda_1\omega_n^2\right) = 0$$

$$\omega_1^2, \omega_2^2 = \frac{-4\mu r^8\omega_n^2 - 16M\mu r^5 - 36m_2^2\lambda_1 \pm \sqrt{D}}{-32\mu r^8} \tag{57}$$

where:

$$D = \left(16\mu^2 r^{16}\omega_n^4 + 256M^2\mu^2 r^{10} + 1296m_2^2\lambda_1^2 + 128M\mu^2 r^{13}\omega_n^2 + 288\mu m_2^2\lambda_1\omega_n^2 r^8 + 1152M\mu m_2^2\lambda_1 r^5\right) - 64\mu r^8\left(9m_2^2\lambda_1\omega_n^2 + 4M\mu r^5\omega_n + 27m_2^2\lambda_1\omega_n^2\right)$$

and the third one is Kepler's $\omega_k^2 = Mr^{-3}$ for comparison.

5.4 Comparing the $\omega(r)$ relations

By drawing the three different $\omega(r)$'s we get a better picture of how these compare for different phases of the binary motion. Starting with the inspiral phase with a frequency below $f = 500Hz$ or $\omega = 0.00525km^{-1}$(or $\omega^2 = 0.276 \cdot 10^{-4}km^{-2}$).

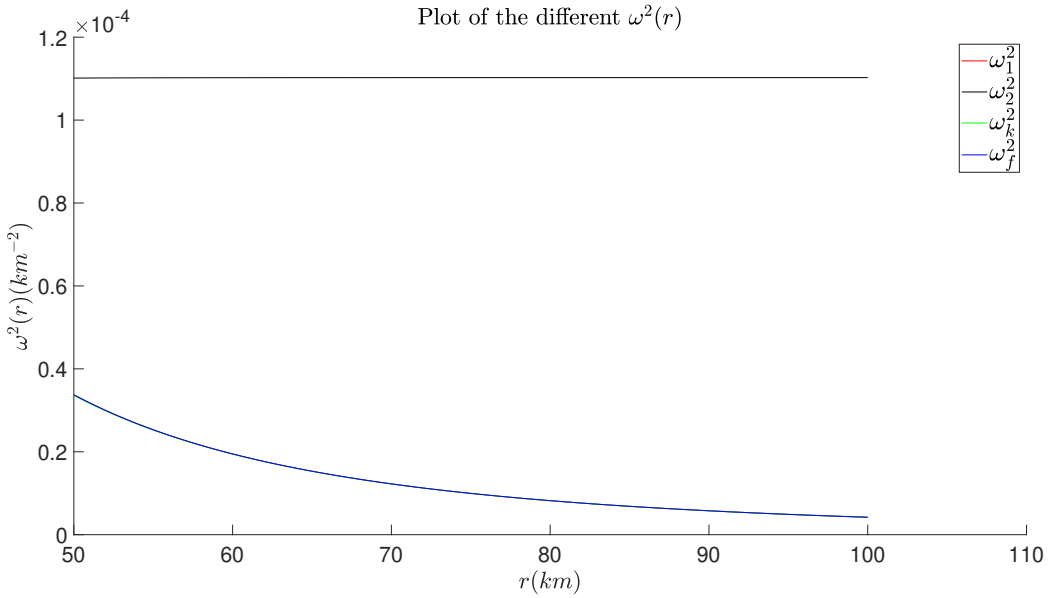

Figure 4: Plot of the different $\omega^2(r)$ for separations in the inspiral phase, where the black line is the "-" solution of 57, the red is the "+" solution, Flanagan-Hinderer's in blue and Kepler's in green.

The "+" solution along with Flanagan-Hinderer's and Kepler's, do not have major differences even when we remove the "-" solution from the graph. This is a good sign, as all three relation should behave similarly to Kepler's for big enough separations.The "-" solution has an irregular behavior (ω increasing with separation),but we will keep it in the future graphs for now to see her full behavior.

We continue in the intermediate phase of the evolution, with frequencies higher than $500Hz$, where the tidal terms become important and finally dominate as the two companions approach the final merger. In this context, we can no longer expect the same accuracy from the r_{fh} relation as it was derived by assuming that the tidal terms are very small compared to the other terms back in 23. For the same reasons, Kepler's relation is also lacking accuracy. In this phase of the evolution, everything we've assumed begins to crumble, $f = 500Hz$ is already considered to be the frequency at the innermost stable circular orbit (ISCO)[6][27] (we remind that the motion's frequency is half the gravitational wave's frequency). From this point onwards, mass transfer begins and for some neutron star models, this marks the end of the quasi-circular orbits, while for others, with bigger polytropic indices there may still be circular orbits while mass transfer is happening[27]. Additionally, the calculations as a whole lack very important aspects, like general relativity and damping effects which become more and more important as we close in on the merger. Even so, we choose to move as close as possible and include every $\omega(r)$ relation in the next plots to see their differences:

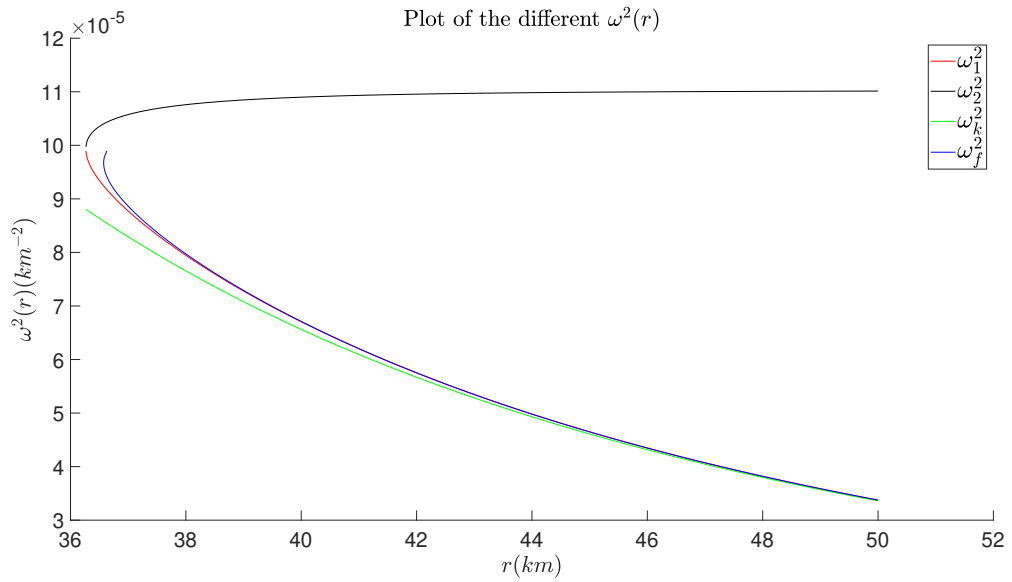

Figure 5: Plot of the different $\omega^2(r)$ for separations after the inspiral phase, where the black line is the "-" solution of 57, the red is the "+" solution, Flanagan-Hinderer's in blue and Kepler's in green.

The "-" solution still shows an irregular behavior, while the other three show almost no difference in bigger separations. However a visible difference appears the closer we get to f=1000Hz (or $\omega^2 = 11 \cdot 10^{-5} km^{-2}$) where the terms $(1 - 4x_n^2) \sim 0$, i.e. close to resonance .

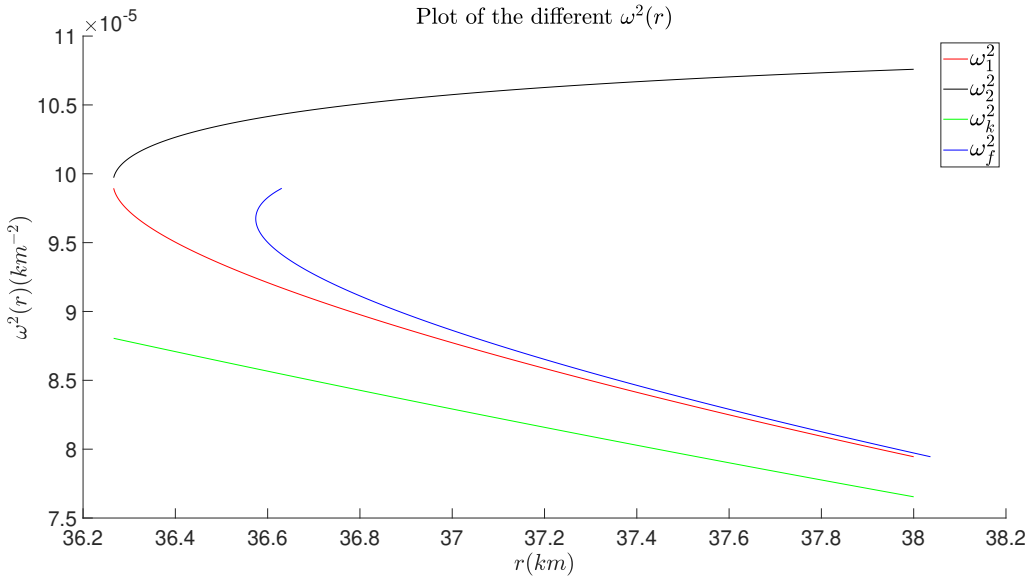

Figure 6: Plot of the different $\omega^2(r)$ for separations close to resonance, where the black line is the "-" solution of 57, the red is the "+" solution, Flanagan-Hinderer's in blue and Kepler's in green.

Even though the ω_{fh} uses a hypothesis that isn't true in this phase of the binary motion, it performs really well even this close to resonance. The "+" solution (ω_1) being the exact version of ω_{fh}, only differs considerably, as we approach resonance and the latter ultimately "fails" at $r = 36.5 - 37km$. The "-" solution is invalid and disregarded for separations larger than roughly $36.25km$. The next question is what happens in even smaller separations with an ultimate limit of $30km$ (where the two $R = 15km$ neutron stars's surfaces touch) but all the solutions behavior is odd, as D becomes negative. Thus, we will stop at the last separation in which D is positive which is calculated to be around $r = 36.2683km$.

6 Results

Having a better understanding of the $\omega(r)$ relations and having locked every other parameter we can now draw the polynomial in 56 and search for Ω and potential instabilities. We begin by plotting for a separation much larger than $53.5km$ were the end of the inspiral phase is (equivalent separation of $f = 500Hz$).

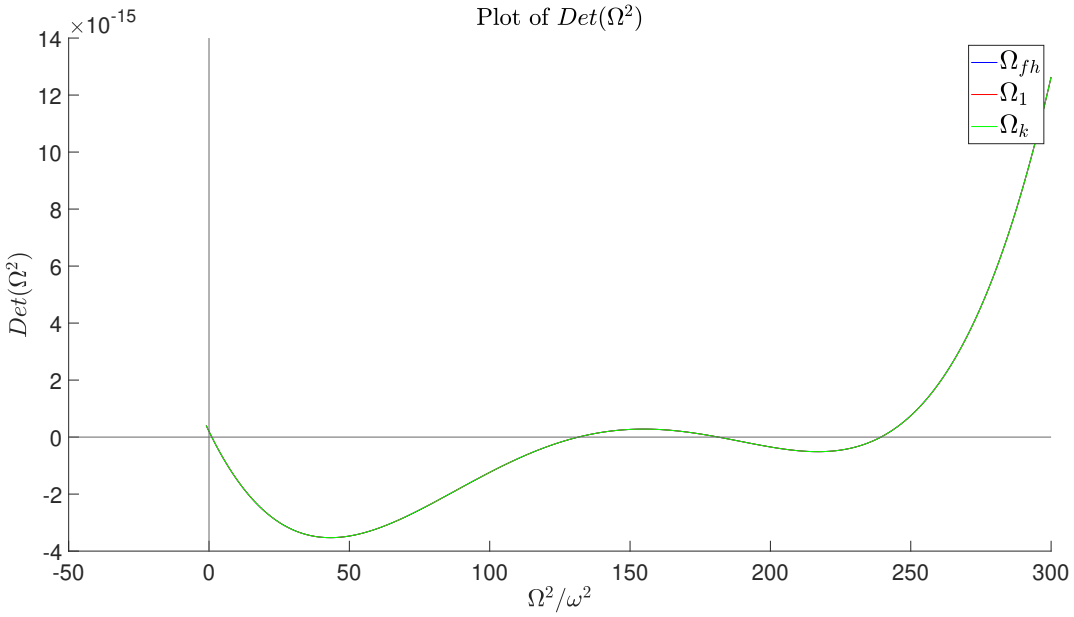

Figure 7: A full plot of the polynomial 56 for $r = 120km$, were all 4 of it's roots are visible for all 3 relations discussed.

In this plot for $r = 120km$ all three relations behave incredibly similar, but that's to be expected as all relations behave like Kepler's for large separations. We can clearly see all 4 roots, however the latter three are not realistic, as for large separations the bulge should face the companion even with a small angle[13], so we focus on the one near 0.

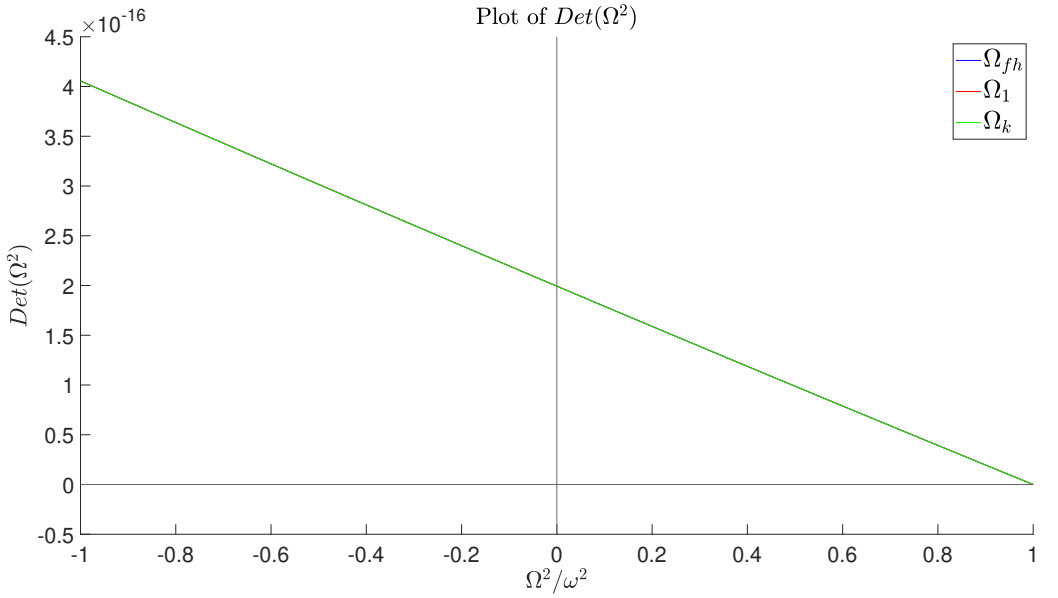

Figure 8: A plot of the polynomial 56 for $r = 120km$, were only the first of it's roots is visible for all 3 relations discussed.

The polynomial behaves like a straight line near 0, with a clear solution for $\omega = \Omega$ which means that the oscillations share the same frequency with the motion which also matches with the argument that the bulge faces the companion. For a big enough separation like this we can ignore most of the terms and simplify the matrix.

$$\begin{pmatrix} -\Omega^2 + 3\omega^2 - \frac{2M}{r^3} & 0 & 0 & 0 \\ 0 & (-\Omega^2 + \omega_n^2) & 0 & 0 \\ 0 & 0 & (-\Omega^2 + \omega_n^2 - 4\omega^2) & -4\omega i\Omega \\ 0 & 0 & 4\omega i\Omega & (-\Omega^2 + \omega_n^2 - 4\omega^2) \end{pmatrix} \tag{58}$$

We can simplify even further using Kepler's relation which is very accurate for big separations as showcased in Figure 4.

$$\Pi = \begin{pmatrix} 0 & 0 & 0 & 0 \\ 0 & (-\omega^2 + \omega_n^2) & 0 & 0 \\ 0 & 0 & (\omega_n^2 - 5\omega^2) & -4\omega^2 i \\ 0 & 0 & 4\omega^2 i & (\omega_n^2 - 5\omega^2) \end{pmatrix} \tag{59}$$

We now see clearly why $\omega = \Omega$ is a solution, as it makes the first term of the matrix equal to zero.

6.1 Results for a BNS

We will additionally plot the polynomial focused around 0 so that we can observe the $\omega = \Omega$ root, using all three of the relations discussed for different separations ranging from $r = 53km$ close to were the end of the inspiral phase is all the way to $r = 37km$ close to the smallest achievable separation in this setting.

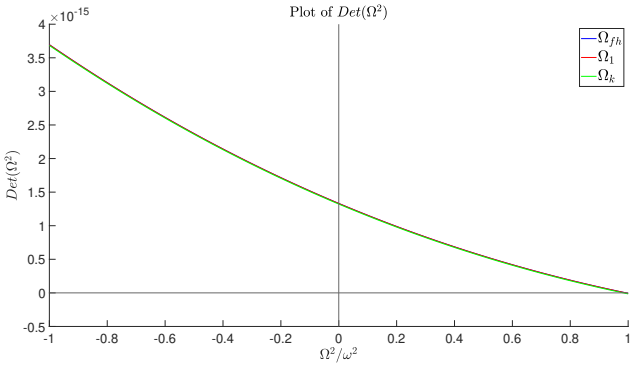

(a) For $r = 53km$

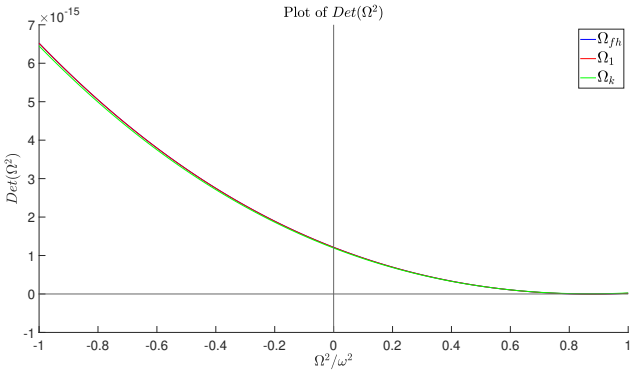

(b) For $r = 43km$

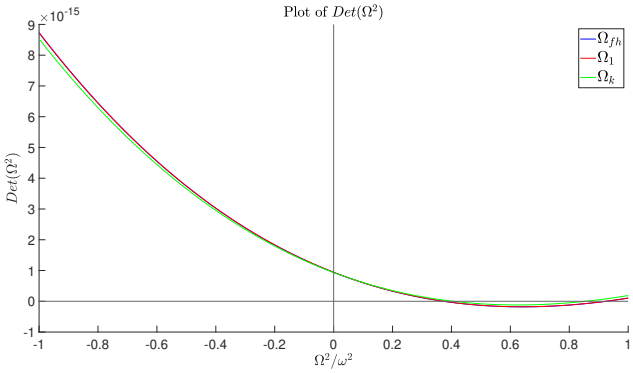

(c) For $r = 40km$

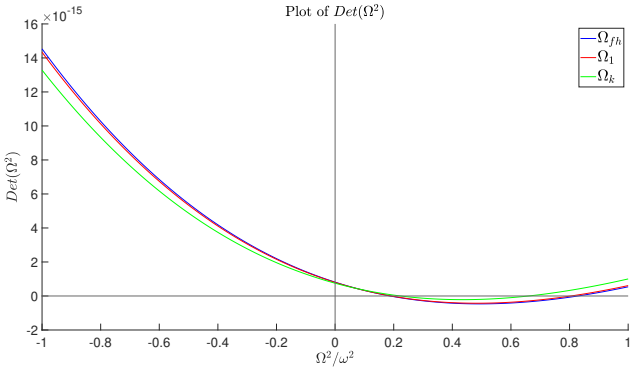

(d) For $r = 37km$

Figure 9: Plots of the Polynomial 56 for different separations focused on it's first root.

As the separation decreases the roots start to move to the left for all 3 relations. For $r = 53km$ the first root lies close to 1 and the straight line behavior begins to fade. The first root gradually moves as we decrease the separation reaching $\Omega^2/\omega^2 = 0.2$ for $r = 37km$. This shift in Ω translates into an unlocked oscillation, where the bulges don't phase each other, and the radial oscillations do not match the frequency of the motion. This particular set of parameters, does not seem to contain any instabilities, even when we get this close to the merger ignoring the fact that the

circular orbits have already stopped and ignoring relativistic and damping effects.
To check out if the other models also contain no instabilities, we will go back to the matrix and express Ω as a fraction of ω, $\Omega = \alpha\omega$. Thus, the matrix becomes:

$$\begin{pmatrix} -\alpha^2\omega^2 + 3\omega^2 - \frac{2M}{r^3} - \frac{m_2}{2\mu}\left[Q'^n + Q^n\right]\frac{36}{r^5} & \frac{9m_2}{2\mu r^4} & \frac{9m_2}{2\mu r^4} & 0 \\ \frac{3}{2}\frac{m_2\lambda_{1,n}\omega_n^2}{r^4} & (-\alpha^2\omega^2 + \omega_n^2) & 0 & 0 \\ \frac{3}{2}\frac{m_2\lambda_{1,n}}{r^4}\frac{(3\omega_n^2+4\omega^2)}{(1-4x_n^2)} & 0 & (-\alpha^2\omega^2 + \omega_n^2 - 4\omega^2) & -4i\alpha\omega^2 \\ \frac{-4i\alpha\omega^2 Q^n}{r} & 0 & 4i\alpha\omega^2 & (-\alpha^2\omega^2 + \omega_n^2 - 4\omega^2) \end{pmatrix} \tag{60}$$

We will test 5 different Equations of State Models in total, to see if this shifting behavior appears in each of them . Each model's name and parameters, including the frequency of oscillations we expect to see in each, are the same ones we introduced in 2.6. The additional information for the induced oscillations are given in the following table[25]:

Model	l	R_0 (km)	v	ν_K (Hz)	ν_f (Hz)
A	4	31.8	0.255	567	2260
	3	29.0	0.267	651	1953
	2	26.0	0.282	767	1534
B	3	22.9	0.300	626	1879
	2	21.0	0.313	711	1422
C	3	21.2	0.312	702	2105
	2	18.9	0.331	835	1671
D	3	15.5	0.365	1119	3358
	2	14.1	0.383	1296	2593
E	3	13.5	0.391	1379	4138

Figure 10: Excited stellar modes and their frequency for a neutron star-point mass binary (mode l,separation of excitation R_0, velocity u, frequency of rotation ν_k and oscillation frequency ν_f) for different Equations of State[25].

From the first table (in figure 3) we will extract the parameters (n, M, r) for two identical neutron stars. From the second table we will ignore higher modes ($l \geq 3$) and take the frequencies of the excited oscillations for $l = 2$. For the model E that doesn't have $l = 2$ we choose to check for $f_n = 3600Hz$. Using the program we used for Figure 9 we will find the parameter α in $\Omega = \alpha\omega$ of the first root, for the smallest achievable radius r_s (i.e. before the discriminant D becomes negative or if the two companion stars touch $r \leq 2R$). We will then begin to lower the frequency of the oscillations with a lower limit of $f_n = 1000Hz$ and observe how the root moves and thus how α changes. There are some combinations of these parameters for which the root disappears entirely, thus the r_s will be increased slightly until the root appears. If no instabilities appear this close to resonance, it will be clear that we cannot expect instabilities in the inspiral phase.

The resulting α for every model and the r_s it was calculated at are listed in the tables 2 & 3. We observe a similar shift of the first root towards 0 in all models, but no matter how much we reduced the frequency of the oscillations (for example in model E) the root never became negative, thus we still do not observe any instabilities.

The results from this analysis show, that even while ignoring the ISCO, relativistic and damping effects (from gravitational waves etc.) and reducing the induced oscillation's frequencies, perhaps beyond their realistic limits there is still no instability($\Omega^2 < 0$). We only observe a shift in the frequency of the small oscillations (Ω^2), but it persistently stays positive and seems to be asymptotically moving towards 0.

Model	$f_n(Hz)$	$r_s(km)$	a^2
A	$1500Hz$	30.6	1.00
A	$1400Hz$	29.0	0.73
A	$1300Hz$	29.0	0.43
A	$1200Hz$	28.6	0.44
A	$1100Hz$	29.9	0.36
A	$1000Hz$	31.6	0.22
B	$1400Hz$	36.3	1.00
B	$1300Hz$	38.5	0.98
B	$1200Hz$	33.2	0.54
B	$1100Hz$	34.6	0.43
B	$1000Hz$	36.3	0.33
C	$1700Hz$	31.8	1.36
C	$1600Hz$	30.5	1.10
C	$1500Hz$	31.0	0.72
C	$1400Hz$	31.0	0.45
C	$1300Hz$	30.9	0.51
C	$1200Hz$	32.2	0.45
C	$1100Hz$	33.8	0.27
C	$1000Hz$	35.7	0.18

Table 2: α^2 for different f_n for the smallest possible separation r_s for models A,B and C.

Model	$f_n(Hz)$	$r_s(km)$	a^2
D	$2600Hz$	20.9	2.53
D	$2400Hz$	21.3	1.99
D	$2200Hz$	22.0	1.54
D	$2000Hz$	23.1	1.06
D	$1800Hz$	24.4	0.82
D	$1600Hz$	26.1	0.45
D	$1400Hz$	28.3	0.26
D	$1200Hz$	31.0	0.14
D	$1000Hz$	34.7	0.07
E	$4200Hz$	19.0	5.95
E	$3800Hz$	19.0	6.09
E	$3400Hz$	20.0	5.42
E	$3000Hz$	19.0	2.26
E	$2600Hz$	19.2	2.28
E	$2200Hz$	21.1	0.88
E	$1800Hz$	23.8	0.38
E	$1400Hz$	27.7	0.14
E	$1000Hz$	34.3	0.03

Table 3: α^2 for different f_n for the smallest possible separation r_s for models D and E.

6.2 Results for a Neutron Star-Point Mass binary

We will now change the configuration slightly. Instead of having a binary consisting of two identical neutron stars, we will consider a binary consisting of a neutron star and a point mass. This allows us to get even closer than before and matches better with the work from which the 5 models and their tidally induced oscillation's frequencies originated [25]. If we consider identical masses, as we did up to this point, nothing really changes in the calculations, except for the theoretical limit of the innermost stable circular orbit, which is now the relativistic $r_{ISCO} = 6M = 12.6km$.

Allowing the separation to take such small values, reveals an interesting new area of separations for which D becomes positive again. To demonstrate this we are going to use Model A's parameters $(m_1 = m_2 = m, R, n, \omega_n)$ and display the $\omega(r)$ relations once again.

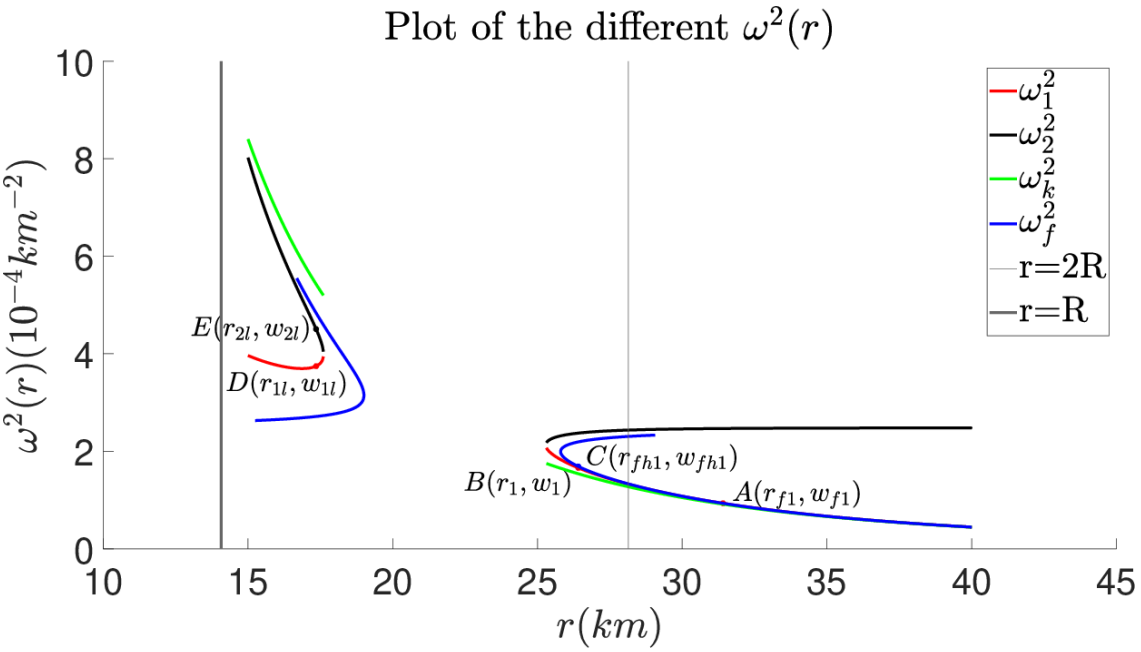

Figure 11: Plot of the different $\omega^2(r)$ for model A , where the black line is the "-" solution of 57, the red is the "+" solution, Flanagan-Hinderer's in blue and Kepler's in green. We also display the horizontal lines r=R and r=2R where R is the neutron star's radius, to visualize how close we let the two objects get.

We may have disregarded the "-" relation in the previous analysis, but that was true only for the right side of this plot. On the left side, the "-" solution seems more realistic than the "+" solution as it converges with both Flanagan-Hinderer's and Kepler's.

Having found no instabilities on the right side of the plot, we wish to check if this new left sector contains any. We pick 5 points, i.e. 5 couples of r, ω for which we will plot the $Det(\Omega^2)$ once again. This points include: (i) Point $A(r_{1f}, \omega_{1f})$ in the "+" solution but for a relatively higher separation (this checks that the "far away" solution is still for $\alpha^2 = 1$), (ii)point $B(r_1, \omega_1)$ in the "+" solution but for a separation close to the last achievable on the right side, (iii)point $C(r_{fh}, \omega_{fh})$ in Flanagan-Hinderer's relation for the exact same separation as point B (for comparison), (iv)point $D(r_{1l}, \omega_{1l})$ in the "+" solution for a separation close to the largest achievable on the left side and (v)point $E(r_{2l}, \omega_{2l})$ in the "-" solution for the same separation with point D.

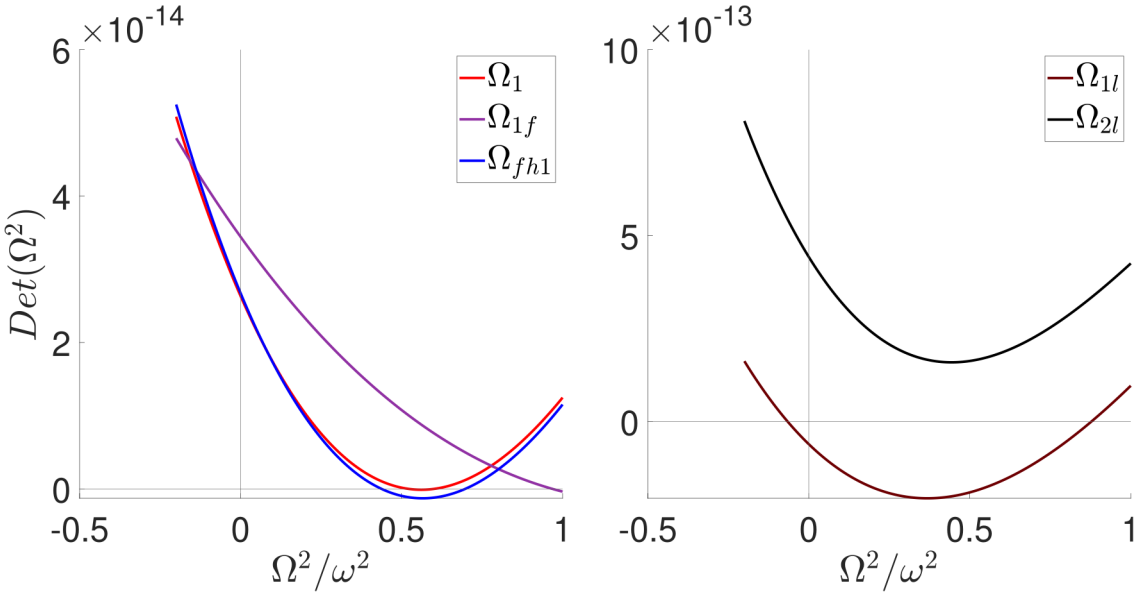

Figure 12: A plot of the polynomial 56 for model A, focused around 0, for points A,B & C on the left and D & E on the right.

The left plot shows us once again, that no instabilities are present in the right sector of the $\omega(r)$ plots, however on the left side ,the "+" solution $D(r_{1l}, \omega_{1l})$ has a negative root, i.e. it is unstable. The "-" solution $E(r_{2l}, \omega_{2l})$ is again stable, and it's first root is not visible on the plot ($\alpha^2 > 2$). We follow the same steps for every model and the resulting plots are given below:

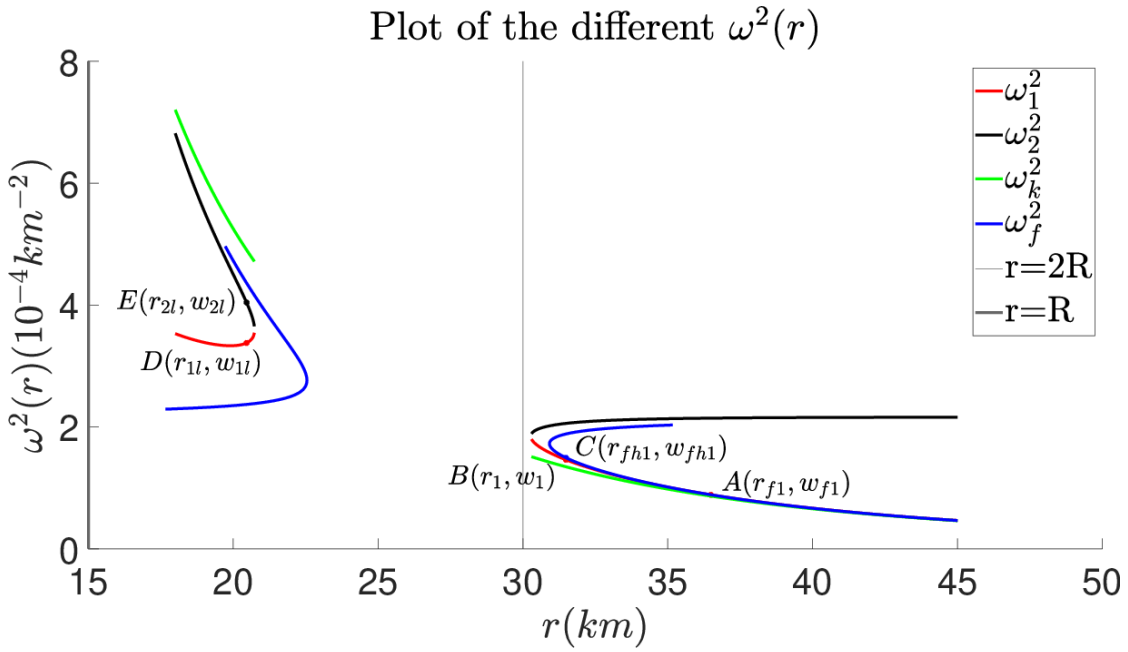

Figure 13: Plot of the different $\omega^2(r)$ for model B, where the black line is the "-" solution of 57, the red is the "+" solution, Flanagan-Hinderer's in blue and Kepler's in green. .

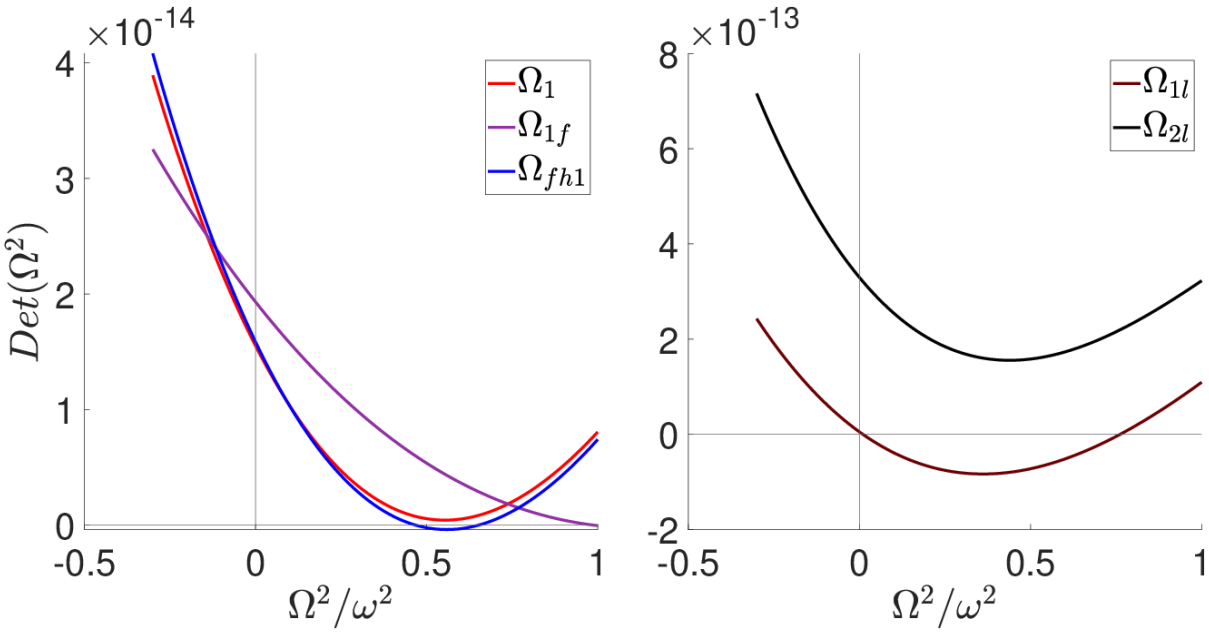

Figure 14: A plot of the polynomial 56 for model B, focused around 0, for points A,B & C on the left and D & E on the right.

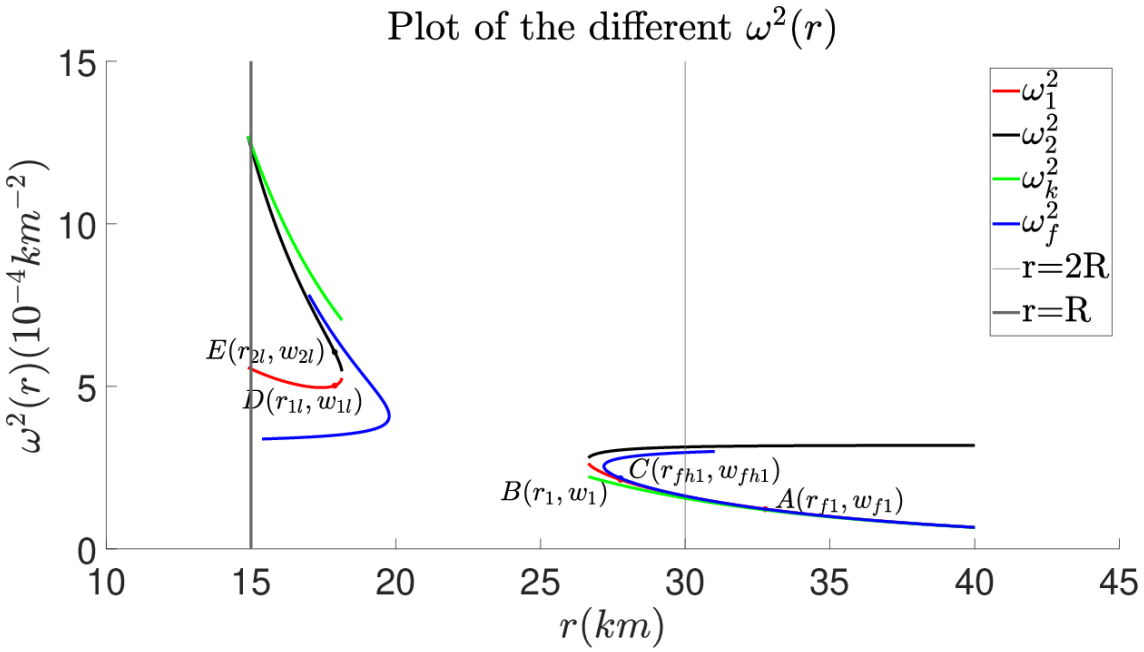

Figure 15: Plot of the different $\omega^2(r)$ for model C, where the black line is the "-" solution of 57, the red is the "+" solution, Flanagan-Hinderer's in blue and Kepler's in green. .

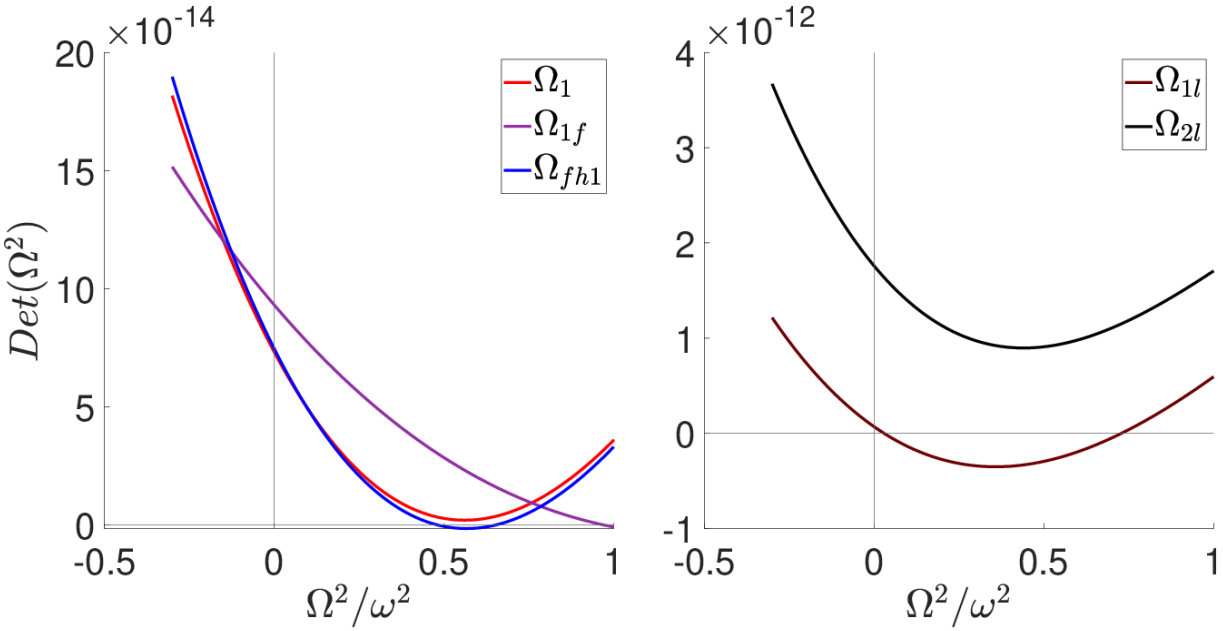

Figure 16: A plot of the polynomial 56 for model C, focused around 0, for points A,B & C on the left and D & E on the right.

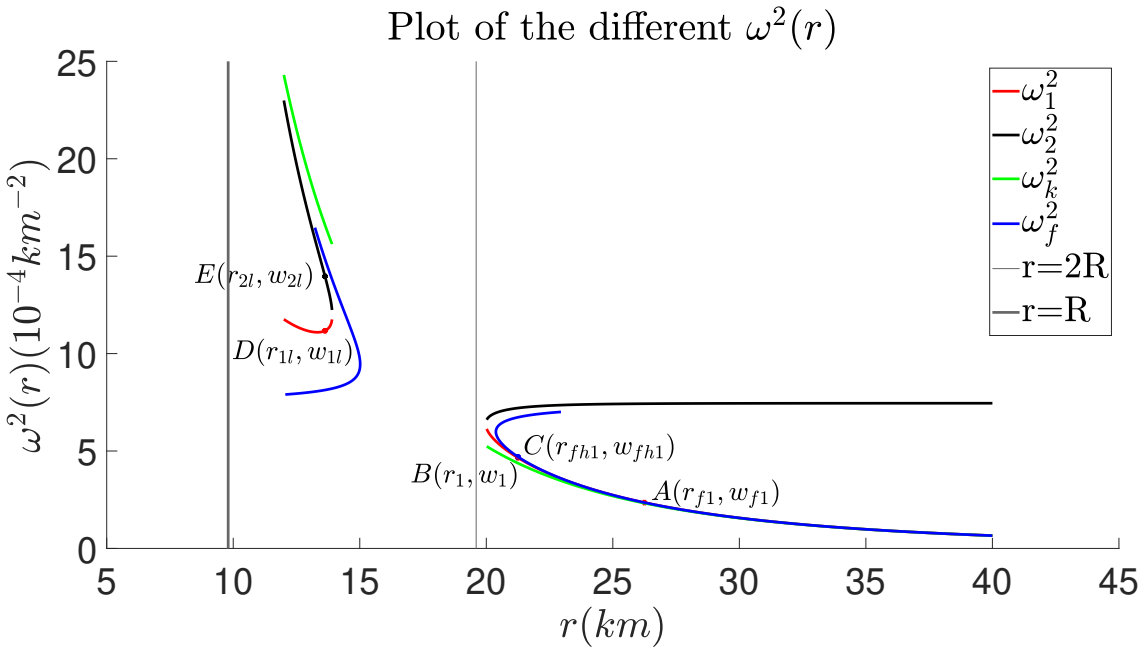

Figure 17: Plot of the different $\omega^2(r)$ for model D, where the black line is the "-" solution of 57, the red is the "+" solution, Flanagan-Hinderer's in blue and Kepler's in green. .

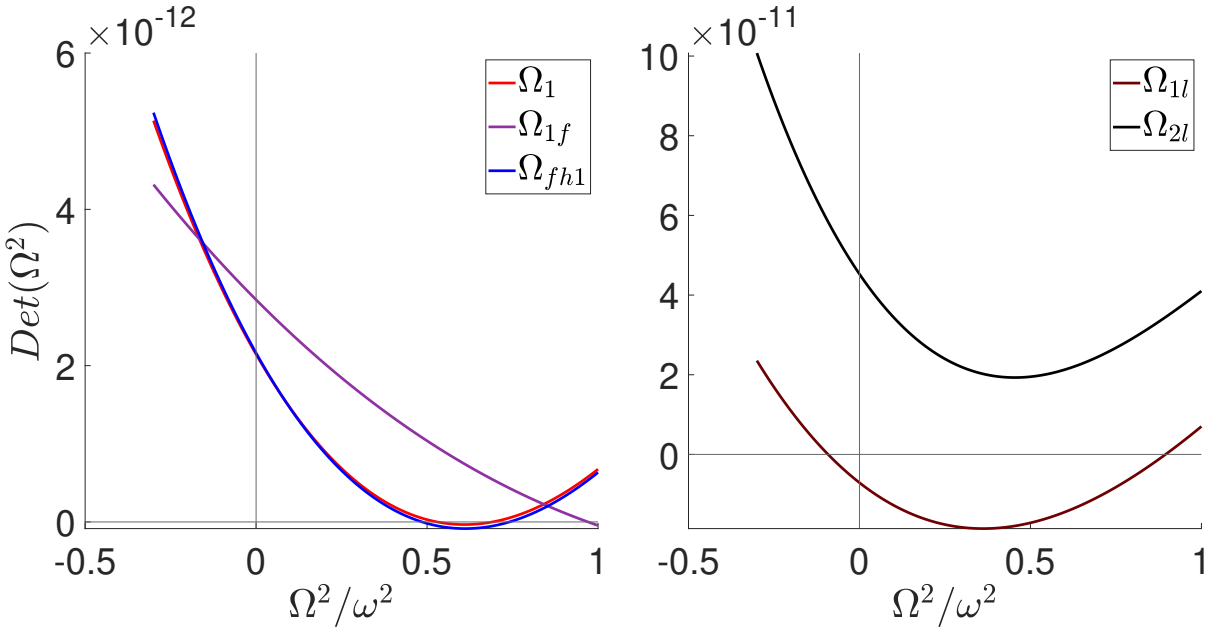

Figure 18: A plot of the polynomial 56 for model D, focused around 0, for points A,B & C on the left and D & E on the right.

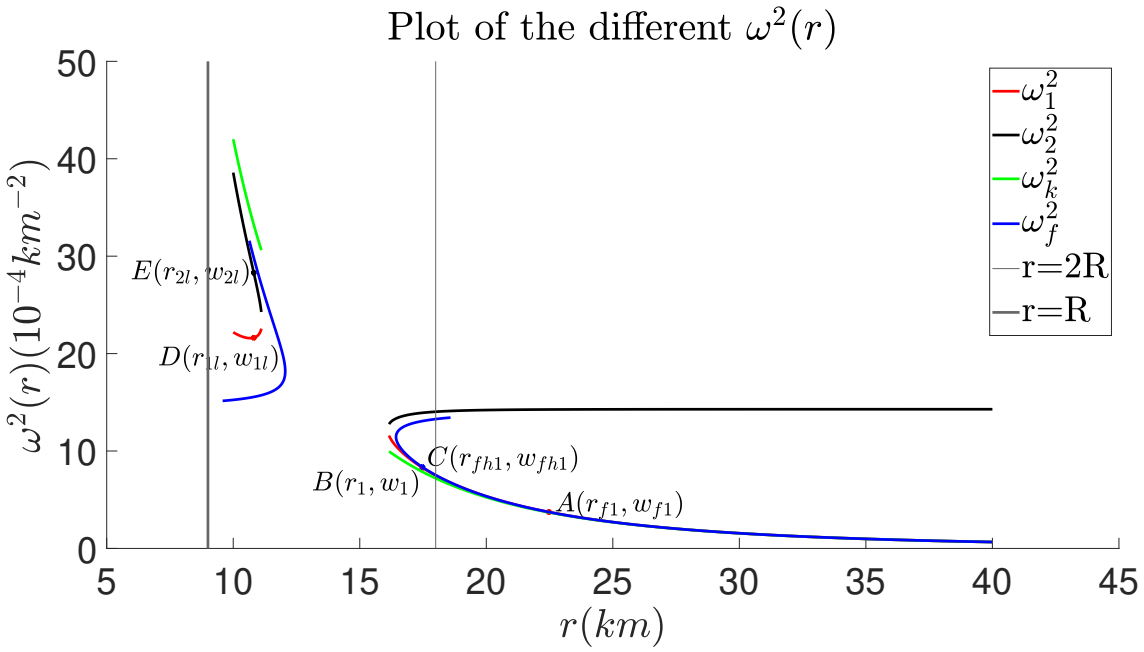

Figure 19: Plot of the different $\omega^2(r)$ for model E, where the black line is the "-" solution of 57, the red is the "+" solution, Flanagan-Hinderer's in blue and Kepler's in green. .

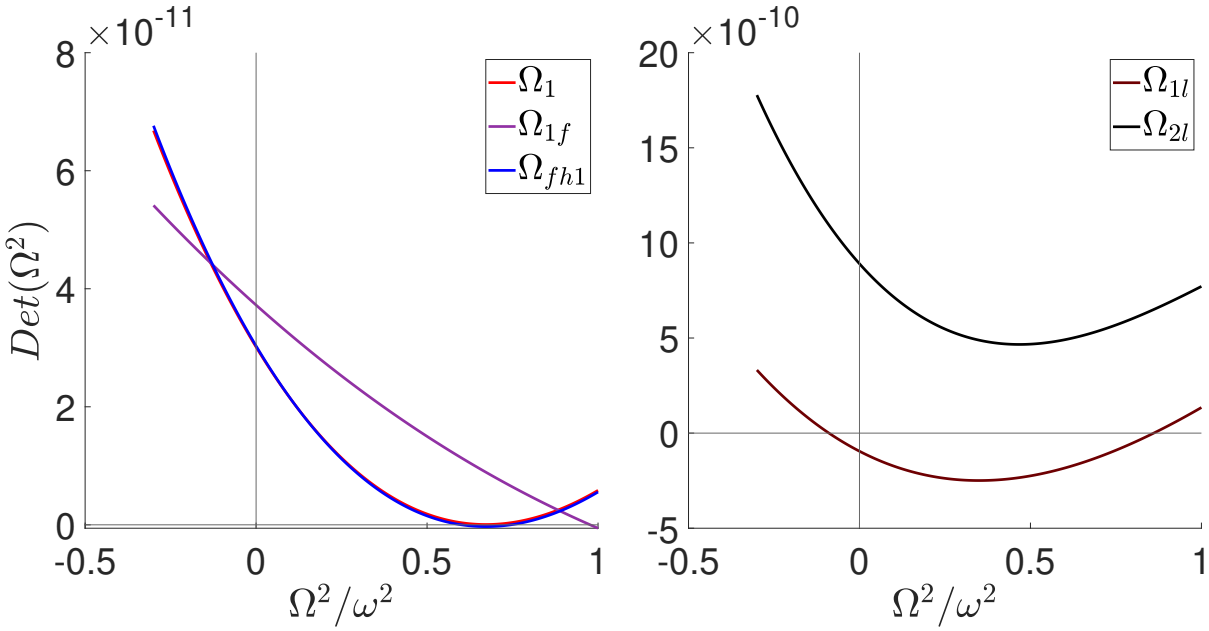

Figure 20: A plot of the polynomial 56 for model E, focused around 0, for points A,B & C on the left and D & E on the right.

Most models repeat the same pattern with model A,i.e. an unstable point D (or close to instability for models B and C) in the left side ω_1 and a stable point E in the left side of ω_2. Model E's instability is found in a separation smaller than $r < 6M = 12.6km$. These instabilities, even though they appeared, they might as well be unrealistic if ω_1 must be disregarded for the left sector just as ω_2 was disregarded in the right one. Of course, the same limitations of not using general relativity and dissipation terms still apply.

We will now repeat the process for smaller love numbers, from the erratum of [15]. For the models B and D we have the exact love numbers and we will use those, but for the rest, we do not have an exact k_2 from the tables, as a result we will use the differences we calculated (see appendix A) to predict how much smaller the real k_2 should be, compared to the fitted one. For simplicity, the tidal love numbers we are going to use for each model is listed below, along with the $Det(\Omega^2)$ plots for each one.

Model	k2	% Of the fitted
A*	0,0603	50
B	0,0776	
C*	0,0482	40
D	0,0253	
E*	0,0241	20

Table 4: List of the smaller tidal love numbers we are going to use. Models with a * indicate that their values are an expected % of what the fitted value is based on the Appendix A's difference percentages of the respective M/R ratios.

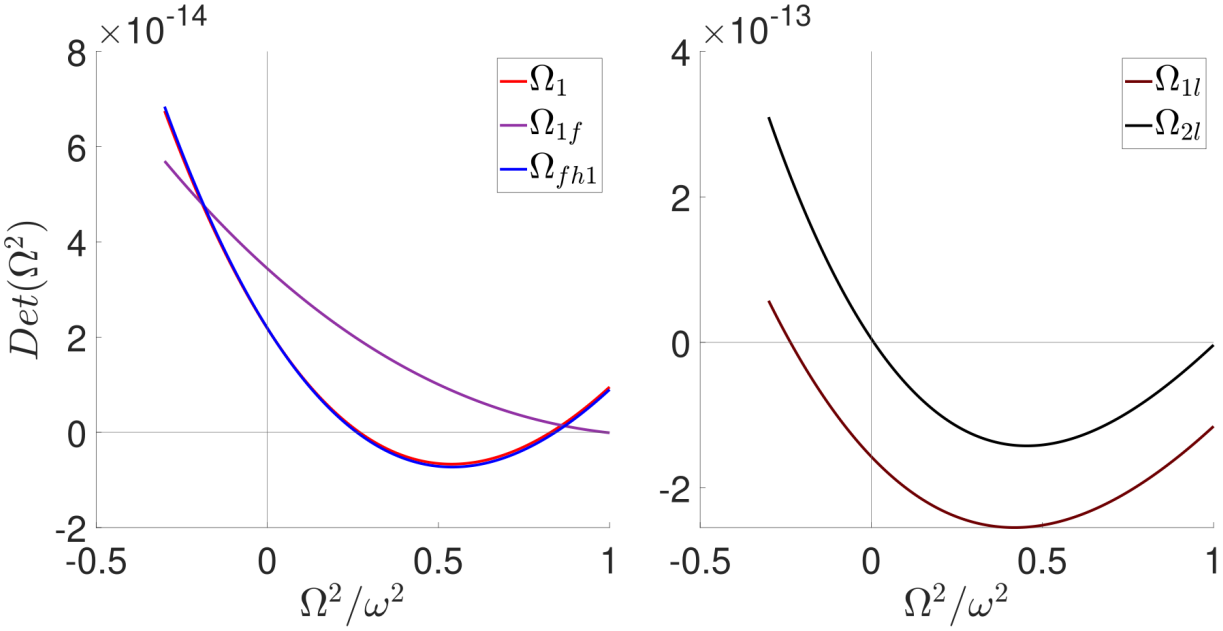

Figure 21: A plot of the polynomial 56 for model A, for $k_2 = 50\%$ of the fitted, focused around 0, for points A,B & C on the left and D & E on the right.

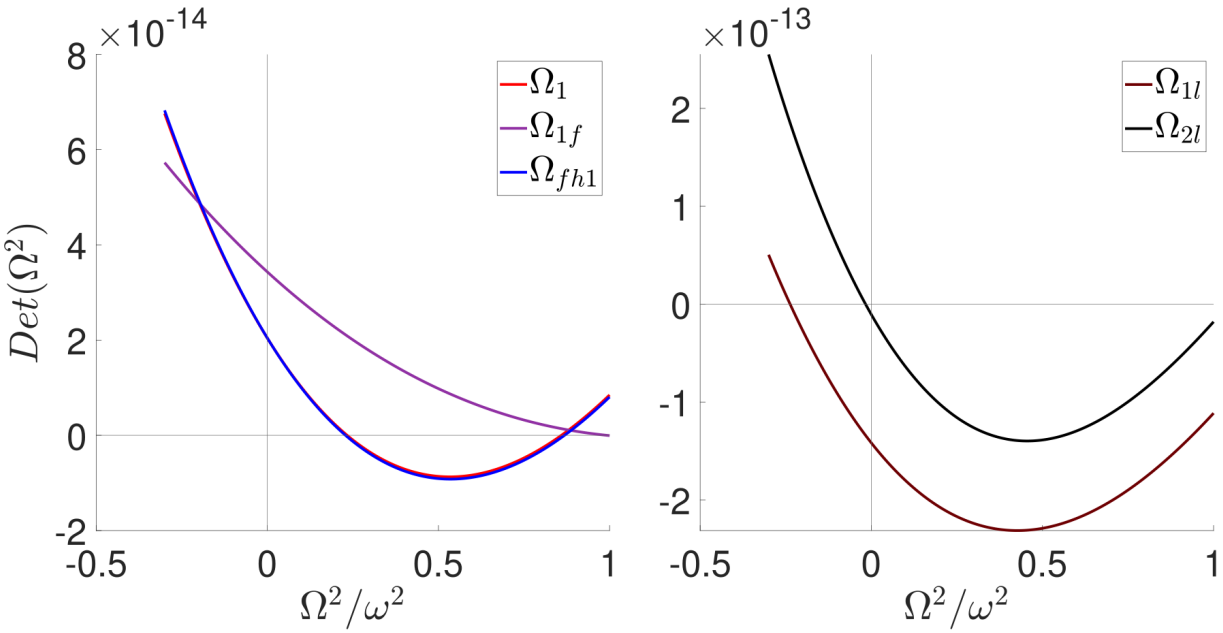

Figure 22: A plot of the polynomial 56 for model A,for $k_2 = 40\%$ of the fitted (just for comparison), focused around 0, for points A,B & C on the left and D & E on the right.

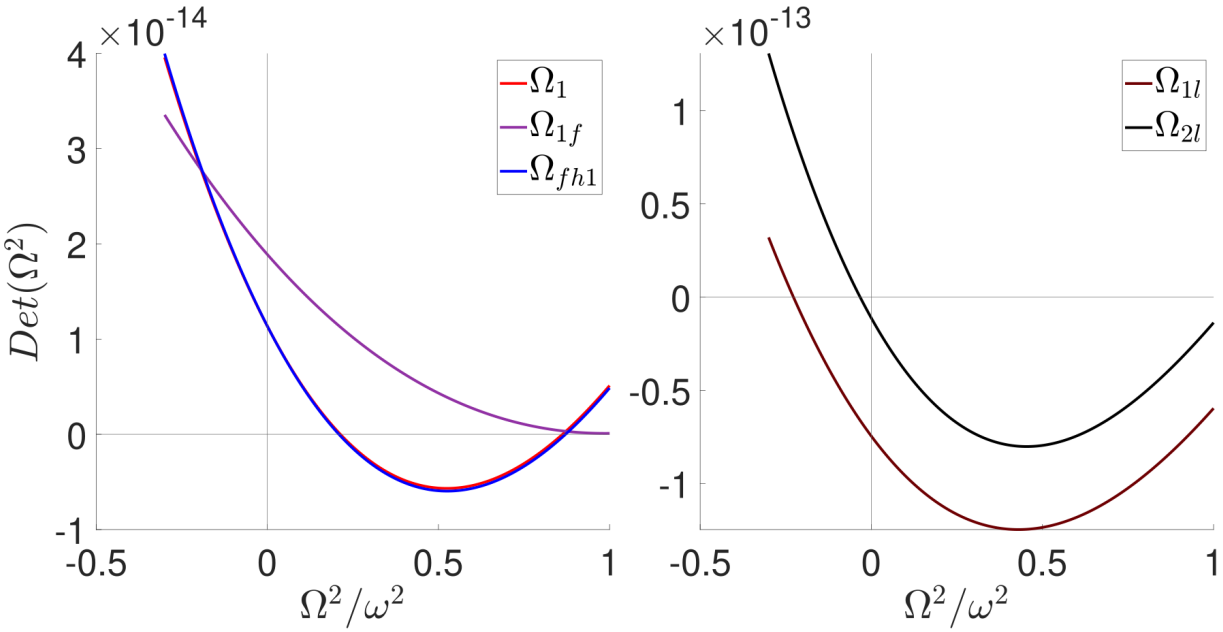

Figure 23: A plot of the polynomial 56 for model B, for $k_2 = 0.0776$, focused around 0, for points A,B & C on the left and D & E on the right.

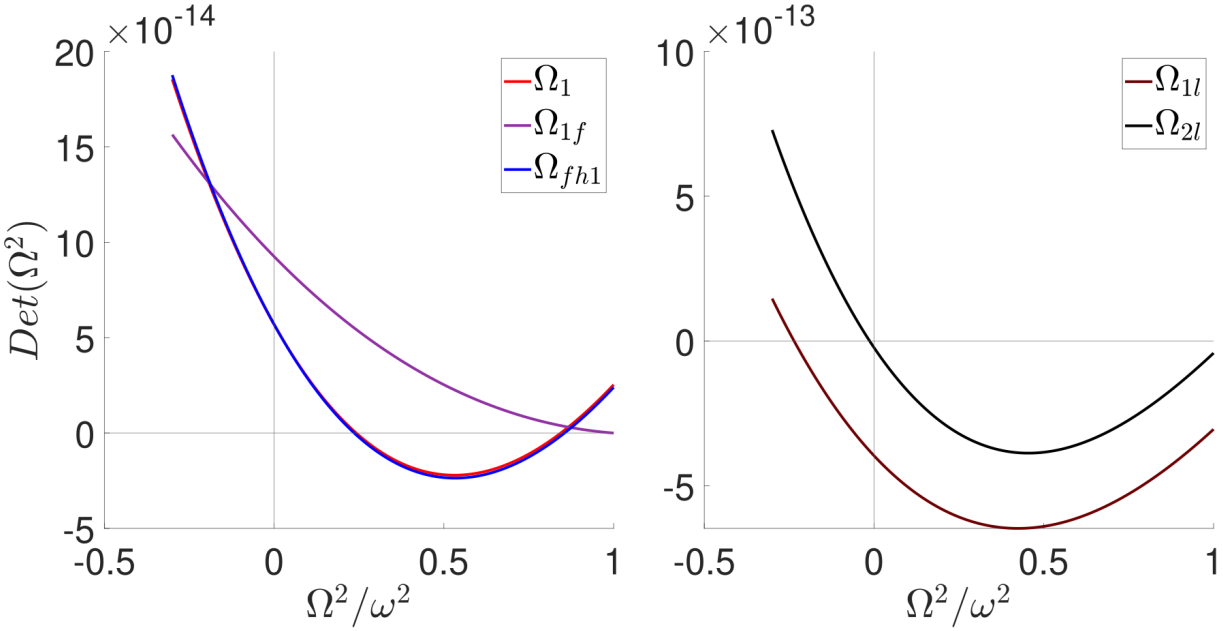

Figure 24: A plot of the polynomial 56 for model C, for $k_2 = 40\%$ of the fitted, focused around 0, for points A,B & C on the left and D & E on the right.

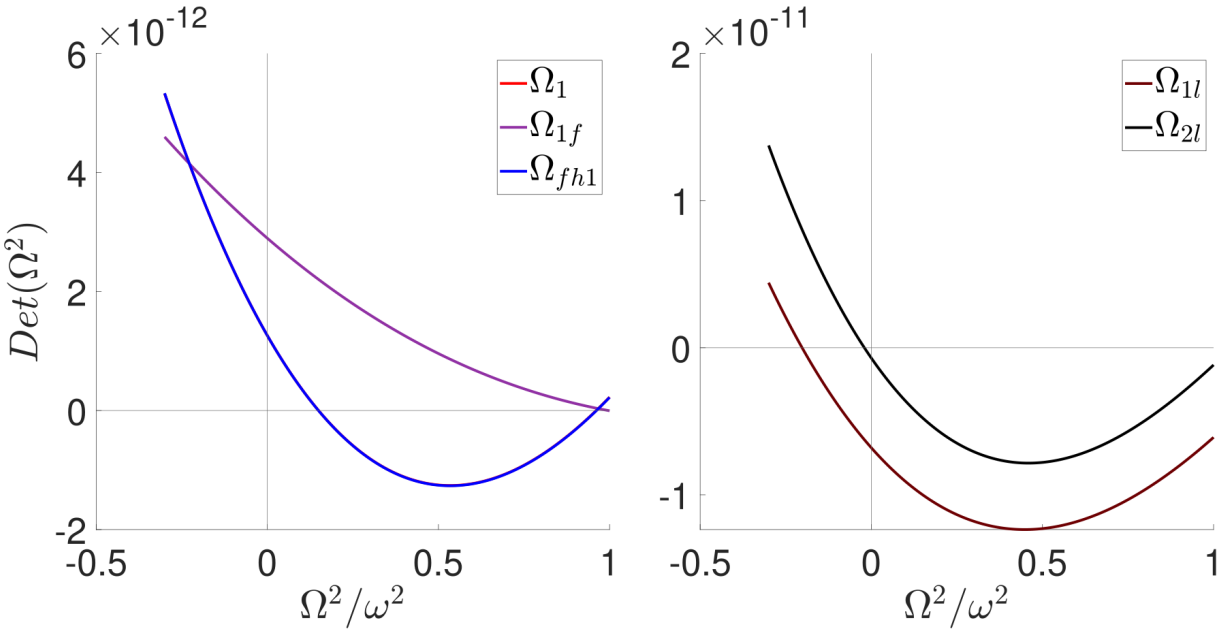

Figure 25: A plot of the polynomial 56 for model D, for $k_2 = 0.0253$, focused around 0, for points A,B & C on the left and D & E on the right.

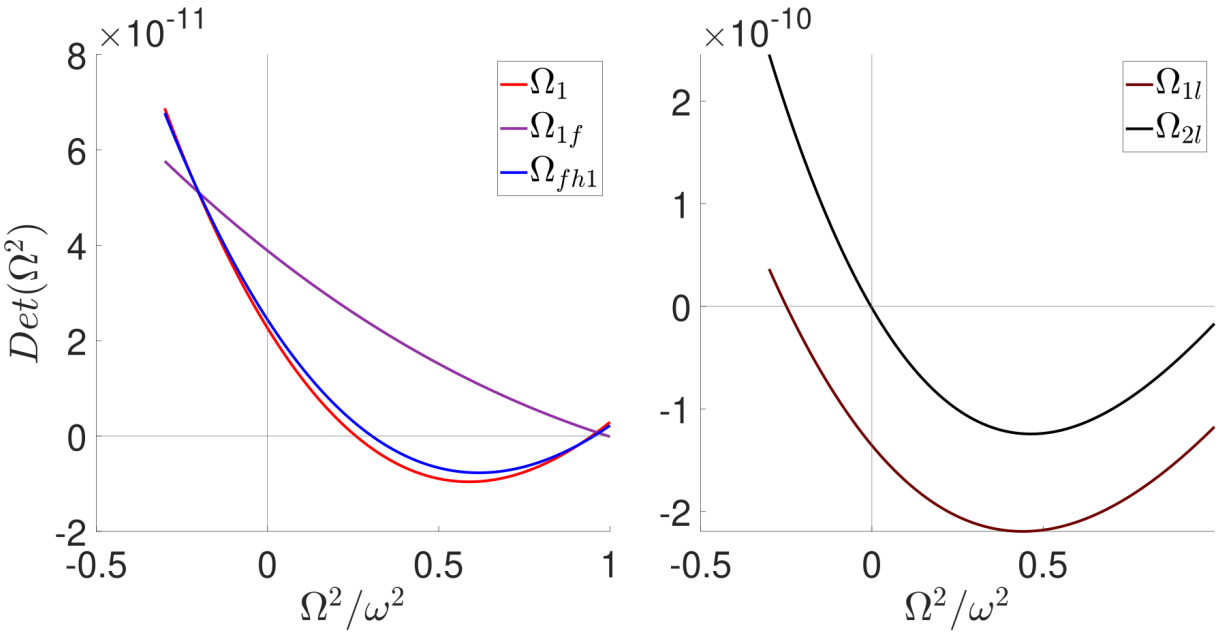

Figure 26: A plot of the polynomial 56 for model E, for $k_2 = 20\%$ of the fitted, focused around 0, for points A,B & C on the left and D & E on the right.

Again, the right side points A,B and C do not show any instabilities. However, it is clear that for the smaller values of the tidal love numbers, the left side's points D and E are both unstable for all models except model A, which can still be unstable for a slightly smaller love number ($k_2 = 40\%$ of the fitted, as seen in figure 22). Even though we found some instabilities, these exist in absurdly small separations, where the ignored effects, not only shouldn't be ignored, but they are the main driving factors of the binary's evolution.

6.3 Combining everything: The case of Model D

We will now combine what we did for model D in 6.2, but we will also lower the frequency like we did in 6.1, as a last attempt to find instabilities for BNSs that happen before the system reaches the ISCO. We will take all the parameters from 3 for model D, set $f_n = 1000Hz$ and use the exact $k_2 = 0.0253$ from [15]. For these parameters the ISCO should be around $f = 750Hz$ or even higher [27] let's assume the quasi-circular orbits could get to $f = 1000Hz$ ($\omega^2 = 1.1 \cdot 10^{-4}$), before stopping. The resulting plots are:

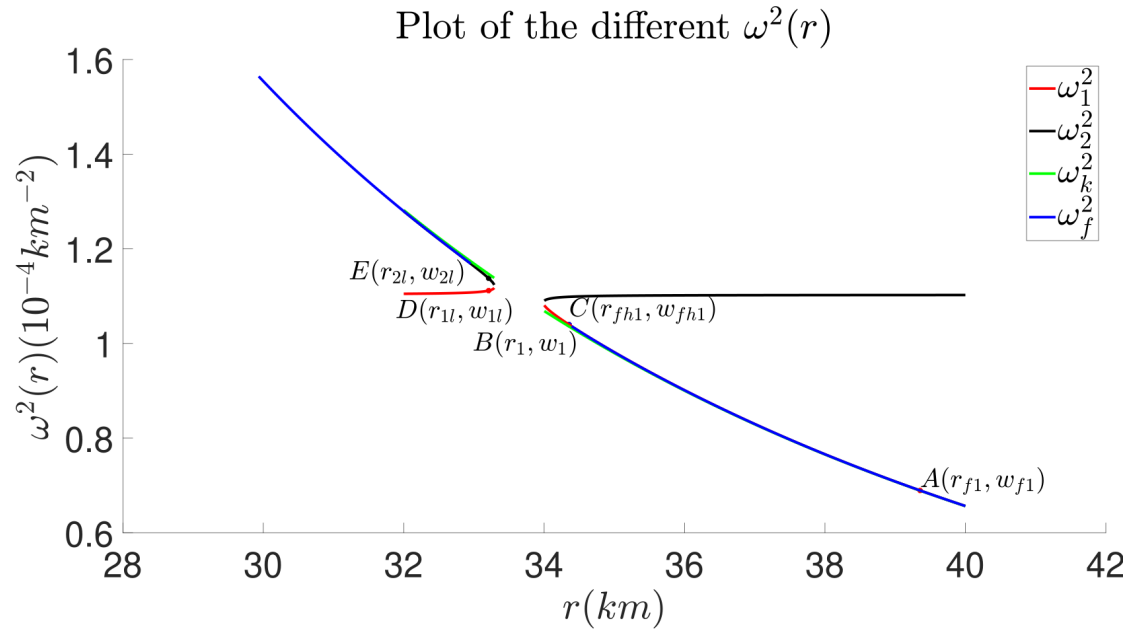

Figure 27: Plot of the different $\omega^2(r)$ for model D, for $k_2 = 0.0253$ and $f_n = 1000Hz$, where the black line is the "-" solution of 57, the red is the "+" solution, Flanagan-Hinderer's in blue and Kepler's in green. .

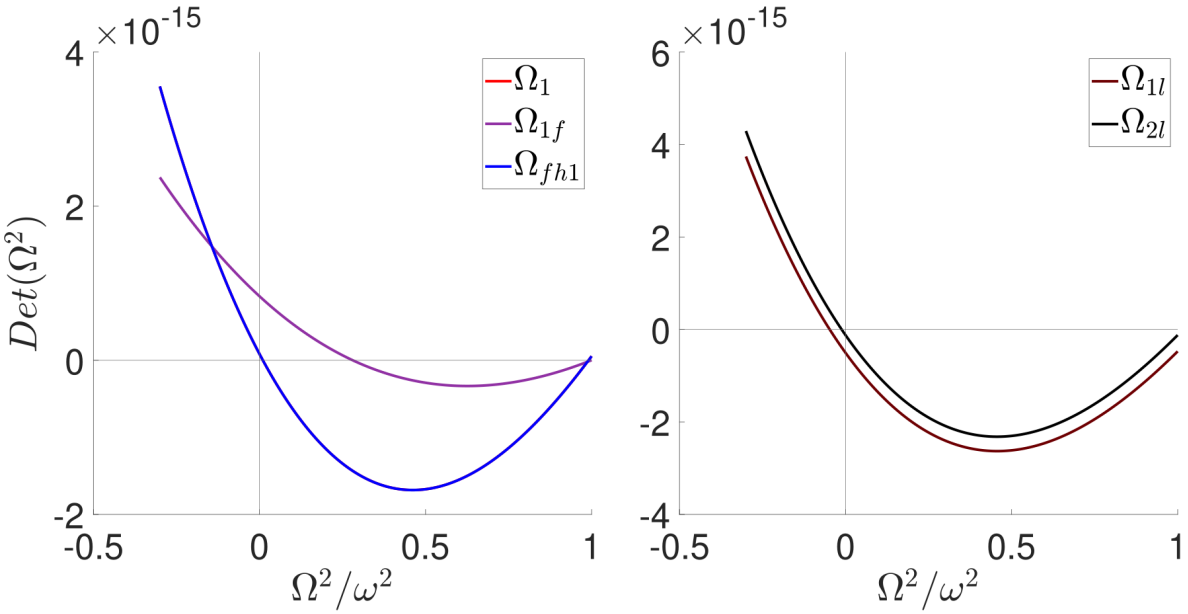

Figure 28: A plot of the polynomial 56 for model D, for $k_2 = 0.0253$ and $f_n = 1000Hz$, focused around 0, for points A,B & C on the left and D & E on the right.

Once again, points A,B & C do not show any instabilities. Points D & E on the other hand are both unstable. However even with all these assumptions, this instability is quite meaningless, as the moment it appears, we reach ISCO (if we haven't passed it already) and the circular orbits stop.

7 Conclusion

In this work, we checked if tidally induced instabilities can appear during the inspiral phase of a binary neutron star's evolution. We assumed small perturbations on the quasi-circular orbits for a binary of two identical neutron stars. Damping effects from gravitational waves or viscosity, along with general relativity corrections were ignored in the inspiral phase. The equation of state models along with the single, assumed, oscillating node's frequency were taken from a similar work [25]. Of the 5 models checked, (figures 3 & 10), for different $\omega(r)$ relations ($\omega_1, \omega_2, \omega_{fh}, \omega_k$), no instability was found in the inspiral phase and we were only able to reinforce the assumption that the bulge faces the companion star[13], as the angle's oscillations for larger frequencies had the same frequency with the motion ($\alpha^2 = 1$ for large separations). We even checked after the inspiral phase, continuing to ignore damping and relativistic effects, which are non-negligible in this phase of the evolution , in an attempt to find instabilities closer to the resonance (where the terms $(1 - 4x_n^2) \sim 0$). However, no instability was found, no matter how close we got to resonance. The perturbation's frequency (Ω^2) closed in on 0 , without ever becoming negative (see tables 2 & 3). This was a shared behaviour among all 5 models and for substantially lowered oscillating shell's frequencies (ω_n), down to a minimum of $f_n = 1000Hz$.

We then replaced the BNS with a Neutron Star-Point Mass binary and searched for instabilities in every possible separation, again ignoring damping and relativistic effects. In this setting a new sector appeared in the $\omega(r)$ plots, that didn't appear thus far, as it was in separations smaller than $2R$ (where the BNS companion's surfaces touch). In this new sector, instabilities did appear, but only for an $\omega(r)$ relation that we think should be considered unrealistic (ω_1 on the left sector in figure 11), as it's behaviour is odd and doesn't agree with Kepler's and Flanagan-Hinderer's when the tidal deformability (λ) is reduced (see 27). Due to an erratum for [15], we repeated this whole process with new love numbers that were substantially smaller (see table 4). Specifically we took the available love numbers from Hinderer's corrected tables for $n = 1.0$ and attempted to predict how much smaller would a realistic k_2 be compared to the fitted one (see Appendix A). Using these love numbers and for realistic oscillation frequencies for all models, we found instabilities for models B,C,D for both ω_1 & ω_2 relations on the left sector of the figures. Model E, was also unstable but for a separation smaller than the relativistic ISCO ($r < 6M = 12.6km$).

Lastly we attempted to combine the latter two, to search for instabilities that could perhaps arise, before the ISCO for a BNS. Model D was chosen as the best candidate. With $M/R = 0.21$ (Figure 3), $k_2 = 0.0253$[15] and for a substantially lowered tidally induced oscillation's frequency ($f_n = 1000Hz$), the same instabilities appeared on the left side for both ω_1 & ω_2. However, even if we assume that the system could still be orbiting quasi-circularly in frequencies this close to resonance ($f = 1000Hz$), the instability happens at the same time we reach the ISCO and the system stops orbiting quasi-circularly. In other words, we found that even in these unrealistic conditions, elliptical orbits can appear, but this happens exactly when orbits stop being circular anyway.

References

[1] LIGO Scientific Collaboration [LSC]. *THE SENSITIVITY OF THE ADVANCED LIGO DETECTORS AT THE BEGINNING OF GRAVITATIONAL WAVE ASTRONOMY*. URL: https://www.ligo.org/science/Publication-O1Noise/index.php.

[2] B. P. Abbott et al. "GW170817: Observation of Gravitational Waves from a Binary Neutron Star Inspiral". In: *Physical review letters* 119.16 (Oct. 2017). DOI: 10.1103/physrevlett.119.161101. URL: https://doi.org/10.1103/physrevlett.119.161101.

[3] Tiziano Abdelsalhin. *Tidal deformations of compact objects and gravitational wave emission*. 2019. arXiv: 1905.00408.

[4] F Acernese et al. "Dynamic matched filters for gravitational wave detection". In: *Classical and quantum gravity* 21.20 (Sept. 2004), S1849–S1854. DOI: 10.1088/0264-9381/21/20/028. URL: https://doi.org/10.1088/0264-9381/21/20/028.

[5] Theocharis Apostolatos et al. "Gravitational radiation from a particle in circular orbit around a black hole. III. Stability of circular orbits under radiation reaction". In: *Physical review. D. Particles, fields, gravitation, and cosmology/Physical review. D. Particles and fields* 47.12 (June 1993), pp. 5376–5388. DOI: 10.1103/physrevd.47.5376. URL: https://doi.org/10.1103/physrevd.47.5376.

[6] M. Bejger et al. "Impact of the nuclear equation of state on the last orbits of binary neutron stars". In: *Astronomy & astrophysics* 431.1 (Feb. 2005), pp. 297–306. DOI: 10.1051/0004-6361:20041441. URL: https://doi.org/10.1051/0004-6361:20041441.

[7] Taylor Binnington and Eric Poisson. "Relativistic theory of tidal Love numbers". In: *Physical review. D. Particles, fields, gravitation, and cosmology/Physical review. D, Particles, fields, gravitation, and cosmology* 80.8 (Oct. 2009). DOI: 10.1103/physrevd.80.084018. URL: https://doi.org/10.1103/physrevd.80.084018.

[8] William E. Boyce and Richard C. DiPrima. *Elementary differential equations and boundary value problems*. Wiley, Dec. 2012.

[9] Patrick Brady, Giovanni Losurdo, and Hisaaki Shinkai. *LIGO, VIRGO, and KAGRA as the International Gravitational Wave Network*. Jan. 2021, pp. 1–21. DOI: 10.1007/978-981-15-4702-7\{_}51-1. URL: https://doi.org/10.1007/978-981-15-4702-7_51-1.

[10] Katerina Chatziioannou. "Neutron-star tidal deformability and equation-of-state constraints". In: *General relativity and gravitation* 52.11 (Nov. 2020). DOI: 10.1007/s10714-020-02754-3. URL: https://doi.org/10.1007/s10714-020-02754-3.

[11] Horng Sheng Chia. "Tidal deformation and dissipation of rotating black holes". In: *Physical review. D/Physical review. D.* 104.2 (July 2021). DOI: 10.1103/physrevd.104.024013. URL: https://doi.org/10.1103/physrevd.104.024013.

[12] Einstein. "Über Gravitationswellen". In: *Zenodo (CERN European Organization for Nuclear Research)* (Jan. 1918). DOI: 10.5281/zenodo.5442768. URL: https://zenodo.org/record/5442768.

[13] Éanna É. Flanagan and Tanja Hinderer. "Constraining neutron-star tidal Love numbers with gravitational-wave detectors". In: *Physical review. D. Particles, fields, gravitation, and cosmology/Physical review. D, Particles, fields, gravitation, and cosmology* 77.2 (Jan. 2008). DOI: 10.1103/physrevd.77.021502. URL: https://doi.org/10.1103/physrevd.77.021502.

[14] Herbert Goldstein, Charles P. Poole, and John L. Safko. *Classical Mechanics*. Addison-Wesley Longman, Jan. 2002.

[15] Tanja Hinderer. "Tidal love numbers of neutron stars". In: *Astrophysical journal/The Astrophysical journal* 677.2 (Apr. 2008), pp. 1216–1220. DOI: 10.1086/533487. URL: https://doi.org/10.1086/533487.

[16] V. S. Imshennik and D. V. Popov. "Evolution of eccentric orbits of neutron star binaries emitting gravitational waves". In: *AstL* 20.5 (Sept. 1994), pp. 529–537. URL: http://ui.adsabs.harvard.edu/abs/1994AstL...20..529I/abstract.

[17] Petros Ioannou and Theocharis Apostolatos. *Elements of Theoretical mechanics(Textbook in Greek)*. 2nd ed. University of Athens, 2007.

[18] T. W. B. Kibble and Frank H. Berkshire. *Classical Mechanics*. Imperial College Press, Jan. 2004.

[19] L D Landau and E.M. Lifshitz. *Mechanics*. Elsevier, Jan. 1976.

[20] Charles W. Misner, Kip S. Thorne, and John Archibald Wheeler. *Gravitation*. Princeton University Press, Oct. 2017.

[21] Stephen O'Sullivan and Scott A. Hughes. "Strong-field tidal distortions of rotating black holes. II. Horizon dynamics from eccentric and inclined orbits". In: *Physical review. D/-Physical review. D.* 94.4 (Aug. 2016). DOI: 10.1103/physrevd.94.044057. URL: https://doi.org/10.1103/physrevd.94.044057.

[22] Stephen O'Sullivan and Scott A. Hughes. "Strong-field tidal distortions of rotating black holes: Formalism and results for circular, equatorial orbits". In: *Physical review. D. Particles, fields, gravitation, and cosmology/Physical review. D, Particles, fields, gravitation, and cosmology* 90.12 (Dec. 2014). DOI: 10.1103/physrevd.90.124039. URL: https://doi.org/10.1103/physrevd.90.124039.

[23] Roger Penrose. "Gravitational collapse and Space-Time singularities". In: *Physical review letters* 14.3 (Jan. 1965), pp. 57–59. DOI: 10.1103/physrevlett.14.57. URL: https://doi.org/10.1103/physrevlett.14.57.

[24] P. C. Peters and J. Mathews. "Gravitational Radiation from Point Masses in a Keplerian Orbit". In: *Physical review* 131.1 (July 1963), pp. 435–440. DOI: 10.1103/physrev.131.435. URL: https://doi.org/10.1103/physrev.131.435.

[25] J. A. Pons et al. "Gravitational signals emitted by a point mass orbiting a neutron star: Effects of stellar structure". In: *Physical review. D. Particles, fields, gravitation, and cosmology/Physical review. D. Particles and fields* 65.10 (May 2002). DOI: 10.1103/physrevd.65.104021. URL: https://doi.org/10.1103/physrevd.65.104021.

[26] Virginia Trimble. "WIRED BY WEBER: the story of the first searcher and searches for gravitational waves". In: *Bulletin of the American Physical Society* 2017 (Jan. 2017). URL: http://absimage.aps.org/image/APR17/MWS_APR17-2016-000089.pdf.

[27] Kōji Uryū, Masaru Shibata, and Yoshiharu Eriguchi. "Properties of general relativistic, irrotational binary neutron stars in close quasiequilibrium orbits: Polytropic equations of state". In: *Physical review. D. Particles, fields, gravitation, and cosmology/Physical review. D. Particles and fields* 62.10 (Oct. 2000). DOI: 10.1103/physrevd.62.104015. URL: https://doi.org/10.1103/physrevd.62.104015.

[28] N. Vlahakis. *Fluid Dynamics(in Greek)*. Publisher Papazissis, 2019.

[29] Yanyan Zheng et al. "A Needle in (Many) Haystacks: Using the False Alarm Rate to Sift Gravitational Waves from Noise". In: *Significance* 18.1 (Feb. 2021), pp. 26–31. DOI: 10.1111/1740-9713.01488. URL: https://doi.org/10.1111/1740-9713.01488.

A The love numbers for different polytropic NS models

n	M/R	k_2 (erratum)	k_2 (fitted)	diff (%)	k_2 (pre erratum)	k_2 (fitted)	diff (%)
0,3	0,10	0,2940	0,6392	54,00	0,5401	0,6392	15,50
0,3	0,15	0,2010	0,6384	68,51	0,5691	0,6384	10,85
0,3	0,20	0,1190	0,6378	81,34	0,6146	0,6378	3,64
0,3	0,25		0,6374			0,6374	
0,5	0,10	0,2300	0,4439	48,19	0,4260	0,4439	4,04
0,5	0,15	0,1580	0,4434	64,37	0,4349	0,4434	1,92
0,5	0,20	0,0950	0,4430	78,56	0,4489	0,4430	-1,33
0,5	0,25	0,0569	0,4427	87,15	0,4589	0,4427	-3,65
0,7	0,10	0,1779	0,3322	46,45	0,3373	0,3322	-1,53
0,7	0,15	0,1171	0,3318	64,71	0,3369	0,3318	-1,53
0,7	0,20	0,0721	0,3315	78,25	0,3363	0,3315	-1,44
0,7	0,25	0,0420	0,3313	87,32	0,3267	0,3313	1,39
1,0	0,10	0,1220	0,2266	46,15	0,2405	0,2266	-6,15
1,0	0,15	0,0776	0,2263	65,71	0,2363	0,2263	-4,43
1,0	0,20	0,0459	0,2261	79,70	0,2282	0,2261	-0,93
1,0	0,25	0,0253	0,2259	88,81	0,2081	0,2259	7,89
1,2	0,10	0,0931	0,1772	47,45	0,1936	0,1772	-9,27
1,2	0,15	0,0577	0,1770	67,39	0,1900	0,1770	-7,37
1,2	0,20	0,0327	0,1768	81,50	0,1811	0,1768	-2,43
1,2	0,25		0,1767			0,1767	
1,5	0,10		0,1206			0,1206	
1,5	0,15		0,1205			0,1205	
1,5	0,20		0,1204			0,1204	
1,5	0,25		0,1203			0,1203	

Table 5: Tidal love numbers (k_2) from [15],before and after the erratum and their differences (%) from the fitting formula.

B The codes

We will now list the MATLAB codes used for the plots and calculations.

B.1 The main code

This the final version of the code we used for all the plots.

```
    clc;
clear all;
close all;
%Mass
m1=0.675*2.1;
m2=0.675*2.1;
m=m2;
M=m1+m2;
mu=m1*m2/M;
npoly=1.5; %Polytropic index
R=14.07; %Radius
k2=0.5*3/2* (-0.41+ (0.56/ (npoly^0.33)))* (m1/R)^ (-0.003); %tidal love number
%k2=2/3*0.0253; %declare a specific k2
l=2/3*R^5*k2; %tidal deformability
n=3.6*0.021; %oscillation frequency
NN=1000;
xi=linspace (-0.3,+1,NN); %adjust the plot values
per=6;%
split=1;%1 if you want to draw separate diagrams for w1l,w2l and 0 if you
```

```
% don't
%print -depsc EOmegaofr.eps
%print -depsc EDet.eps

drawomegaofr=1; %don't change this i broke it
rc=linspace (10,40,NN); %adjust the radius plot values
ii=1;
iii=1;
i4=1;

if drawomegaofr==1
Diakc=16*mu^2.*rc.^16.*n^4+256*M^2*mu^2.*rc.^10+128*mu^2*M.*rc.^13.*n^2 ...
+36*36*m2^4*l^2+8*36*mu*m2^2*l*n^2.*rc.^8+32*36*M*mu*m2^2*l.*rc.^5 ...
-64*mu.* (9*m2^2*l*n^2.*rc.^8+4*M*mu*n^2.*rc.^13+27*m2^2*l*n^2.*rc.^8);

Diaktsek=Diakc; %this is for checking D
for i=1:NN-1 %finds the parts where D is negative and removes them from the plot
    if Diakc(i)*Diakc(i+1)<0
        if Diakc(i)>0
            ii=i;
            r1c=rc(1:ii);
            for iii=ii:NN-1
                if Diakc(iii)*Diakc(iii+1)<0
                i4=iii+2;
                r2c=rc(i4:end);
                rc=cat(2,r1c,NaN,r2c);
                end

            end

        else
            ii=i+1;
            for iii=ii:NN-1
                if Diakc(iii)*Diakc(iii+1)<0
                i4=iii;
                rc=rc(ii:i4);
                end
            end
            if i4==1
                rc=rc(ii:end);
            end
        end
    end

    if ii==1
     rc=rc(ii:end);
    end

end
Diakc=16*mu^2.*rc.^16.*n^4+256*M^2*mu^2.*rc.^10+128*mu^2*M.*rc.^13.*n^2 ...
+36*36*m2^4*l^2+8*36*mu*m2^2*l*n^2.*rc.^8+32*36*M*mu*m2^2*l.*rc.^5 ...
-64*mu.* (9*m2^2*l*n^2.*rc.^8+4*M*mu*n^2.*rc.^13+27*m2^2*l*n^2.*rc.^8);
root=sqrt(Diakc);
w1c= (-4*mu.*rc.^8.*n^2-16*M*mu.*rc.^5-36*m2^2*l+root)./ (-32*mu.*rc.^8);
w2c= (-4*mu.*rc.^8.*n^2-16*M*mu.*rc.^5-36*m2^2*l-root)./ (-32*mu.*rc.^8);

wkc=M.*rc.^ (-3);
ac= (1-4.* (sqrt(w1c)/n).^2);

wtf1=linspace (min(w1c), (100-per)/100* (n^2/4),NN/2);
wtf2=linspace ( ( ( (100+per)/100)* (n^2/4)),1.4*max(w1c),NN/2);
```

```
wtf=[wtf1 ,NaN, wtf2 ];
atf= (1-4.* (wtf./ (n^2)));
rf=M^ (1/3).*sqrt (wtf).^ (-2/3)+3/4*l* (1+3./atf).*M^ (-4/3).*sqrt (wtf).^ (8/3);

%set the 5 different r's,omega's
r1=r2c (45); % first common for omega_1
Diak1=16*mu^2.*r1.^16.*n^4+256*M^2*mu^2.*r1.^10+128*mu^2*M.*r1.^13.*n^2 ...
+36*36*m2^4*l^2+8*36*mu*m2^2*l*n^2.*r1.^8+32*36*M*mu*m2^2*l.*r1.^5 ...
-64*mu.* (9*m2^2*l*n^2.*r1.^8+4*M*mu*n^2.*r1.^13+27*m2^2*l*n^2.*r1.^8);
root1=sqrt (Diak1);
w1=sqrt ( (-4*mu.*r1.^8.*n^2-16*M*mu.*r1.^5-36*m2^2*l+root1)./ (-32*mu.*r1.^8));

r1f=r1+5; % far for omega_1
Diak1f=16*mu^2.*r1f.^16.*n^4+256*M^2*mu^2.*r1f.^10+128*mu^2*M.*r1f.^13.*n^2 ...
+36*36*m2^4*l^2+8*36*mu*m2^2*l*n^2.*r1f.^8+32*36*M*mu*m2^2*l.*r1f.^5 ...
-64*mu.* (9*m2^2*l*n^2.*r1f.^8+4*M*mu*n^2.*r1f.^13+27*m2^2*l*n^2.*r1f.^8);
root1f=sqrt (Diak1f);
w1f=sqrt ( (-4*mu.*r1f.^8.*n^2-16*M*mu.*r1f.^5-36*m2^2*l+root1f)./ (-32*mu.*r1f.^8));

%Find the right wfh1 for that r1 with a questionable surely optimizable
%way
wt=linspace (0.001,0.03,100*NN);
at= (1-4.* (wt./n).^2);
rt=M^ (1/3).*wt.^ (-2/3)+3/4*l.* (1+3./at).*M^ (-4/3).*wt.^ (8/3);
t=linspace (1,1,100*NN);
t=r1*t;
tt=abs (rt-t);
wtt=min (tt);
it=find (tt==wtt,1);
wfh1=wt (it);
%calculating it with flanagan/hinderer
afh1= (1-4* (wfh1/n)^2);
%Calculate r
rfh1=M^ (1/3)*wfh1^ (-2/3)+3/4*l* (1+3/afh1)*M^ (-4/3)*wfh1^ (8/3);

%left part of plot
i2l=length (r1c)-10;

r1l=r1c (i2l); %left part for omega_1
Diak1l=16*mu^2.*r1l.^16.*n^4+256*M^2*mu^2.*r1l.^10+128*mu^2*M.*r1l.^13.*n^2 ...
+36*36*m2^4*l^2+8*36*mu*m2^2*l*n^2.*r1l.^8+32*36*M*mu*m2^2*l.*r1l.^5 ...
-64*mu.* (9*m2^2*l*n^2.*r1l.^8+4*M*mu*n^2.*r1l.^13+27*m2^2*l*n^2.*r1l.^8);
root1l=sqrt (Diak1l);
w1l=sqrt ( (-4*mu.*r1l.^8.*n^2-16*M*mu.*r1l.^5-36*m2^2*l+root1l)./ (-32*mu.*r1l.^8));

r2l=r1l; %left part for omega_2
Diak2l=16*mu^2.*r2l.^16.*n^4+256*M^2*mu^2.*r2l.^10+128*mu^2*M.*r2l.^13.*n^2 ...
+36*36*m2^4*l^2+8*36*mu*m2^2*l*n^2.*r2l.^8+32*36*M*mu*m2^2*l.*r2l.^5 ...
-64*mu.* (9*m2^2*l*n^2.*r2l.^8+4*M*mu*n^2.*r2l.^13+27*m2^2*l*n^2.*r2l.^8);
root2l=sqrt (Diak2l);
w2l=sqrt ( (-4*mu.*r2l.^8.*n^2-16*M*mu.*r2l.^5-36*m2^2*l-root2l)./ (-32*mu.*r2l.^8));


figure (1);
hold on;
plot (r1f,w1f^2*10^4, 'r*','LineWidth',3, 'HandleVisibility', 'off');
text (1.01*r1f,1.2*w1f^2*10^4, '$A-(r_{f1},w_{f1})$' ,'Interpreter','latex', ...
    'FontSize', 30);
plot (r1,w1^2*10^4, 'r*','LineWidth',3, 'HandleVisibility', 'off');
text (0.75*r1,0.8*w1^2*10^4, '$B-(r_{1},w_{1})$' ,'Interpreter','latex', ...
    'FontSize', 30);
```

```
plot (rfh1,wfh1^2*10^4, 'b*','LineWidth',3, 'HandleVisibility', 'off');
text (1.01*rfh1,1.1*wfh1^2*10^4, '$C-(r_{fh1},w_{fh1})$' ,'Interpreter','latex', ...
    'FontSize', 30);
plot (r1l,w1l^2*10^4, 'r*','LineWidth',3, 'HandleVisibility', 'off');
text (0.65*r1l,0.9*w1l^2*10^4, '$D-(r_{1l},w_{1l})$' ,'Interpreter','latex', ...
    'FontSize', 30);
plot (r2l,w2l^2*10^4, 'black*','LineWidth',3, 'HandleVisibility', 'off');
text (0.55*r2l,1*w2l^2*10^4, '$E-(r_{2l},w_{2l})$' ,'Interpreter','latex', ...
    'FontSize', 30);

plot (rc,w1c*10^4, 'r','LineWidth',3);
plot (rc,w2c*10^4, 'black','LineWidth',3);
plot (rc,wkc*10^4,'g','LineWidth',3);
plot (rf,wtf*10^4,'b','LineWidth',3);
xline (2*R);
xline (R,'LineWidth',3);
title ('Plot of the different $\omega^2 (r)$' ,'Interpreter','latex')
xlabel ('$r (km)$','Interpreter','latex')
ylabel ('$\omega^2 (r) (10^{-4} km^{-2})$','Interpreter','latex')
legend ('$\omega_1^2$','$\omega^2_2$','$\omega^2_k$','$\omega^2_f$' ...
    ,'r=2R','r=R','Interpreter','latex');
fontsize (legend ,40,'points')
ax = gca;
ax.FontSize = 40;
end




y=Det (w1,r1,m,mu,M,n,l,xi);
y1=y;%Det for r1,w1

y=Det (w1f,r1f,m,mu,M,n,l,xi);
y1f=y;%Det for r1f,w1f

y=Det (wfh1,rfh1,m,mu,M,n,l,xi);
yfh1=y;%Det for rfh1,wfh1

y=Det (w1l,r1l,m,mu,M,n,l,xi);
y1l=y;%Det for r1l,w1l

y=Det (w2l,r2l,m,mu,M,n,l,xi);
y2l=y;%Det for r2l,w2l



if split==1
%Draw the Dets separately:
figure (2);
tiledlayout (1,2)

nexttile
hold on;
semilogy (xi,y1, 'red','LineWidth',3);
semilogy (xi,y1f, 'Color',[0.568627 0.192157 0.643137],'LineWidth',3);
semilogy (xi,yfh1, 'blue','LineWidth',3);
xlabel ('$\Omega^2/\omega^2$','Interpreter','latex');
ylabel ('$Det-(\Omega^2)$','Interpreter','latex');
xline (0);
yline (0);
legend ('$\Omega_{1}$','$\Omega_{1f}$','$\Omega_{fh1}$','Interpreter','latex')
```

```
fontsize (legend,40,'points')
ax = gca;
ax.FontSize = 40;

nexttile
hold on;
semilogy (xi,y1l,'Color',[0.431373 0.000000 0.007843],'LineWidth',3)
semilogy (xi,y2l, 'black','LineWidth',3);
xlabel ('$\Omega^2/\omega^2$','Interpreter','latex');
xline (0);
yline (0);
legend ('$\Omega_{1l}$','$\Omega_{2l}$','Interpreter','latex')
fontsize (legend,40,'points')
ax = gca;
ax.FontSize = 40;
else
%Draw the Det:
figure (2);
hold on;
plot (xi,y1, 'red','LineWidth',3);
plot (xi,y1f, 'Color',[0.568627 0.192157 0.643137],'LineWidth',3);
plot (xi,yfh1, 'blue','LineWidth',3);
plot (xi,y1l,'Color',[0.431373 0.000000 0.007843],'LineWidth',3)
plot (xi,y2l, 'black','LineWidth',3);

title ('Plot of $Det (\Omega^2)$','Interpreter','latex');
xlabel ('$\Omega^2/\omega^2$','Interpreter','latex');
ylabel ('$Det (\Omega^2)$','Interpreter','latex');
hold on;
xline (0);
yline (0);
legend ('$\Omega_{1}$','$\Omega_{1f}$','$\Omega_{fh1}$','$\Omega_{1l}$' ...
    ,'$\Omega_{2l}$','Interpreter','latex')
fontsize (legend,40,'points')
ax = gca;
ax.FontSize = 40;
end
```

B.2 The function Det.m

This is the function Det.m that is used in the previous code:

```
    function y=Det (w,r,m,mu,M,n,l,xi)
a= (1-4* (w/n)^2);
W4=1;
W3=9*m^2*l/ (r^8*mu)+27*m^2*l/ (r^8*a*mu)+2*M/r^3-3*n^2-11*w^2;
W2=-81*m*n^2/ (4*r^8*a*mu)-135*m^2*l*n^2/ (4*r^8*mu)-81*m^2*l*n^2/ (a*r^8*mu) ...
    -6*M*n^2/r^3+3*n^4-27*m*w^2/ (r^8*a*mu)-72*m^2*n^2*l/ (r^8*mu) ...
    -108*m^2*n^2*l/ (r^8*a*mu)-16*M*w^2/r^3+9*n^2*w^2+40*w^4;
W1=81*m*n^4/ (2*r^8*a*mu)+81*m^2*l*n^4/ (2*r^8*mu)+81*m^2*l*n^4/ (a*r^8*mu) ...
    +6*M*n^4/r^3-n^6-27*m*n^2*w^2/ (r^8*a*mu)+54*m^2*l*n^2*w^2/ (r^8*mu)- ...
    108*m^2*l*n^2*w^2/ (r^8*a*mu)-n^4*w^2-108*m*w^4/ (4*r^8*a*mu) ...
    +144*m^2*l*w^4/ (r^8*mu)+432*m^2*l*w^4/ (r^8*a*mu)+32*M*w^4/r^3 ...
    -16*n^2*w^4-48*w^6;
W0=-81*m*n^6/ (4*r^8*a*mu)-63*m^2*l*n^6/ (4*r^8*mu)-27*m^2*l*n^6/ (a*r^8*mu) ...
    -2*M*n^6/r^3+54*m*n^4*w^2/ (a*r^8*mu)+126*m^2*l*n^4*w^2/ (r^8*mu) ...
    +216*m^2*l*n^4*w^2/ (a*r^8*mu)+16*M*n^4*w^2/r^3+3*n^6*w^2 ...
    +108*m*n^2*w^4/ (a*r^8*mu)-252*m^2*l*n^2*w^4/ (a*r^8*mu)-32*M*n^2*w^4/r^3 ...
    -24*w^4*n^4+48*n^2*w^6;
x=xi*w^2;
y=W4.*x.*x.*x.*x+W3.*x.*x.*x+W2.*x.*x+W1.*x+W0;
```